

SYNAPTIC MITOCHONDRIA
REGULATE HAIR CELL SYNAPSE
SIZE AND FUNCTION

by
Hiu-tung Candy Wong

A dissertation submitted to Johns Hopkins University in conformity with the requirements for
the degree of Doctor of Philosophy

Baltimore, Maryland
January, 2020

Abstract

Mechanosensitive hair cells of the inner ear and lateral line are specialized sensory cells that are required to evoke vital behaviors such as hearing, maintaining an upright posture and evading predators. To encode these sensory signals, hair cells use specialized ribbon synapses. Mitochondrial dysfunction has been implicated in hearing loss but the role of healthy mitochondria in hair cells or at ribbon synapses is unclear. I show that mitochondrial Ca^{2+} couples with presynaptic activity and plays distinct roles at hair cell synapses in mature and developing cells. I show that in mature hair cells, evoked-presynaptic- Ca^{2+} influx initiates mitochondrial- Ca^{2+} uptake; block of mitochondrial- Ca^{2+} uptake depresses presynaptic- Ca^{2+} activity and long-term block of mitochondrial- Ca^{2+} uptake can impact synapse integrity. I show that in developing hair cells, mitochondrial- Ca^{2+} uptake coincides with spontaneous presynaptic rises in Ca^{2+} . Block of spontaneous presynaptic rises in Ca^{2+} or mitochondrial- Ca^{2+} uptake in developing hair cells enlarges presynaptic ribbon structure during synapse formation. Presynaptic ribbon size is composed primarily of the self-aggregating structural protein Ribeye. My work indicates that mitochondrial- Ca^{2+} may impact ribbon formation by modulating Ribeye-Ribeye protein interactions via the NAD(H) binding domain on Ribeye. Spontaneous mitochondrial- Ca^{2+} loading lowers cellular NAD^+/NADH and ultimately downregulates ribbon formation. Furthermore, I found that direct application of NAD^+ or NADH can directly increase or decrease ribbon formation respectively. Our results propose that mitochondrial- Ca^{2+} is an important component of presynaptic function and formation.

Advisory committee:

Dr. Katie S. Kindt (Thesis advisor)

Dr. Paul A. Fuchs (Second reader)

Dr. Marnie E. Halpern (Chair)

Dr. Wei Li

Dr. Chen-Ming Fan

Dedication

I dedicate this thesis to my parents, Yuen Han and Tak Sing.

A special thank you to Dr. Daniel Cummins, who shares his life with me, and provided plentiful encouragement and deoxygenated water to support this work.

To every wonderful person who have influenced me and my work; know that I am grateful for your companionship and support.

Acknowledgments

I would like to extend a heartfelt thanks to past and current lab members for their suggestions, friendship, and influence. It cannot be said enough that Dr. Katie Kindt is everything I could hope to look for in a good mentor. Alisha Beirl is a wonderful friend and dependable source of amazing immunohistochemistry and dry humor. Former postbaccalaureate researcher Suna Li is a friend and an inspiration and provided helpful knowledge on zebrafish handling when I was learning the craft.

Thank you to Dr. Doris Wu for her invaluable advice, especially in times of uncertainty.

A special feeling of gratitude to my thesis committee, Drs. Paul Fuchs, Marnie Halpern, Wei Li, and Chen-Ming Fan for their support for both my academic endeavors and personal growth.

Much thanks to the office of the Johns Hopkins Biology department, whose support is indispensable during my thesis work.

My undergraduate research training from Dr. Yehoash Raphael and his laboratory staff, especially Dr. Don Swiderski and Lisa Beyer, shaped my interest which eventually cumulated in this thesis.

Table of Contents

Abstract.....	ii
Dedication	iv
Acknowledgments.....	v
List of Tables	vi
List of Figures	xi
Abbreviations.....	xiii
Chapter 1: Introduction	1
Overview	1
Anatomy of the mammalian inner ear.....	4
Hair cell ribbon synapse formation.....	25
Ca ²⁺ imaging using genetically-encoded Ca ²⁺ indicators.....	28
Mitochondrial Ca ²⁺ uptake in hair cell physiology and pathology.....	33
Zebrafish posterior lateral line	42
Chapter 2: Synaptic mitochondria are critical for hair-cell synapse function and integrity	48
Abstract	49
Introduction.....	50
Results.....	52
Mitochondria are located near presynaptic ribbons.....	52

Mitochondrial-Ca ²⁺ uptake at ribbons is MCU and Cav1.3 dependent	55
Mitochondrial-Ca ²⁺ uptake occurs in cells with presynaptic-Ca ²⁺ influx.....	62
Blocking mitochondrial-Ca ²⁺ entry impairs presynaptic Ca ²⁺ signals in mature hair cells	65
Evoked mitochondrial-Ca ²⁺ uptake is important for mature synapse integrity and cell health	68
MCU and Cav1.3 channel activities regulate subcellular Ca ²⁺ homeostasis	76
Discussion	80
Role of evoked mitochondrial-Ca ²⁺ uptake in mature hair cells	80
Role of mitochondrial-Ca ²⁺ in hair cell death and synapse integrity	82
Materials and Methods	83
Zebrafish husbandry and genetics	83
Cloning and transgenic fish production.....	84
Pharmacological treatment of larvae for immunohistochemistry.....	86
<i>In vivo</i> imaging of evoked Ca ²⁺ signals.....	86
Electron microscopy.....	87
Immunofluorescence staining and Airyscan imaging	88
Quantification and Statistical Analysis.....	89
Analysis of Ca ²⁺ signals, processing, and quantification	89
Image processing and quantification of synapse morphology	90
Statistics	92
Acknowledgements	93

Chapter 3: Spontaneous mitochondrial-Ca ²⁺ uptake modulates ribbon synapse formation.....	94
Abstract	95
Introduction.....	96
Results.....	98
Blocking mitochondrial-Ca ²⁺ entry does not impair presynaptic-Ca ²⁺ signals in immature hair cells	98
Spontaneous presynaptic and mitochondrial-Ca ²⁺ influx pair in developing hair cells.....	102
Spontaneous mitochondrial-Ca ²⁺ uptake regulates ribbon formation.....	108
MCU and Ca _v 1.3 channel activities regulate subcellular Ca ²⁺ homeostasis	117
Mitochondrial-Ca ²⁺ levels regulate NAD(H) redox in developing hair cells	118
NAD ⁺ and NADH directly influence ribbon formation.....	122
Discussion	127
Functional significance of ribbon size	127
Ribeye and CtBP localization at synapses	129
Role of spontaneous mitochondrial-Ca ²⁺ uptake in developing hair cells.....	131
Materials and Methods	133
Zebrafish husbandry and genetics	133
Cloning and transgenic fish production	133
Pharmacological treatment of larvae for immunohistochemistry	135
<i>In vivo</i> imaging of baseline Ca ²⁺ and NAD(H) redox.....	135

<i>In vivo</i> imaging of evoked Ca ²⁺ signals	136
<i>In vivo</i> imaging of spontaneous Ca ²⁺ signals.....	137
Immunofluorescence staining and Airyscan imaging	138
Quantification and Statistical Analysis.....	139
Analysis of Ca ²⁺ and NAD(H) signals, processing, and quantification.....	139
Image processing and quantification of synapse morphology	141
Statistics	143
Acknowledgements	144
Chapter 4: Conclusion	145
Future directions	151
Role of Ribeye NAD(H)-binding domain in presynaptic ribbon formation	151
The role of mitochondrial-Ca ²⁺ uptake in hair cells	156
Endoplasmic reticulum Ca ²⁺ handling	161
References	172
Appendix	172
Image analysis	173
Bibliography	176
Curriculum Vitae	239

List of Tables

Table 1.1. Estimated average ribbon number, size and synapse innervation in different organs and species.....	18
Table 2.1. Primers used to generate $Tg(myo6b:mitoRGECO1)^{idc12Tg}$	85
Table 3.1. Primers used to generate $Tg(myo6b:Rex-YFP)^{idc13Tg}$	134

List of Figures

Figure 1.1. Sensory hair cells that populate sensory epithelia of the auditory and vestibular organs utilize ribbon synapses.....	5
Figure 1.2 Hair cell and ribbon synapse structure and function.....	11
Figure 1.3. Synaptic ribbon size variation between and within hair cells.	19
Figure 1.4 Transgenic biosensors expressed in zebrafish hair cells.....	31
Figure 1.5. Mitochondrial Ca^{2+} uptake influences mitochondrial respiration and NAD^+/NADH redox homeostasis.....	34
Figure 1.6 Zebrafish lateral line afferent pathway for escape behavior.....	44
Figure 2.1. Mitochondrial- Ca^{2+} uptake initiates adjacent to ribbons.....	53
Figure 2.2. The time course of mechanically-evoked mitochondrial- Ca^{2+} signals are longer-lasting than cytosolic- Ca^{2+} signals and is additive.	57
Figure 2.3. Mitochondrial- Ca^{2+} uptake occurs in anterior lateral-line hair cells.	59
Figure 2.4. Mitochondrial- Ca^{2+} uptake can impact presynaptic Ca^{2+} signals.	63
Figure 2.5. Hair-cell bundle mechanotransduction Ca^{2+} signals and presynaptic Ca^{2+} signals during MCU and VDAC block.	66
Figure 2.6. Mitochondrial- Ca^{2+} is important for ribbon size and synapse integrity in mature hair cells.	70
Figure 2.7. Ribbon and postsynapse size in mature ALL neuromasts.....	72
Figure 2.8. MCU block does not impact postsynapse size in mature hair cells.....	74

Figure 2.9. Cytosolic-Ca ²⁺ , mitochondrial-Ca ²⁺ baseline measurements in mature hair cells.....	78
Figure 3.1. Mitochondrial-Ca ²⁺ uptake does not impact presynaptic Ca ²⁺ signals in immature hair cells.....	100
Figure 3.2. Spontaneous presynaptic-Ca ²⁺ influx is linked with Mitochondrial-Ca ²⁺ uptake.....	104
Figure 3.3. Spontaneous presynaptic and mitochondrial-Ca ²⁺ signals are abolished by Cav1.3 channel antagonist isradipine.	106
Figure 3.4. Mitochondrial-Ca ²⁺ regulates ribbon formation.....	110
Figure 3.5. Ribbon and postsynapse size in immature ALL neuromasts.....	112
Figure 3.6. MCU and Cav1.3 block do not impact postsynapse size.....	115
Figure 3.7. Cytosolic-Ca ²⁺ , mitochondrial-Ca ²⁺ and NAD ⁺ /NADH redox baseline measurements.....	120
Figure 3.8. NAD ⁺ and NADH directly influence ribbon formation.....	123
Figure 3.9. NAD ⁺ and NADH treatment do not impact postsynapse size.....	125
Figure 4.1. Schematic model of mitochondrial-Ca ²⁺ activity and function in developing and mature hair cells.....	146
Figure 4.2. Contacts between mitochondria and ER cisternae.....	163
Figure 4.3. ER-localized Ca ²⁺ indicator R-CEPIA1-er.....	168
Figure A1. Image analysis scheme for identification and measurement of Ribeye and MAGUK puncta.....	174

Abbreviations

#- number (of)

%- percent

°C- degree Celsius

ATP- adenosine 5'-triphosphate

Ca²⁺- calcium

DNA- deoxyribonucleic acid

dpf- days post-fertilization

hr- hour/hours

Hz- Hertz

IMM- inner mitochondrial membrane

K⁺- potassium

min- minute/minutes

mito- mitochondrial

mM- millimolar

mRNA- messenger ribonucleic acid

Na⁺- sodium

NAD- nicotinamide adenine dinucleotide

NM- neuromast

nm- nanometer

OMM- outer mitochondrial membrane

P- postnatal day

PCR- polymerase chain reaction

Redox- reduction-oxidation

RFP- red fluorescent protein

ROI- region of interest

ROS- reactive oxygen species

s- second(s)

TEM- transmission electron microscopy

μM- micromolar

μm- micrometer

Chapter 1: Introduction

Overview

In the U.S., 40 million people suffer from hearing loss (Blackwell et al., 2014). Hearing loss can be a result of many factors including genetic predisposition, environmental factors such as noise-exposure, as well as aging (Blackwell et al., 2014). In the majority of these cases, hearing loss is sensorineural, resulting from a disruption of auditory sensory cells or afferent neurons. Emerging research indicates that noise-exposure and aging may result in synaptopathy, a type of sensorineural hearing loss where the synapses that connect auditory sensory cells and afferent neurons are damaged or lost (Furman et al., 2013; Kujawa and Liberman, 2009; Stamatakis et al., 2006; Wan and Corfas, 2015). Acquired synaptopathy-related hearing impairment may contribute to auditory pathologies such as tinnitus—ringing or buzzing heard without an external stimulus, and hyperacusis—abnormal sensitivity to moderate sounds (Knipper et al., 2013; Roberts et al., 2010). Therefore, the study of auditory sensory cell synaptic function, formation and maintenance is essential to understanding sensorineural hearing loss.

The sensory cells of the inner ear are notable for their hair-like projections on their apical cell surface and are aptly named—hair cells. In mammals, hair cells detect sensory cues including sound, as well as gravity and acceleration. Hair cells use specialized synapses rapidly and efficiently to convert these sensory cues into electrical signals that are carried to the brain. Proper hair cell function is closely tied to local changes in intracellular Ca^{2+} . In hair cells, both the detection and transmission of sensory cues trigger local changes in

intracellular Ca^{2+} . The apical hair-like stereocilia projections, also called hair bundles, detect sensory stimuli. Deflection of hair bundles causes a cationic influx of ions, including Ca^{2+} , into the hair bundles. This apical influx of cations depolarizes the membrane to trigger voltage-dependent presynaptic- Ca^{2+} influx that drives neurotransmitter release. If either apical mechanosensitive channels or presynaptic- Ca^{2+} channels are disrupted, sensory neurotransmission is lost. Loss of either of these Ca^{2+} signals results in sensorineural hearing loss in mice and humans (Michalski and Petit, 2015; Moser and Starr, 2016). Some examples include mutations in *pcdh15* (Ahmed et al., 2001; Alagramam, 2001; Alagramam et al., 2001; Seiler et al., 2005) or *cdh23* (Bolz et al., 2001; Palma et al., 2001; Söllner et al., 2004), which are required for apical influx of Ca^{2+} into hair bundles, and mutations in *cav1.3* (Namkung et al., 2001; Platzer et al., 2000; Sidi, 2004), which disrupt presynaptic- Ca^{2+} influx.

Within all cells, including hair cells, both intracellular Ca^{2+} and mitochondrial Ca^{2+} are tightly regulated. For example, in developing hair cells, spontaneous presynaptic Ca^{2+} activity in auditory and vestibular hair cells is an essential component of synapse and circuit formation (Holman et al., 2019; Tritsch et al., 2007; Johnson et al., 2013). In mature hair cells, excessive increase in intracellular Ca^{2+} can lead to mitochondrial- Ca^{2+} overload and ultimately cell death and hearing loss (Esterberg et al., 2013). Mitochondrial- Ca^{2+} overload is associated with excitotoxic insults such as excess noise and ototoxin exposure (Esterberg et al., 2013, 2014; Jensen-Smith et al., 2012; Patron et al., 2013; Qiu et al., 2013; Wang et al., 2019). Further, after these insults, dying hair cells display signs of mitochondria distress, such as swollen cristae and generation of reactive oxygen species (ROS) (Esterberg et al., 2014, 2016; Mangiardi et al., 2004; Olivari et al., 2008; Owens et al., 2007; Sha et al., 2001). In further support of the importance of mitochondria, several forms of hearing loss in humans are associated with mutations in mitochondrial genes (Ballana et al., 2006; Kameoka et al.,

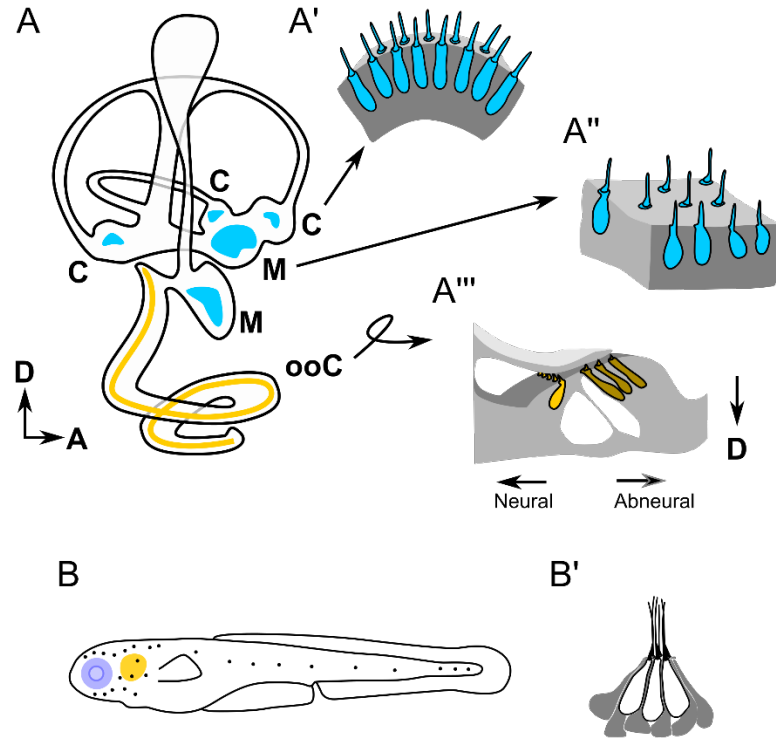
1998; van den Ouweland et al., 1992; Reardon et al., 1992; Scaglia et al., 2006; Verhoeven et al., 1999; Vialettes et al., 1997). Based on these studies, it is clear that mitochondria are critical for hair cell function and survival and for proper hearing. The importance of mitochondria in hair cells make the mitochondria a potential therapeutic target for hearing loss prevention. Despite the well-defined role of mitochondria in pathology, the inherent roles mitochondria and mitochondrial Ca^{2+} play in hair cell and hearing are less defined.

In the following sections, I outline the state of knowledge on the function of mitochondria in hair cells and more broadly the role mitochondria play at synapses. I also outline the development and function of the sensory hair cell synapse. Overall, understanding the formation and integrity of these synapses is critical to the protection and restoration of these structures, contributing to the development of therapies that treat and prevent hearing loss.

Anatomy of the mammalian inner ear

Animals have evolved specialized sensory organs to detect environmental sounds, as well as their own movement, and postural adjustments to gravity. Mammals achieve these behaviors using their inner ear, which contains a cochlea to detect sound, and a vestibular labyrinth to detect gravitational, linear and angular acceleration (Figure 1.1A). Amphibians and aquatic animals have an additional, related sensory organ—the lateral line—that is used to detect water flow and pressure.

Figure 1.1. Sensory hair cells that populate sensory epithelia of the auditory and vestibular organs utilize ribbon synapses.



A. The mammalian inner ear detects auditory and vestibular cues using specialized sensory epithelia. The fluid-filled compartments of the inner ear (black outline) are illustrated from a dorsal-view. Auditory signals are detected by the organ of Corti (yellow), while linear and angular acceleration and gravity are detected by 5 vestibular sensory epithelia (blue): 2 maculae and 3 cristae within semicircular canals. Enlarged are representative drawings of cross sections through a crista (A'), macula (A'') and organ of Corti (A'''). The organ of Corti is made up of two population of hair cells that form a defined and repeating spiral pattern through the organ. Inner hair cells (light yellow) form a single row closer to the cell bodies of the afferent neurons (neural), while outer hair cells (dark yellow) form 3 rows adjacent to the inner hair cells. B, Zebrafish larvae lateral line distribution. Black dots along the body represent location of hair cells. B', Each black dot in B is a cluster of hair cells (white) tightly packed within a structure called a neuromast. The neuromast hair cells are located just beneath the zebrafish skin. A, anterior; C, crista; D, dorsal; M, macula; ooC, organ of Corti

In mammals, hearing begins in the spiral-shaped cochlea. Sound, conducted through air, is converted into oscillations in fluid pressure along the spiral of the cochlea (Von Békésy and Wever, 1989). Subtle variations in the mechanical properties along the cochlea tune different segments to vibrate in response to different sound frequencies (Emadi et al., 2004; Karavitaki and Mountain, 2007; Naidu and Mountain, 1998; Reichenbach and Hudspeth, 2014; Teudt and Richter, 2014). On the other hand, the sense of balance requires the vestibular labyrinth. In mammals, the labyrinth is a fluid-filled pouch that can be subdivided into 5 sensory epithelia: 3 semicircular canals and 2 maculae (Eatock and Songer, 2011; Khan and Chang, 2013). Each canal is a loop that contains an ampulla, a bulbous sack which houses a flexible barrier called the cupula on top of a sensory organ, the crista ampullaris. Mammals have 3 canals aligned in near perpendicular directions to enable optimal rotational sensitivity in each corresponding plane (Cullen and Minor, 2002). Additionally, mammals have two maculae to detect linear acceleration—the utricle and saccule (Fritzsche and Beisel, 2004).

Teleost fishes, including zebrafish, also have an inner ear. In zebrafish, the larval inner ear is structured similar to the mammalian inner ear, although no obvious auditory organ equivalent to the mammalian cochlea is present (Platt, 1993). Instead, auditory signals are detected by a macular epithelium (Ladich, 2014; Popper and Fay, 1993, 2011). Zebrafish larval ears contain an anterior and a posterior macula, upon which an otolithic structure is anchored to translate stimuli to the macular hair cells (Popper et al., 2005). Additionally, 3 semicircular canals support the detection of rotational movements (Platt, 1993). Upon adulthood, the fish ear develops an additional macula, the lagena (Haddon and Lewis, 1996). The inner ear of the zebrafish larva is functional by 4 days post-fertilization (dpf) and is able to support behaviors such as acoustic startle and righting reflexes (Eaton and Farley, 1973;

Eaton et al., 1977a; Moorman et al., 1999; Riley and Moorman, 2000). In addition to an inner ear, teleosts, amphibians and certain aquatic animals also have a related sensory organ system called the lateral line. The lateral line system is present on or near the surface of the skin as a dispersed collection of flow-detecting epithelia called neuromasts (Coombs and Montgomery, 1999; McHenry et al., 2009; Montgomery et al., 2003).

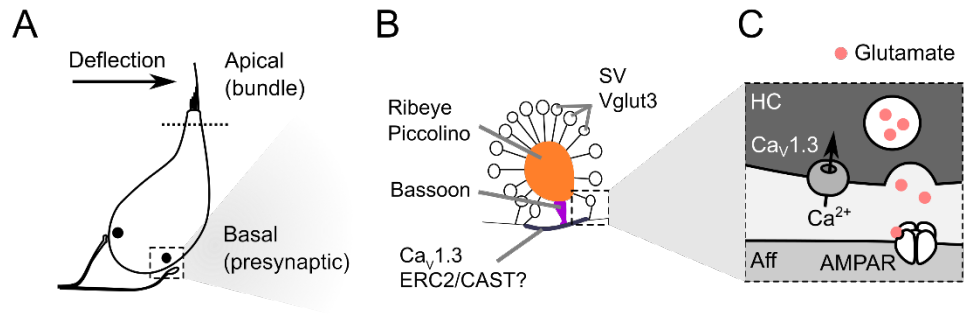
To detect auditory and vestibular cues, these sensory organs use sensory receptors called hair cells (Figure 1.1A'-A''). In the auditory organ of the mammalian cochlea, there are two types of hair cells, inner and outer hair cells. When sound travels within the cochlea, the vibration of is detected by inner hair cells (Figure 1.1 A'', Fuchs et al., 2003; Nouvian et al., 2006). To further enhance frequency specificity, the vibration is filtered and amplified in mammals by the uniquely electromotile outer hair cells (Liberman et al., 2002; Mellado Lagarde et al., 2008; Reichenbach and Hudspeth, 2014; Zheng et al., 2006). In the vestibular portion of the mammalian inner ear, rotation of the head is propagated to the fluid within the semicircular canals, which is detected by hair cells in the cristae (Figure 1.1A'). Additionally, linear acceleration from movement or gravity pulls the otoconia, a gelatinous matrix weighted with calcium carbonate crystals, which is detected by hair cells in the utricle and saccule (Figure 1.1A''; Anniko et al., 1988; Jones et al., 1999, 2004; Riley and Moorman, 2000; Salvinelli et al., 2004; Simmler et al., 2000; Sollner et al., 2004; Trune and Lim, 1983). In the larval zebrafish inner ear, the vestibular organs follow a similar activation paradigm—the 3 cristae act as rotation sensors, while the maculae respond to linear acceleration and gravity. In the zebrafish inner ear, one of the maculae also acts to detect sound in the place of the mammalian organ of Corti (Platt, 1993). In adult zebrafish, an additional macula, the lagena, also aids in hearing (Popper and Fay, 2011).

The hair cells within these sensory organs are specialized epithelial cells with distinct apical and basal structures. These distinct structures impart unique functional domains within hair cells (Figure 1.2A). In the apical compartment of hair cells are mechanosensory bundles that function to transform mechanical stimuli into membrane depolarizations. Mechanosensory hair bundles are composed of actin-rich protrusions, called the stereocilia (Flock and Cheung, 1977; Wiederhold, 1976). Stereocilia contain mechano-electrical transduction (MET) channels, non-specific cation channels that pass both K^+ and Ca^{2+} (reviewed in Cunningham and Müller, 2019). Deflection of the hair bundle mechanically opens the MET channels and initiates a depolarization of the hair cell membrane. In contrast to neuronal action potential, in which depolarization generates an all-or-none response, hair cell depolarizations are graded. Hair cells use graded depolarizations to encode stimulus intensity (Corey and Hudspeth, 1983; Torre et al., 1995).

MET opening in the hair bundle instantly depolarizes the electrically compact hair cell, including the basal compartment (Figure 1.2A). The basal compartment contains a specialized synapse, known as a ribbon synapse (Figure 1.2B). The role of this synapse is to convert graded membrane potentials of the hair cell into action potentials in the innervating afferent neuron. At the hair cell synapse, membrane depolarization opens voltage-gated L-type Ca^{2+} channels ($Ca_v1.3$) localized at the presynapse (Figure 1.2B-C; Brandt et al., 2003; Sidi, 2004). The resulting Ca^{2+} influx triggers synaptic vesicle fusion and release of the neurotransmitter glutamate into the synaptic cleft (Figure 1.2C; Obholzer et al., 2008; Pangršič et al., 2010; Ruel et al., 2008; Seal et al., 2008; Vincent et al., 2014). When released into the cleft, glutamate binds and opens AMPA (α -amino-3-hydroxy-5-methyl-4-isoxazole propionic acid) receptors at the afferent postsynapse to allow an influx of cations into the

postsynapse (Glowatzki and Fuchs, 2002; Sebe et al., 2017). At a sufficient intensity of cation influx, an action potential is generated and propagates down the neuronal fiber to the brain.

Figure 1.2 Hair cell and ribbon synapse structure and function



A, Deflection of the apical stereocilia bundle depolarizes the hair cell membrane to trigger synaptic activity at the presynapse. B, Hair cell presynapse structures include synaptic vesicles and ribbon body (orange), which is tethered by Bassoon protein (purple) to the presynapse membrane. C, At the presynaptic membrane, hair cell depolarization opens the voltage-gated Ca^{2+} channel $\text{Ca}_v1.3$. Nearby synaptic vesicles (white circle) containing neurotransmitter glutamate (pink circle) fuse in response to Ca^{2+} influx and release glutamate into the synaptic cleft. The released glutamate binds to and activates the ionotropic glutamate receptors AMPAR at the postsynapse of the afferent neuron. Aff, afferent neuron; AMPAR, α -amino-3-hydroxy-5-methyl-4-isoxazole propionic acid receptor; HC, hair cell; SV, synaptic vesicle.

The postsynaptic innervation patterns of hair cells differ between sensory organs. Auditory inner hair cells are innervated by a bouton-like postsynapse. Each auditory inner hair cell is innervated by many afferent neurons, and each afferent neuron forms a single contact or synapse (Liberman, 1982; Liberman et al., 1990). In contrast, auditory outer hair cells are innervated by relatively few afferent neurons, and each afferent neuron can form bouton-like synapses on many outer hair cells (Berglund and Ryugo, 1987; Liberman et al., 1990). In the mammalian vestibular epithelia, hair cells are classified as “type I” and “type II” based on their morphology (Desai et al., 2005a, 2005b). Similar to auditory hair cells, mammalian type II vestibular hair cells are also innervated by bouton-like postsynapses, and similar to the outer hair cells, one afferent neuron can form many synapses on multiple hair cells (Eatock and Songer, 2011). In comparison, type I vestibular hair cells are innervated by an enveloping, or calyceal type of postsynapse (Lysakowski and Goldberg, 1997). The innervation pattern of the lateral line hair cells of aquatic and amphibian animals is most similar to type II vestibular hair cells, where afferent neurons form bouton-like postsynapses onto multiple hair cells (Dow et al., 2018; Nagiel et al., 2008, 2009).

Hair cell ribbon synapse structure and function

Classical neuronal presynapse activity is limited by the refractory period of the neuron as well as the supply of releasable neurotransmitter local to the presynapse. Because the onset, duration and intensity represent important aspects of the sensory information hair cells receive, the synapses in hair cells must rapidly and continuously transmit information to the innervating afferent neuron (Matthews and Fuchs, 2010). Hair cells accomplish these requirements by using specialized ribbon synapses. Ribbon synapses also are utilized in retinal bipolar and photoreceptor cells, in electroreceptors, and in pinealocytes (Fritzsche and

Wahnschaffe, 1983; Gleisner et al., 1973; Matsushima et al., 1983; Sjöstrand, 1958; Smith and Sjostrand, 1961; Vollrath et al., 1983). In hair cells, ribbon synapses respond to graded membrane depolarizations to quickly and continuously transmit sensory information without a refractory period and can encode signal duration as well as intensity (van Hateren, 1992; de Ruyter van Steveninck and Laughlin, 1996).

To perform these tasks, hair cell synapses have adapted structures and molecules from the classical neuronal synapse to create a specialized ribbon synapse. Both neuronal and ribbon synapses concentrate neurotransmitter release machinery to form a presynaptic density. Hair cells additionally have a unique presynaptic structure called a “ribbon” (Figure 1.2B). Ribbons are visible in electron microscopy as a characteristic electron-dense structure (for example: Figure 2.1C). The presence of this density distinguishes ribbon synapses from classical neuronal synapses (Smith and Sjostrand, 1961). In the hair cells, ribbons are thought to be important for the overall function of the synapse. For example, mutant mice lacking ribbons were found to have altered synaptic function and afferent neuron firing behavior (Becker et al., 2018; Jean et al., 2018; Maxeiner et al., 2016). Loss of ribbon densities in zebrafish was found to disrupt presynaptic active zone formation and alter synapse function (Lv et al., 2012; Sheets et al., 2011). Overall these works indicate that the ribbon is required for the fidelity of synaptic activity in hair cells.

The main component of ribbons is the protein Ribeye. Ribeye was first identified from immunoprecipitation of ribbons from the bovine retina, and later from the mouse retina as well as the chicken basilar papilla (Schmitz et al., 2000; tom Dieck et al., 2005; Uthaiiah and Hudspeth, 2010). Ribeye is a protein of around 120 kDa that is unique to vertebrates (Schmitz et al., 2000). Ribeye is a splice variant of the transcriptional co-repressor

Carboxyl-terminal binding protein 2 (CtBP2) (Schmitz et al., 2000). Ribeye protein is divided into 2 main domains, the A- and B-domain. The unique N-terminus of Ribeye is the A-domain. The C-terminal terminus of Ribeye is the B-domain, which is nearly identical to full-length CtBP2.

Because the B-domain of Ribeye is essentially CtBP2, a considerable amount of information on this domain is inferred from studies on CtBP2. The B-domain and CtBP2 both contains a nicotinamide adenine dinucleotide (NAD⁺, NADH or NAD(H)) binding site (Magupalli et al., 2008; Schmitz et al., 2000). Studies on CtBP2 have shown that NAD(H) binding leads to dimerization and possibly tetramerization of CtBP2 (Bellesi et al., 2018; Fjeld et al., 2003; Thio et al., 2004). Interestingly, cellular metabolism, reflected in the NAD⁺/NADH ratio, may be coupled to dimerization of CtBP2; this dimerization is important for the transcriptional corepressor function of CtBP2. In hair cells, no clear function is assigned to the B-domain of Ribeye. But in photoreceptors, the B-domain of Ribeye has been shown to interact with other presynaptic proteins (Alpadi et al., 2008; Dembla et al., 2014; Venkatesan et al., 2010; Wahl et al., 2016). However, these interacting partners identified in photoreceptors—Munc119, ArfGAP3, GCAP2, and Tulp2—are not known components of the hair cell ribbon synapse. Despite the divergent molecular composition of ribbon synapses in photoreceptors and hair cells, the B-domain in hair cells is poised to interact similarly with presynaptic proteins: in zebrafish hair cells, Ribeye B-domain has been shown to localize preferentially within the ribbon near the presynaptic membrane (Sheets et al., 2014). The localization of Ribeye B domain near the presynapse suggests that presynaptic structures may attract the Ribeye B domain preferentially or alternatively, repel the A domain.

Recent work has confirmed that Ribeye protein is required to form electron-dense ribbons in hair cells. For example, Ribeye knockdown has been associated with the loss of presynaptic ribbon structure in mice and in zebrafish (Becker et al., 2018; Jean et al., 2018; Sheets et al., 2011; Wan et al., 2005). In zebrafish, morpholinos have been used to transiently knockdown Ribeye in zebrafish. This work found that the Ribeye knockdown led to a loss of ribbons and an overall disruption of synapse formation in hair cells (Sheets et al., 2011). A more recent study in zebrafish introduced a frameshift mutation in *ribeye* and observed less severe changes on ribbon synapse structure (Lv et al., 2016). In this frameshift mutant, ribbons no longer appear electron dense in TEM, were smaller, and associated with fewer synaptic vesicles. Interestingly, both studies found that Ribeye knockdown disrupted Cav1.3 Ca²⁺ channels clustering at the synapse. In contrast to this work on Ribeye loss of function, complementary work in zebrafish also examined hair cells that exogenously overexpressed Ribeye. In this work, Ribeye overexpression produced enlarged ribbons (Sheets et al., 2011, 2017). Overall, these studies show Ribeye protein is a critical component of ribbon synapses.

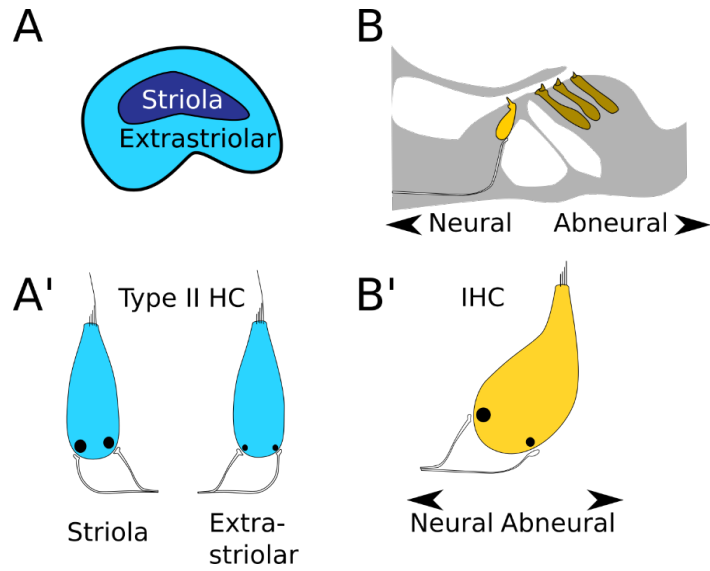
Ribbons can occur in a variety of numbers and sizes depending on the sensory organ, stage of development, and species of the organism (Table 1; reviewed in Moser et al., 2006). Studies indicate that differences in ribbon size within or between hair cell types can correlate with differences in ribbon synapse function. For example, in the mammalian vestibular system, the ribbons of type II dimorphic hair cells in the striola region are larger than those in the extrastriola region (Figure 1.3A-A'; Lysakowski and Goldberg, 1997). Functionally, afferent neurons that innervate hair cells with larger ribbons in the striola have lower rates of spontaneous activity compared to afferents that innervate the extrastriola (Eatock et al., 2008; Goldberg et al., 1984; Risner and Holt, 2006). Similarly, in the mammalian auditory system, inner hair cells utilize at least two populations of ribbon

synapses that can be distinguished based on ribbon size and the threshold sensitivity of the innervating afferent neuron (Figure 1.3B-B'; Liberman and Liberman, 2016; Liberman et al., 2011; Song et al., 2016). It is believed that these functional differences may be important to increase the range of sensitivity for auditory hair cells (Ohn et al., 2016). In addition to work in mammals, in zebrafish lateral line hair cells, ribbon size was enlarged to directly demonstrate the effect of ribbon morphology on ribbon synapse function. In zebrafish, synapses with enlarged ribbons had afferent neurons with lower spontaneous activity (Sheets et al., 2017). Furthermore, the onset encoding, or the timing of the first afferent spike upon stimulation, was significantly delayed at synapses with larger ribbons. Together, these findings suggest that synaptic function is related to differences in ribbon size, albeit in perhaps unexpected ways.

Table 1.1. Estimated average ribbon number, size and synapse innervation in different organs and species

<u>Hair cell type</u>	<u>Publication</u>	<u>Species</u>	<u>Age</u>	<u>Subtype</u>	<u># ribbon per hair cell</u>	<u>Average ribbon diameter (nm)</u>	<u>Postsynapse shape</u>	<u>Afferent neuron organization</u>
Post-hearing IHC	(Khimich et al., 2005)	mouse	3-8 weeks	-	9.8 ± 0.9	260	Bouton	1 hair cell to 1 neuron
	(Sonntag et al., 2018)	mouse	P27-P30	apical	11.8 ± 1.1	-		
	(Johnson et al., 2008)	gerbil	P21-P69	midbasal apical	16.3 ± 7 20.6 ± 0.6	- 114 ± 20		
	(Hashimoto et al., 1990)	guinea pig	adult	basal apical	22.4 ± 0.8 17	- -		
	(Lieberman et al., 1990)	cat	adult	basal abneural	26 -	- 180		
Vestibular	(Lenzi et al., 1999)	frog	-	saccular	-	468 ± 65	Bouton	Many hair cells to 1 neuron
	(Lenzi et al., 2002)	frog	-	saccular, inhibited saccular, stimulated	-	401 ± 22 391 ± 15		
	(Lysakowski and Goldberg, 1997)	chinchilla	adult	type I	15-20	90	Calyx	Many hair cells to 1 neuron
				type II, central	15-22	Similar to type I	Bouton	Many hair cells to 1 neuron
Lateral line	(Sheets et al., 2017; Suli et al., 2016)	zebrafish	5 dpf	posterior lateral line neuromast	2-4	288 (.065 μm ² , assume circular)	Bouton	Many hair cells to 1 neuron

Figure 1.3. Synaptic ribbon size variation between and within hair cells.



A, Some vestibular epithelia are structurally segregated into distinct regions. For example, the mammalian utricle contains a striola and an enveloping extrastriolar region. A' type II hair cells (blue) are found in the striolar and extrastriolar regions. Ribbon synapses of these type II hair cells in the striolar region are on average larger than those in the hair cells within the extrastriolar region. B, Synapses of cochlear hair cell may be described according to their location (neural or abneural) relative to neuronal somata ganglion within the center of the spiral shaped cochlea. B', Auditory inner hair cell (yellow) synapses may also be sorted into two ribbon sizes; larger ribbons preferentially reside on the neural side of the cell.

Although Ribeye is an important determinant of ribbon size at ribbon synapses, it is not present at classic neuronal presynapses. Despite this difference, both hair cell and neuronal synapses share similar structural and functional requirements. At both synapses, during synaptic transmission, neurotransmitters are focally released at a specialized area of the membrane called the presynaptic “active zone”. The active zone contains an arrangement of synaptic vesicles and exocytotic machinery in close association with Ca^{2+} channels organized and maintained by specialized structural proteins. At both hair cell and classical neuronal synapses, synaptic vesicles are filled with neurotransmitters, then recruited to the synapse, and ultimately their contents are released by fusion of the vesicles with the cell membrane.

In hair cells, synaptic vesicles are filled with the neurotransmitter glutamate much the same way as at classical synapses—through vesicular glutamate transporters. To fill vesicles with glutamate, hair cells utilize Vesicular glutamate transporter 3 (Vglut3), a molecule that is critical for hearing and balance in zebrafish, mouse and humans (Obholzer et al., 2008; Ruel et al., 2008; Seal et al., 2008). At classical neuronal synapses, vesicle fusion is mechanically driven by SNAP (soluble N-ethylmaleimide sensitive factor attachment protein) and SNARE (SNAP receptors) complexes (Fernández-Busnadiego et al., 2010). For example, at neuronal synapses, SNARE proteins such as Vesicle-associated membrane proteins (VAMP1 and 2), Syntaxin 1A and SNAP-25 are required for exocytosis (Chen and Scheller, 2001; Söllner et al., 1993). Biochemical and immunohistochemical approaches indicate that these key proteins are also present in hair cells (Safieddine and Wenthold, 1999; Uthaiiah and Hudspeth, 2010). On the other hand, genetic studies indicate that these proteins are not required for hair cell synaptic function (Nouvian et al., 2011). Similarly, essential proteins required for neuronal synapses such as Synaptophysin 1 and 2 (Safieddine and Wenthold,

1999) and Complexins (Strenzke et al., 2009) also are not present in hair cells. Therefore, currently it is not clear whether SNARE proteins are required or what equivalent release machinery is required for exocytosis at hair cells synapses (Matthews and Fuchs, 2010; Safieddine et al., 2012). One clear exception is the hair-cell-specific Ca^{2+} -sensor Otoferlin, discussed later in this section.

Although SNARE proteins may not be required at hair cell synapses, other important structural components are shared between neuronal and ribbon synapses. Two examples are the large structural proteins Bassoon (400 kDa) and Piccolo/Aczonin (550 kDa). Bassoon and Piccolo are structurally related proteins with multiple domains for interacting with many presynaptic protein partners—including each other (reviewed in: Gundelfinger and Fejtova, 2012; Gundelfinger et al., 2016; Torres and Inestrosa, 2018). At the neuronal presynapse, Bassoon and Piccolo colocalize (Dani et al., 2010). Both proteins interact with CtBP1, a protein which is in the same family as Ribeye (Ivanova et al., 2015). While Bassoon and Piccolo proteins share many homologous regions, some regions and therefore functions are protein specific (tom Dieck et al., 1998; Fenster et al., 2000; Gundelfinger et al., 2016; Wang et al., 1999). Bassoon and Piccolo contribute to synapse function by forming a scaffold that clusters presynaptic components near the presynaptic active zone in neurons (Cases-Langhoff et al., 1996; tom Dieck et al., 1998; Hagiwara et al., 2005; Ohtsuka et al., 2002; Takao-Rikitsu et al., 2004). Both proteins are involved in many aspects of neuronal synapse function, such as synaptic vesicle replenishment and vesicle localization near the active zone (Altrock et al., 2003; Hallermann et al., 2010; Mendoza Schulz et al., 2014; Mukherjee et al., 2010; Parthier et al., 2018). These proteins also bridge the presynapse with the actin cytoskeleton (reviewed in: Ackermann et al., 2015; Gundelfinger et al., 2016), and are required for general synaptic

maintenance such as turnover of presynaptic components (Okerlund et al., 2017; Waites et al., 2013).

In hair cells, Bassoon also serves an important presynaptic structural role at ribbon synapses. Bassoon is a key scaffolding protein at the presynaptic ribbon and is located beneath the ribbon (Figure 1.2B). In inner hair cells, Bassoon is required to anchor the ribbon body to the active zone, and disruption of Bassoon results in floating ribbons (Buran et al., 2010; Frank et al., 2010; Jing et al., 2013; Khimich et al., 2005; Meyer et al., 2009). Ribbon synapses have a smaller (about 330 kDa), ribbon-specific splice isoform of Piccolo named Piccolino (Dick et al., 2001; Khimich et al., 2005; Michanski et al., 2019; Regus-Leidig et al., 2013). Unlike Bassoon, which is found beneath the ribbons, Piccolino is localized to the ribbon (Michanski et al., 2019). Currently, the function of Piccolino at hair cell ribbon synapses remains unexplored. However, a clue to Piccolino function may be found in recent studies on ribbon synapses in retinal photoreceptor cells, where Piccolino interacts with Ribeye through PXDLS-motifs (Figure 1.2B; Müller et al., 2019)

Neurotransmitter released during hair cell synaptic activity is stored in synaptic vesicles associated with or near the ribbon. At neuronal presynapses, synaptic vesicles are docked or tethered to the plasma membrane by filaments in preparation for release. The number of filament-tethered vesicles decreases during synaptic activity, which suggests that the filaments are a component of synaptic vesicle turnover (Fernández-Busnadiego et al., 2010). At ribbon presynapses, synaptic vesicles are similarly tethered by thin filaments to the plasma membrane, and also to the ribbon (Buran et al., 2010; Khimich et al., 2005; Lenzi et al., 1999; Smith and Sjostrand, 1961). Presynaptic- Ca^{2+} influx occurs near ribbons in hair cells to drive vesicle exocytosis, and it is likely that the membrane-docked vesicles fuse first

at stimulus onset (Frank et al., 2009; Zenisek et al., 2003). A distinct “readily-releasable pool” (RRP) of vesicles at ribbon synapses can be defined by capacitance measurements. This RRP may be the functional equivalent of the membrane-docked vesicles (Krunner et al., 2017; Moser and Beutner, 2000; Pangršič et al., 2010; Parsons et al., 1994; Schnee et al., 2005; Spassova et al., 2004). In hair cells, the RRP requires anchored ribbons, which implies that the ribbon may play a role in minimizing the delay between stimulation and onset of neurotransmitter release (Jing et al., 2013; Khimich et al., 2005).

At both classical and ribbon synapses, synaptic vesicle release is triggered by presynaptic- Ca^{2+} influx. At hair cell ribbon synapses, this coupling is performed by the L-type Ca^{2+} channel $\text{Ca}_v1.3$ (Figure 1.1B'; reviewed in: Pangršič et al., 2018). Similar to *Vglut3*, $\text{Ca}_v1.3$ is critical for hearing in zebrafish, mice and humans (Brandt et al., 2003; Namkung et al., 2001; Platzer et al., 2000; Sidi, 2004). In mouse and zebrafish, $\text{Ca}_v1.3$ is not required for ribbon synapse formation, but it is required for synapse stability (Nemzou N et al., 2006; Sheets et al., 2012). At neuronal synapses, the Ca^{2+} sensors Synaptotagmins I and II are required to couple Ca^{2+} influx to neurotransmitter release. These Ca^{2+} sensors are absent from the hair cell ribbon synapse (Pang and Südhof, 2010; Safieddine and Wenthold, 1999). Instead, hair cells appear exclusively to use Otoferlin to couple Ca^{2+} influx to neurotransmitter release (Roux et al., 2006; Vincent et al., 2014; Yasunaga et al., 1999). Similar to mutations in *vglut3* and *cav1.3*, mutations in *otof* in zebrafish, mice and humans lead to deafness and loss of balance (Roux et al., 2006; reviewed in: Pangršič et al., 2012).

Currently many structural aspects required for hair cell ribbon synapse function are still not known. More insights on functions of identified or unidentified proteins, and presynapse organization may be gained from drawing parallels from presynaptic proteins of neuronal synapses and ribbon synapses in the retina.

Hair cell ribbon synapse formation

In order for proper hair cell synapse function, ribbons must first form properly. Among hair cell types and species, ribbon synapse development is most thoroughly described in mammalian auditory inner hair cells (Fuchs et al., 2003; Nouvian et al., 2006). In mice, hearing onset occurs at postnatal day 12 (Mikaelian and Ruben, 1965). But prior to hearing onset, ribbon synapses are formed and refined in developing inner hair cells. While mouse auditory hair cells are developed *in utero* (Anniko, 1983), the majority of synapse formation and refinement occurs after birth (Roux et al., 2009; Sobkowicz et al., 1986). During synapse formation and until hearing onset, immature inner hair cells engage in spontaneous bursts of action potentials that drive auditory afferent neuron activity (Johnson et al., 2011; Marcotti et al., 2003; Tritsch and Bergles, 2010). In developing mouse hair cells, bursts of action potentials require presynaptic $Ca_v1.3$ channels (Brandt et al., 2003; Eckrich et al., 2018; Platzer et al., 2000). Therefore, even without auditory input, ribbon synapses develop in an environment with robust presynaptic activity.

During this time, in mammalian hair cells, ribbon precursors are thought to develop extrasynaptically as electron-dense spheres already surrounded by a halo of vesicles (Sobkowicz et al., 1986). These extrasynaptic ribbon precursors are thought to migrate to the base of the hair cell and form larger structures where opposing post-synaptic structures are developing (Dow et al., 2015; Michanski et al., 2019; Safieddine et al., 2012; Sobkowicz et al., 1982, 1986). In mice, as the synapse matures, presynaptic $Ca_v1.3$ channel distribution is refined in concert with the postsynaptic glutamate receptors to form mature synapses (Frank et al., 2010; Johnson et al., 2009; Wong et al., 2014).

The structural changes that occur during inner hair cell synaptic maturation are reflected in electrophysiological measurements (Johnson et al., 2009; Kros, 2007; Safieddine et al., 2012). For example, in auditory hair cells of postnatal rodents, the exocytotic machinery measured by membrane capacitance strengthens as the ribbon is anchored and ribbons synapse structure matures (reviewed in: Kros, 2007; Safieddine et al., 2012) (Johnson et al., 2009). Prior to these evoked measurements, spontaneous presynaptic- Ca^{2+} influx is already present in the rodent auditory hair cells *in utero* (Johnson et al., 2011; Marcotti et al., 2003; Tritsch and Bergles, 2010). During the period of synapse refinement and $\text{Ca}_v1.3$ clustering, total, whole-cell presynaptic- Ca^{2+} influx is decreased, followed by a gradual rise and greater efficiency in triggering exocytosis (reviewed in: Kros, 2007; Safieddine et al., 2012).

The formation of zebrafish ribbon synapses has not been studied at this level of detail. But interestingly, work in zebrafish suggests that $\text{Ca}_v1.3$ activity regulates ribbon size during a critical period of development—block of $\text{Ca}_v1.3$ activity leads to the formation of larger ribbons (Sheets et al., 2012). The impact of $\text{Ca}_v1.3$ activity on ribbon formation suggests a form of presynaptic-activity-dependent regulation of synapse maturation. However, it is not known how presynaptic- Ca^{2+} influx mechanistically influences ribbon formation, and how the sensitivity to presynaptic- Ca^{2+} influx is lost upon hair cell maturation.

Ribbon formation is postulated to depend on self-assembly of Ribeye proteins via Ribeye-Ribeye interactions (Magupalli et al., 2008). In support of this idea, exogenous expression of Ribeye in non-hair cell culture was shown to be sufficient to form size-limited Ribeye puncta reminiscent of ribbons (Chen et al., 2018; Magupalli et al., 2008). Both *in vivo*

studies and cell culture work have explored how Ribeye domains interact with each other to achieve self-aggregation. For example, the unique N-terminal A-domain of Ribeye has been shown to be sufficient for Ribeye protein self-aggregation *in vitro* and *in vivo* (Chen et al., 2018; Magupalli et al., 2008). In contrast, the B-domain alone does not self-aggregate into multimeric puncta.

Although the B-domain does not self-aggregate, it can interact with other B-domains and A-domains in a manner regulated by NAD(H) binding site within the B-domain. This effect of NAD⁺ and NADH on Ribeye is proposed to modulate preference for A-domain to B-domain interaction and reduce A-domain-driven Ribeye self-aggregation. For example, the presence of NAD⁺ or NADH has been shown to affect Ribeye self-aggregation *in vitro* (Magupalli et al., 2008). Further, in the context of ribbons in hair cells, the B-domain has been shown to concentrate at the interface between the ribbon and the presynaptic membrane (Sheets et al., 2014). This indicates that the Ribeye B-domain could aid in seeding Ribeye protein at the presynapse.

Although the role of the B-domain of Ribeye remains unclear, the B-domain is essentially the well-studied transcriptional co-repressor CtBP2. In CtBP2, NAD(H) binding preferentially leads to dimerization and possibly tetramerization (Bellesi et al., 2018; Fjeld et al., 2003; Thio et al., 2004). This mechanism couples to the NAD⁺/NADH ratio, which serves as a reflection of cellular metabolic state, and enhances CtBP2 transcriptional corepressor function. Currently, whether Ribeye B domain at ribbons can detect NAD⁺/NADH ratio in order to regulate Ribeye self-aggregation has not yet been demonstrated *in vivo*. In more general terms, it is not known if NAD⁺ and NADH levels within hair cells relate to Ribeye-Ribeye interactions and ribbon formation *in vivo*.

Ca²⁺ imaging using genetically-encoded Ca²⁺ indicators

Many important aspects of hair cell function and development are reflected by the location and duration of Ca²⁺ influx into the cell. These Ca²⁺ signals represent a valuable readout of both spontaneous activity and evoked presynapse activity. For example, prior to hearing onset, immature hair cells engage in spontaneous presynaptic-Ca²⁺ activity akin to action potentials that drive auditory afferent neuron activity (Johnson et al., 2011; Marcotti et al., 2003; Tritsch and Bergles, 2010). In mature hair cells, presynaptic-Ca²⁺ influx is an integral part of evoked synaptic activity that triggers synaptic vesicle exocytosis to release neurotransmitter (Roux et al., 2006; Vincent et al., 2014).

A simple and effective way to visualize Ca²⁺ flux in the hair cell is with fluorescent Ca²⁺-sensitive dyes. Based on their Ca²⁺-binding affinity, they can be used to visualize Ca²⁺ in distinct subcellular domains within the hair cell. These dyes can be introduced into the hair cell by a pipette that breaches the cell membrane. Alternatively, if the dye is cell permeant, it can enter the hair cell directly. Using these methods, Ca²⁺ influx into hair bundles has been observed (Lumpkin and Hudspeth, 1995; Ricci and Fettiplace, 1998; Beurg et al., 2010). Such approaches have been used to determine the site of Ca²⁺ influx and the location of MET channels in hair bundles (Lumpkin and Hudspeth, 1995; Ricci and Fettiplace, 1998). Ca²⁺ dyes can also achieve sufficient resolution to visualize subcellular Ca²⁺ signals in other locations within inner hair cells. For example, in combination with a fluorescent peptide to mark the presynapse, Ca²⁺-sensitive dyes have been used to study the function of Ca²⁺ flux at the presynapse of auditory hair cells (Meyer et al., 2009; Neef et al., 2009, 2018). Ca²⁺-sensitive dyes have also been used to study the interaction between postsynaptic efferent and presynaptic afferent Ca²⁺ domains (Moglie et al., 2018), and demonstrate the prevalence of

ER Ca^{2+} -induced Ca^{2+} release (Kennedy and Meech, 2002). Overall, Ca^{2+} -sensitive dyes have been successfully used for detailed study of subcellular Ca^{2+} flux at the single cell level.

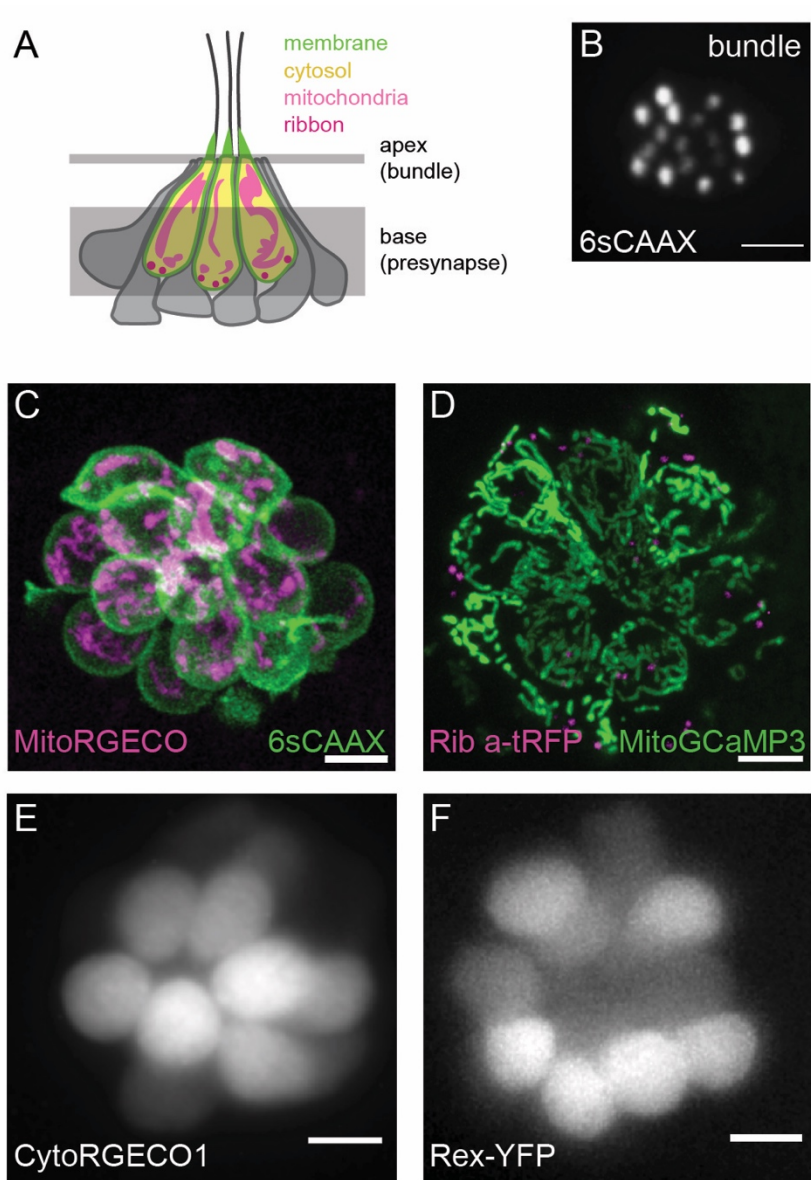
Another powerful way to measure Ca^{2+} signals is by using genetically-encoded Ca^{2+} indicators (GECIs). These indicators are modified fluorescent proteins that are fused to Ca^{2+} -binding motifs. When Ca^{2+} levels increase, these modified fluorescent proteins increase in fluorescence intensity (Higashijima et al., 2003; Zhang et al., 2016). Because GECI are genetically encoded, they can be expressed in specific cells types. In addition, GECIs can be localized subcellularly to specifically measure Ca^{2+} domains. Subcellular Ca^{2+} domains can be detected by localizing GECIs to organelles within cells. In hair cells, GECIs have been used to reveal critical Ca^{2+} -dependent events, such as MET and presynaptic function (Higashijima et al., 2003; Zhang et al., 2016).

Ca^{2+} imaging using GECIs is a valuable way to complement powerful electrophysiological methods to study hair cell function. Numerous studies have shown that whole-cell electrophysiological recordings can yield nuanced measurement of ion channel function within hair cells and at the afferent postsynapse with high temporal resolution (reviewed in: Fuchs, 2005; Example: Goutman and Glowatzki, 2007). Unfortunately, using this approach, it is difficult to localize where these signals are occurring within the cell. In addition, it is not possible to isolate both MET and presynaptic- Ca^{2+} currents in the same cell (Figure 1.4A). Furthermore, in contrast to electrophysiology, it is more feasible to use Ca^{2+} image to make simultaneous measurements from multiple hair cells (Figure 1.4).

Overall, Ca^{2+} imaging can enable powerful studies of discrete Ca^{2+} domains, as well as system-wide activity patterns among multiple cells. For example, previous work in zebrafish has shown that measurements using membrane-localized GECIs enable

simultaneous measurements of MET-channel- and $Ca_v1.3$ -dependent Ca^{2+} influx within the same hair cell as well as among populations of hair cells (Zhang et al., 2018). GECIs have also been localized to different subcellular structures within cells by other alteration to protein localization. For example, in zebrafish hair cells, mitochondria- and ER-localized GECIs were used to show the temporal dynamic of Ca^{2+} influx into each organelle prior to ototoxin-induced hair cell death (Figure 1.4D MitoGCaMP3; Esterberg et al., 2014). Overall this work indicates that GECIs can be used to reveal coordinated Ca^{2+} activity of targeted cell types within an organ with subcellular resolution. This level of information is immensely useful for studying Ca^{2+} signals present at developing and mature hair cell synapses in the context of the whole hair cell.

Figure 1.4 Transgenic biosensors expressed in zebrafish hair cells



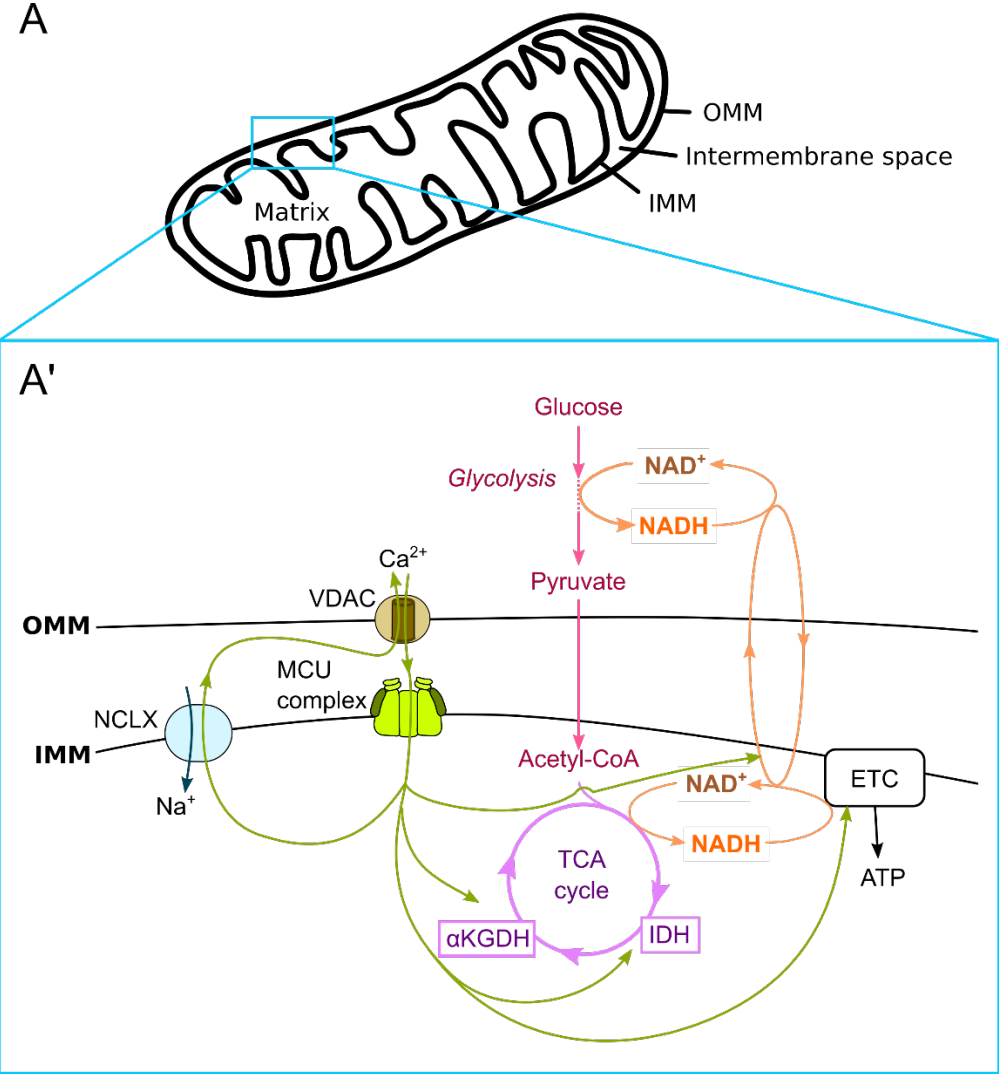
A, Illustration of a neuromast and the imaging planes used to study within lateral line hair cells from apex to base. Localization of membrane- (green), cytosol- (yellow), ribbon- (magenta), or mitochondria-localized (pink) fluorescent proteins are illustrated in their respective colors. B, Example live lateral line hair cells at 5 dpf expressing membrane localized GCaMP6s (GCaMP6sCAAX) highlight hair bundles. This localized indicator can be used to detect Ca^{2+} changes associated with mechanotransduction. C-F, Live neuromast hair cells imaged from midbody to base. Hair cells of 5 dpf larvae are expressing MitoRGECO1 (C, magenta), MitoGCaMP3 (D, green) and GCaMP6sCAAX (C, green) to measure mitochondrial- and presynaptic localized Ca^{2+} . Ribeye α -tagRFP (D, magenta) can also be used detect ribbon location to measure Ca^{2+} influx relative to ribbon location. In addition, CytoRGECO1 (E) or Rex-YFP (F) can be used to show to show cytosolic Ca^{2+} and NAD^+ / $NADH$ changes respectively. Scale bars = 5 μm in B-F.

Mitochondrial Ca^{2+} uptake in hair cell physiology and pathology

It is clear that evoked and spontaneous synaptic activity coincides with Ca^{2+} influx into hair cells; but activity does not end when Ca^{2+} enters the cell. Ca^{2+} can be extruded, buffered or further sequestered within subcellular domains. One major subcellular domain that can sequester intracellular Ca^{2+} is the mitochondria. In many cell types, mitochondria have been shown to take up and store Ca^{2+} (Carafoli and Lehninger, 1971; Williams et al., 2013). Within cells, mitochondrial- Ca^{2+} uptake can play a role in modulating bioenergetics, shaping intracellular Ca^{2+} changes, and triggering or preventing cell death (Glancy and Balaban, 2012; Orrenius et al., 2003).

Mitochondria take up and sequester Ca^{2+} within 2 compartments, the intermembrane space and matrix. These compartments are segregated by 2 phospholipid bilayers: the outer mitochondrial membrane (OMM) which separates the cytosol from the intermembrane space and inner mitochondrial membrane (IMM), which defines the boundary between the intermembrane space and matrix. Mitochondria-specific channels in the outer and inner membranes directs the influx and efflux of mitochondrial Ca^{2+} (Figure 1.5). The outer mitochondrial membrane is permeable to Ca^{2+} mainly through the highly conserved, 30-35 kDa Voltage-dependent anion channel (VDAC) (reviewed in: Colombini, 2012). As a porin, VDAC is permeable to ions and metabolites of up to 5 kDa (Shoshan-Barmatz et al., 2010). VDAC is voltage-gated and is permeable to both anions and cations including Ca^{2+} (reviewed in: De Pinto et al., 2008; Gincel et al., 2001; Shoshan-Barmatz and Gincel, 2003).

Figure 1.5. Mitochondrial Ca^{2+} uptake influences mitochondrial respiration and NAD^+/NADH redox homeostasis



Ca^{2+} enters and exits the mitochondria through mitochondria-specific channels. A, Mitochondria are composed of two phospholipid bilayers (black line): the outer mitochondrial membrane (OMM) and the inner mitochondrial membrane (IMM). The intermembrane space resides between the OMM and the IMM, and the matrix is defined by the IMM. A', Matrix Ca^{2+} levels may regulate mitochondrial respiration. Ca^{2+} (green arrow) passes the OMM from the cytosol (top) through the voltage-dependent anion channel (VDAC). Mitochondrial Ca^{2+} uniporter (MCU) complex and mitochondrial Na^+ - Ca^{2+} exchanger (NCLX) are embedded in the IMM and are the major pathways for Ca^{2+} influx into and efflux from the mitochondrial matrix (bottom). Glycolysis (pink arrows) in the cytosol feeds metabolic products into the tricarboxylic cycle (TCA, purple arrows), which drives the electron transport chain (ETC, black) to generate ATP. Glycolysis, TCA cycle and ETC processes reduce or oxidize nicotinamide adenine dinucleotide (NAD, orange arrows) between the oxidized form (NAD^+) and the reduced form (NADH). While NAD(H) cannot permeate the IMM, its electrons can be shuttled indirectly through the IMM. Mitochondrial Ca^{2+} modulates ETC activity, as well as isocitrate dehydrogenase (IDH) and α -ketoglutarate dehydrogenase (α KGDH) activity in TCA. Mitochondrial Ca^{2+} also regulates the rate of electron exchange between the NAD(H) pool in the matrix and in the cytosol.

Ca^{2+} enters the inner mitochondrial membrane (IMM) mainly through the mitochondrial- Ca^{2+} uniporter (MCU) complex (Baughman et al., 2011; Chaudhuri et al., 2013; De Stefani et al., 2011). The MCU complex is composed of the MCU channel, and associated proteins that modulate channel function, such as MICU1 and MICU2 (reviewed in Giorgi et al., 2018). The MCU complex is a highly Ca^{2+} selective channel (Baradaran et al., 2018; Kirichok et al., 2004). However, channel opening is inhibited until cytoplasmic- Ca^{2+} reaches around 20 μM (Csordás et al., 2013; Kamer and Mootha, 2014), which is high when compared to the average cytosolic Ca^{2+} concentration of around 100-200 nM (Carafoli, 2003; Chaudhuri et al., 2013; Williams et al., 2013). However, if mitochondria and its associated MCU complex are near sources with the potential for large changes in intracellular Ca^{2+} , such as near Ca^{2+} channels, these domains of high Ca^{2+} concentration can enable the fast, MCU-dependent uptake into the mitochondrial matrix (Csordás et al., 1999; Filadi and Pozzan, 2015; Pinton et al., 1998).

High concentrations of Ca^{2+} have been observed at hair cell synapses. For example, live Ca^{2+} imaging of turtle hair cells has shown $\text{Ca}_v1.3$ -dependent microdomain Ca^{2+} domains at the presynapse. In these microdomains, Ca^{2+} concentration is estimated to reach at least 85 μM (Tucker and Fettiplace, 1995). Based on these concentrations, it is possible that MCU-dependent uptake could occur at ribbon synapses, but currently this has not been demonstrated. However, there is precedent in organellar uptake of presynaptic- Ca^{2+} in the hair cell. At mammalian hair cell presynapses, the ER is thought to help maintain a low level of cytosolic- Ca^{2+} by taking up excess Ca^{2+} at the presynapse (Kennedy, 2002; Tucker and Fettiplace, 1995).

Opposing mitochondrial- Ca^{2+} influx is its efflux. Ca^{2+} efflux is mainly sodium-dependent (reviewed in: Sekler, 2015; Carafoli, 1974) and mediated by the mitochondrial Na^+ - Ca^{2+} exchanger (NCLX), an inner mitochondrial membrane protein (Luongo et al., 2017; Palty et al., 2010). The exchanger exchanges a Ca^{2+} ion for 3 Na^+ ions across the membrane for a net import of one positive charge into the mitochondrial matrix (Marinelli et al., 2014). In addition to NCLX, a proton-dependent Ca^{2+} efflux pathway has also been detected in the mitochondria (Pozzan et al., 1977). Although the protein for this pathway has not been identified, a candidate mechanism involves the Leucine zipper EF-hand-containing transmembrane protein 1 (Letm1) at the IMM (Jiang et al., 2009). Letm1 may directly participate as a H^+ - Ca^{2+} exchanger (Jiang et al., 2009), or indirectly modulate Ca^{2+} efflux through modulating mitochondrial- Na^+ homeostasis (Austin et al., 2017).

A major role of moderate mitochondrial- Ca^{2+} uptake under physiological conditions is to regulate ATP production. In the cytosol, glycolysis feeds pyruvate into the mitochondria to generate ATP through oxidative phosphorylation, which is modulated by Ca^{2+} at multiple points of the process (Figure 1.2; Rizzuto et al., 2012). Mitochondrial- Ca^{2+} modulates the conversion of pyruvate to acetyl-CoA (Denton et al., 1972, 1980; Marshall et al., 1984), isocitrate dehydrogenase (IDH) (Denton et al., 1978) and α -ketoglutarate dehydrogenase (α KGDH) (Lai and Cooper, 1986; Lawlis and Roche, 1981a; McCormack and Denton, 1979) in the tricarboxylic (TCA) cycle (reviewed in: Glancy and Balaban, 2012; Gunter and Sheu, 2009; Llorente-Folch et al., 2015). Downstream of the TCA cycle, in the electron transport chain (ETC), increased matrix Ca^{2+} concentration may also increase complex III function (Murphy et al., 1990). In general, mitochondrial- Ca^{2+} can increase ATP production by acting on mitochondrial metabolism.

In addition to ATP production, mitochondrial Ca^{2+} also regulates the cyclic reduction and oxidation of NAD(H), an integral part of mitochondrial metabolism. NADH levels in the cytosol and mitochondria has been shown to be less than 10 % of total NAD(H) content, indicating that the majority of NAD(H) is in the NAD^+ state (Williamson et al., 1967). Enzymes of glycolysis and TCA cycle reduce NAD^+ to NADH, while ETC oxidizes NADH back to NAD^+ (Krebs, 1970; Wallace, 2012). In the mitochondria, TCA cycle enzymes IDH (Denton et al., 1978; Vaughan and Newsholme, 1969; Zammit and Newsholme, 1976) and αKGDH (Lawlis and Roche, 1981b, 1981a) both reduce NAD^+ and are both regulated by mitochondrial Ca^{2+} (reviewed in: Glancy and Balaban, 2012). Ca^{2+} also modulates the connection between the discrete NAD^+/NADH ratio in the cytosol and the mitochondria. While NAD(H) can pass the OMM through VDAC, it cannot permeate the IMM and can only be shuttled through by reducing an equivalent amount of NAD^+ on one side of the IMM as NADH is oxidized on the other (Borst, 1962). The main mechanism for shuttling NADH into the IMM is through the malate-aspartate shuttle, the function of which is also positively regulated by mitochondrial Ca^{2+} (reviewed in: Satrústegui and Bak, 2015).

Because NAD(H) reduction-oxidation (redox) homeostasis is an important component of cell metabolism, it is tightly regulated, and changes in NAD(H) redox can trigger metabolic and physiological adaptations (Bogan and Brenner, 2008; Imai, 2009; Li and Sauve, 2015). For example, in mouse hippocampal neurons, presynaptic activity level has been found to correlate positively with the NAD^+/NADH ratio (Ivanova et al., 2015). A change in the NAD^+/NADH ratio is communicated to the nucleus through the presynaptic-resident CtBP1 protein, which also functions as a transcriptional co-repressor (Ivanova et al.,

2015). Currently it is not known if, similarly to CtBP1, Ribeye localization also is regulated by NAD(H) redox homeostasis in hair cells.

Modest mitochondrial- Ca^{2+} uptake is a normal part of cell physiology. At neuronal presynapses, mitochondria may alter synaptic activity by anchoring to or simply passing by the presynapse structure (reviewed in: Devine and Kittler, 2018; Wan et al., 2012).

Conversely, presynaptic- Ca^{2+} influx may be taken up by axonal mitochondria in transit, which slows the mitochondria (Chang et al., 2011). This purposeful localization may be beneficial to support a spatially variable metabolic demand and ATP production.

In hair cells, mitochondrial- Ca^{2+} uptake has been shown in association with stereocilia bundle deflection, but its role is unclear in presynaptic Ca^{2+} activity. In auditory outer hair cells, mitochondria distinctly pack the space at the base of the hair bundle, near the site of mechanotransduction (Beurg et al., 2010; Fettiplace and Nam, 2019; Weaver and Schweitzer, 1994). There, mitochondrial- Ca^{2+} uptake, plasma membrane Ca^{2+} ATPase (PMCA) pump and Na^+ - Ca^{2+} exchanger (NCX) are thought to contribute to Ca^{2+} clearance from the hair bundle (Beurg et al., 2010; Boyer et al., 2001; Yamoah et al., 1998). In zebrafish hair cells, mitochondria also take up Ca^{2+} during hair cell activation (Pickett et al., 2018). Mitochondria also are distributed around the synaptic region of hair cells (Bullen et al., 2015). However, the contribution of mitochondrial- Ca^{2+} uptake to presynaptic- Ca^{2+} clearance or activity is unclear (Frank et al., 2009; Kennedy, 2002).

While modest mitochondrial- Ca^{2+} uptake occurs as a part of normal cell physiology, high levels of mitochondrial- Ca^{2+} uptake is cytotoxic (reviewed in: Orrenius et al., 2003; Szabo and Zoratti, 2014). In many instances, mitochondrial dysfunction and Ca^{2+} overload lead to cell death (Baumgartner et al., 2009; Giorgi et al., 2012; Kakkar and Singh, 2007; Peng and Jou, 2010). This has been shown in many cell types, including hair cells (Adam-

Vizi and Starkov, 2010; Jensen-Smith et al., 2012; Luongo et al., 2017; Owens et al., 2007). Mitochondrial- Ca^{2+} overload increases ROS production in the cell and triggers the assembly of a permeability transition pore (mPTP) composed of mitochondrial proteins such as VDAC (reviewed in: Giorgi et al., 2012; Nicholls, 2005; Pinton et al., 2008; Stowe and Camara, 2009). While transitory opening of mPTP may assist in the maintenance of the IMM potential and mitochondrial- Ca^{2+} homeostasis, permanent opening of mPTP leads to pro-apoptotic mitochondrial proteins leaking into the cytosol (Crompton, 1999). High levels of ROS can aid in mPTP formation and trigger other apoptotic pathways such as c-Jun N-terminal kinases (JNKs) signaling (Clerici et al., 1995; García-Berrocal et al., 2007; Shen and Liu, 2006; Tajeddine, 2016). Ultimately, mitochondrial- Ca^{2+} overload and mPTP opening triggers cell death.

In mammalian models of acquired hearing loss, such as that induced by noise overexposure or ototoxic drugs, mitochondrial- Ca^{2+} overload reliably precedes hair cell death. Mitochondrial- Ca^{2+} overload has been studied after ototoxic antibiotic aminoglycoside exposure (Jackson et al., 2013; Poulikakos and Falagas, 2013). In zebrafish hair cells, robust mitochondrial ultrastructural changes and Ca^{2+} uptake have been shown immediately prior to aminoglycoside-induced cell death (Esterberg et al., 2014, 2016; Owens et al., 2007). Furthermore, blocking MCU reduced aminoglycoside-induced hair cell death (Esterberg et al., 2014). Higher hair cell metabolism also is correlated with vulnerability to aminoglycoside-induced cell death (Jensen-Smith et al., 2012; Pickett et al., 2018). This may be due to mitochondrial-DNA damage from excessive ROS exposure acting synergistically with aminoglycoside-induced disruption of mitochondrial protein synthesis (Hamasaki and Rando, 1997; Hobbie et al., 2008; Huth et al., 2015; Xing et al., 2007; Zhao et al., 2004, 2005).

In the mammalian cochlea, pharmacological and genetic block of cytosolic- and mitochondrial- Ca^{2+} uptake can both protect hair cells from noise damage (Heinrich et al., 1999; Shen et al., 2007; Wang et al., 2019). Similar to aminoglycoside exposure, ROS also are generated at higher levels in the cochlea during noise exposure (Ohinata et al., 2000; Yamane et al., 1995). The subsequent hair-cell death and the decrease in auditory-sensitivity threshold can both be partially rescued by application of antioxidants prior to or shortly after noise exposure (reviewed in: Oishi and Schacht, 2011). These studies implicate mitochondrial- Ca^{2+} uptake with concurrent ROS overproduction as a causal factor of noise-induced hair-cell death and hearing loss. Overall, mitochondrial- Ca^{2+} uptake is a part of, and may be required for hair-cell death, making it a potential therapeutic target for hearing-loss prevention.

Recent studies have revealed that a more subtle form of noise-induced hearing deficit (Liberman and Dodds, 1984; Lindquist et al., 1954). This deficit is reflected in decreases in auditory-neural-response amplitude as decreases in the amplitude of wave I auditory brain stem (ABR) responses (Kujawa and Liberman, 2009). Correspondingly, rodents with noise exposure and reduced ABR wave I amplitude and humans post-mortem ears can show auditory inner hair cells with altered morphology and loss of synapses, as well as swelling of innervating afferent nerve terminal at surviving synapses (Kujawa and Liberman, 2009; Makary et al., 2011; Robertson, 1983; Spoendlin, 1971; Valero et al., 2017). These functional and morphological pathologies define a form of hearing loss known as “synaptopathy” (Kujawa and Liberman, 2009). In addition to loss of synapses in auditory hair cells, some studies show that, ribbon size distribution is expanded after noise exposure (Jensen et al., 2015; Kujawa and Liberman, 2009; Liberman and Liberman, 2015; Song et al., 2016). Postsynaptically, the afferent postsynaptic boutons also are enlarged, likely as a result of Ca^{2+} overload and excitotoxicity (Puel et al., 1994; Pujol et al., 1985; Sebe et al., 2017). However,

it is not clear how ribbons in auditory hair cells dynamically restructure during or after acoustic overexposure. More work is needed to interpret the significance of changes in ribbon morphology, and whether these changes compensate for, or contribute to the functional deficits.

Zebrafish posterior lateral line

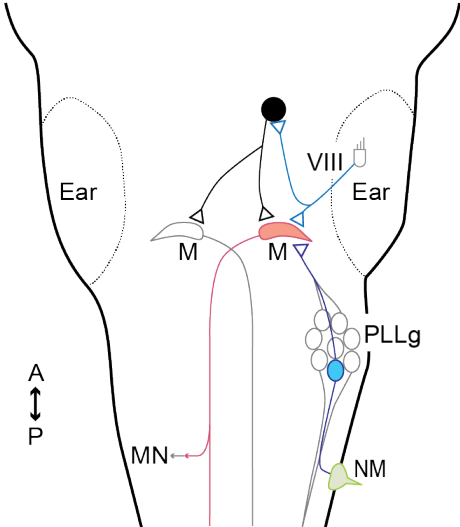
Studying hair cell function and mitochondrial Ca^{2+} *in vivo* is difficult in mammals. The sensory organs of the mammalian inner ear are difficult to access, as they are encased within the temporal bone of the skull. Therefore, live mammalian hair cells are studied in *ex vivo* organ explants (Lim et al., 2011; Nordemar, 1983; Russell and Richardson, 1987; Sobkowicz et al., 1975, 1982, 1993). Zebrafish larvae, on the other hand, are transparent, enabling *in vivo* imaging of cellular morphology and function. This feature has made zebrafish a valuable system to study hearing and balance and sensory hair cells.

Overall, the form, function and development of hair cells are well conserved across vertebrates such as zebrafish and mammals (Nicolson, 2005, 2017; Raible and Kruse, 2000; Whitfield et al., 2002). Genetic studies have also demonstrated that many of the same molecules are required for hearing and hair cells in zebrafish and mammals (Nicolson, 2005, 2017; Whitfield et al., 2002). Zebrafish are also amenable to other genetic manipulation through the creation of transgenic lines expressing bio-sensing fluorescent proteins (Kwan et al., 2007). These transgenic lines, combined with the optical transparency of zebrafish larvae, make zebrafish an ideal system for physiologically-intact imaging (Amsterdam et al., 1995). Intact imaging can be used for *in vivo* observation of biomolecules, such as Ca^{2+} , to examine the

functional properties of the mitochondria, endoplasmic reticulum, cytosol, and presynapse at rest, during activity and during perturbations.

In transparent zebrafish, hair cells can be observed *in vivo* in the inner ear, as well as in an additional sensory organ called the lateral line. The lateral line system detects water movement associated with other shoaling or schooling members or predation (Coombs and Montgomery, 1999; McHenry et al., 2009; Montgomery et al., 2003). This sensory system is composed of small sensory epithelia, called neuromasts, embedded just beneath the skin of fish (reviewed in: Chitnis et al., 2012). Neuromasts of the posterior lateral line (PLL) are innervated by multiple afferent PLL neurons (Dow et al., 2018), which projects their axons to the hindbrain, where they extend along all rhombomeres (Metcalf et al., 1985). The afferent PLL neurons notably innervate the ipsilateral of the two Mauthner neurons within in the fourth rhombomere of the hindbrain (Figure 1.6; Metcalfe et al., 1985, 1986). In teleosts, Mauthner neurons also receives other sensory input such as from hair cells in the anterior lateral line and ears, as well as inhibitory interneurons that were shown to be activated by auditory stimuli (Marti et al., 2008; Mirjany and Faber, 2011; Szabo et al., 2006, 2007). The Mauthner cell makes synaptic connections with the contralateral motor neurons along the spinal cord (Eaton et al., 1977a, 1977b). Activation of the Mauthner neuron, triggered by abrupt sensory stimuli, is a component in the fast escape behavior (Eaton and Farley, 1975; Eaton et al., 2001; Nissanov et al., 1990).

Figure 1.6 Zebrafish lateral line afferent pathway for escape behavior



Posterior lateral line (PLL) neuromasts (NM, green) are innervated by multiple afferent PLL neurons. An example neuron is drawn in blue. The ganglion of the PLL neurons (PLLg) are located in the cranium posterior to the ear, and project their axons to the hindbrain to innervate the ipsilateral Mauthner neuron (pink). The Mauthner neurons also receives sensory input from hair cells in the ears through the cranial nerve VIII (VIII, light blue). The Mauthner cell project its axon to the contralateral spinal cord and make synaptic connections with the contralateral motor neurons (MN) along the spinal cord. Auditory stimuli were also shown to activate inhibitory interneurons (filled black) that innervate both ipsilateral and contralateral (gray outline) Mauthner cells.

In the lateral line, each neuromast is made up of a cluster of hair cells. A gelatinous cupula encases the apical hair bundles of each neuromast, separating them from the external aquatic environment. Water movement deflects the cupula atop the neuromast, and this movement is transferred to the hair bundles within. Because the neuromast is superficially located and relatively exposed, they are particularly amenable to *in vivo* pharmacology, stimulation and visualization.

Unlike mammals, zebrafish embryos do not develop in utero, which enables direct observation of hair cell development *in vivo*. During development, the lateral line system is derived from migrating primordia. The primary PLL is derived from a primordium, primI, that migrates down the trunk of the fish and deposits a trail of posterior lateral line neuromasts along the body (reviewed in: Ghysen and Dambly-Chaudiere, 2007). The nascent PLL ganglion neurons concurrently form growth cones, which are towed by the migrating primI to innervate the deposited neuromast (Gilmour et al., 2004; Metcalfe, 1985). PrimI begins migration at around 1 dpf, depositing neuromasts and a trail of dormant neuromast progenitors until it reaches the end of the trunk by around 2 dpf (Kimmel et al., 1995). After proto-neuromasts are deposited, hair cells begin to form.

Within developing neuromasts, hair cells form in pairs from mitosis of precursor cells residing in the neuromast. In each subsequent day post-fertilization, neuromasts add 2 to 6 hair cells per day with declining frequency. Following mitosis, hair cells precursors quickly develop the structure to support mechanotransduction and synaptic function in 12 to 18 hr (Dow et al., 2015). During this time window, each lateral line hair cell ultimately forms 2-4 ribbon synapses (Sheets et al., 2017; Suli et al., 2016). In larvae between 2 to 3 dpf, all neuromast hair cells are newly differentiated, but by 5-6 dpf, the majority of hair cells are mature and the lateral line system is functional (Kindt et al., 2012; McHenry et al., 2009;

Metcalf, 1985; Murakami et al., 2003; Santos et al., 2006). Overall, this rapid *in vivo* development makes zebrafish an amenable model for the study of ribbon synapse formation in hair cells.

In the following chapters, I outline my work describing the relationship between mitochondrial Ca^{2+} and ribbon synapse function and development in zebrafish hair cells. In Chapter 2, I present work where I characterized evoked-mitochondrial- Ca^{2+} influx in the mature hair cells. Further, I discuss how mitochondrial- Ca^{2+} uptake in mature hair cells may affect ribbon synapse function and stability. In Chapter 3, I describe work where I characterized spontaneous presynaptic and mitochondrial- Ca^{2+} influx in developing hair cells. I outline mechanistically how this spontaneous activity is important for ribbon size determination. In Chapter 4, I discuss the main conclusions of my work, as well as future studies that could answer some outstanding questions. In particular, I relate the findings of my thesis work on the mitochondria to preliminary work on the endoplasmic reticulum. Overall this body of work seeks to outline the framework of current and future work on mitochondrial Ca^{2+} in hair cell synapse development and function.

Chapter 2: Synaptic mitochondria are critical for hair-cell synapse function and integrity

Hin-tung C. Wong^{1,2}, Qinxiang Zhang¹, Alisha J. Beir¹, Ronald S. Petralia³, Ya-Xian Wang³, and Katie S. Kind¹

Affiliations

¹Section on Sensory Cell Development and Function, NIDCD/National Institutes of Health, Bethesda, MD 20892 USA

²National Institutes of Health-Johns Hopkins University Graduate Partnership Program, NIDCD/National Institutes of Health, Bethesda, MD 20892 USA

³Advanced Imaging Core, NIDCD/National Institutes of Health, Bethesda, MD 20892, USA

Work presented in Chapter 2 was published in eLife, volume 8, 2019, page e48914. DOI: 10.7554/eLife.48914. Licensed under Creative Commons Attribution (CC BY 4.0).

Abstract

The auditory and vestibular hair cell ribbon synapse is a specialized synapse that provides indefatigable release of neurotransmitter. Hair cell neurotransmission relies on voltage-gated influx of Ca^{2+} through presynaptic $\text{Ca}_v1.3$ channels. At the presynapse, increases in Ca^{2+} at presynaptic ribbons are critical for neurotransmission. Tight spatial regulation of presynaptic Ca^{2+} is thought to be important for ribbon-synapse function. Previous studies have shown that ER- Ca^{2+} stores can impact hair-cell neurotransmission, but whether mitochondrial- Ca^{2+} stores play a role at this synapse remains unclear. We show that in mature hair cells, presynaptic- Ca^{2+} influx is evoked through $\text{Ca}_v1.3$ channels to initiate mitochondrial- Ca^{2+} uptake adjacent to ribbons. Block of mitochondrial- Ca^{2+} uptake in mature cells depresses presynaptic activity and can impact synapse integrity. Our results present a mechanism where presynaptic- and mitochondrial- Ca^{2+} couple for proper presynaptic function.

Introduction

Neurotransmission is an energy demanding process that relies heavily on mitochondria. In neurons, mitochondrial dysfunction has been implicated in synaptopathies that impact neurodevelopment, learning and memory, and can contribute to neurodegeneration (Flippo and Strack, 2017; Lepeta et al., 2016; Todorova and Blokland, 2017). In hair cells, sensory neurotransmission relies on specialized ribbon synapses to facilitate rapid and sustained vesicle release that is particularly energy demanding (reviewed in: Johnson et al., 2019; Lagnado and Schmitz, 2015; Matthews and Fuchs, 2010; Safieddine et al., 2012). Although mitochondrial dysfunction has been implicated in hearing loss (Böttger and Schacht, 2013; Fischel-Ghodsian et al., 2004; Kokotas et al., 2007), the precise role mitochondria play in hair-cell neurotransmission remains unclear.

Ribbon synapses are characterized by a unique presynaptic structure called a “ribbon” that tethers and stabilizes synaptic vesicles at the active zone (reviewed in: Matthews and Fuchs, 2010). In hair cells, neurotransmission at ribbon synapses requires the presynaptic- Ca^{2+} channel Cav1.3 (Brandt et al., 2003; Kollmar et al., 1997; Sidi, 2004). Hair-cell depolarization opens Cav1.3 channels, resulting in a spatially restricted increase in Ca^{2+} at presynaptic ribbons that triggers vesicle fusion. Tight spatial regulation of presynaptic Ca^{2+} is important for ribbon-synapse function and requires efficient Ca^{2+} clearance through a combination of Ca^{2+} pumps, Ca^{2+} buffers and intracellular- Ca^{2+} stores (Carafoli, 2011; Mulkey and Malenka, 1992; Tucker and Fettiplace, 1995; Yamoah et al., 1998; Zenisek and Matthews, 2000). While ER- Ca^{2+} stores have been implicated in hair-cell neurotransmission,

whether mitochondrial- Ca^{2+} stores play a role in this process remains unclear (Castellano-Muñoz and Ricci, 2014; Kennedy, 2002; Lioudyno et al., 2004; Tucker and Fettiplace, 1995).

To study the impact of mitochondrial- Ca^{2+} on ribbon synapse function, we examined hair cells in the lateral-line system of larval zebrafish. Within the lateral-line, hair cells are arranged in clusters called neuromasts. This system is advantageous for our studies because it contains hair cells with easy access for *in vivo* pharmacology, mechanical stimulation and imaging cellular morphology and function. For example, previous work has shown that GECIs can be used in lateral line hair cells to measure both evoked presynaptic and mitochondria- Ca^{2+} signals (Pickett et al., 2018; Zhang et al., 2018). By 5-6 dpf (days post-fertilization), the majority of hair cells and synapses are mature, and the system is functional (Kindt et al., 2012; McHenry et al., 2009; Metcalfe, 1985; Murakami et al., 2003; Santos et al., 2006). Thus, these hair cells can be used to study evoked presynaptic- and mitochondrial- Ca^{2+} uptake in hair cells.

Using this sensory system, we find that evoked presynaptic- Ca^{2+} influx drives mitochondrial- Ca^{2+} uptake. In mature hair cells, mitochondrial- Ca^{2+} uptake initiates near the presynapse. Short-term, partial block of mitochondrial- Ca^{2+} uptake impairs sustained presynaptic function. Long-term block of mitochondrial- Ca^{2+} uptake lead to a loss of synapse integrity. Overall our results suggest that in hair cells presynaptic- Ca^{2+} influx and mitochondrial- Ca^{2+} uptake couple to impact synapse function and integrity.

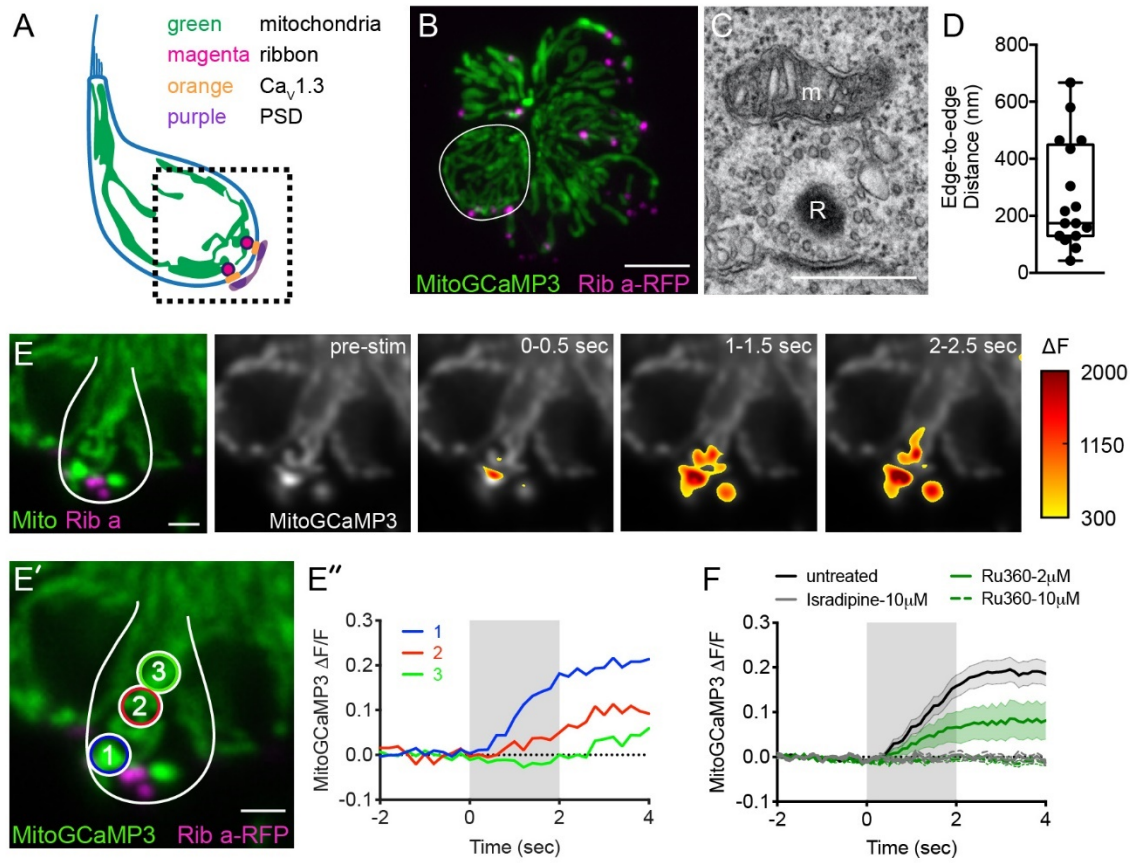
Results

Mitochondria are located near presynaptic ribbons

In neurons, synaptic mitochondria have been shown to influence synapse size, plasticity and function (Flippo and Strack, 2017; Todorova and Blokland, 2017). Based on this work, we hypothesized that mitochondria may impact synapses in hair cells. Therefore, we examined the proximity of mitochondria relative to presynaptic ribbons in zebrafish lateral-line hair cells. We visualized mitochondria and ribbons using transmission electron microscopy (TEM) and in live hair cells using Airyscan confocal microscopy.

Using TEM, we examined sections that clearly captured ribbons (Example, Figure 2.1C). Near the majority of ribbons (81 %) we observed a mitochondrion in close proximity ($< 1 \mu\text{m}$) (Figure 2.1D, median ribbon-to-mitochondria distance = 174 nm, $n = 17$ out of 21 ribbons). To obtain a more comprehensive understanding of the 3D morphology and location of mitochondria relative to ribbons in live cells, we used Airyscan confocal microscopy. To visualize these structures in living cells, we used transgenic zebrafish expressing MitoGCaMP3 (Esterberg et al., 2014) and Ribeye a-tagRFP (Sheets et al., 2014) in hair cells to visualize mitochondria and ribbons respectively. Using this approach, we observed tubular networks of mitochondria extending from apex to base of each hair cell (Figure 2.1A-B, E-E', Figure 2.2A). At the base of the hair cell, we observed ribbons nestled between branches of mitochondria. Overall our TEM and Airyscan imaging suggests that in lateral-line hair cells, mitochondria are present near ribbons.

Figure 2.1. Mitochondrial- Ca^{2+} uptake initiates adjacent to ribbons.



A, Cartoon illustration of a lateral-line hair cell containing: an apical mechanosensory bundle (blue), mitochondria (green), presynaptic ribbons (magenta), $Ca_v1.3$ channels (orange) and postsynaptic densities (purple). B, Airyscan confocal image of 6 live hair cells (1 cell outlined in white) expressing MitoGCaMP3 (mitochondria) and Ribeye a-tagRFP (ribbons) in a developing neuromast at 2 dpf. Also see Figure 2.2. C, A representative TEM showing a mitochondrion (m) in close proximity to a ribbon (R) at 4 dpf. D, Quantification of mitochondrion to ribbon distance in TEM sections ($n = 17$ ribbons). E, Side-view of a hair cell (outlined in white) shows the spatio-temporal dynamics of evoked mitochondrial- Ca^{2+} signals during a 2-s stimulation at 6 dpf. The change in MitoGCaMP3 signal (ΔF) from baseline is indicated by the heatmap and are overlaid onto the pre-stimulus grayscale image. E'-E'', Circles 1-3 (1.3 μm diameter) denote regions used to generate the normalized ($\Delta F/F_0$) temporal traces of mitochondrial- Ca^{2+} signals in E'': adjacent to the presynapse ("1"), and midbody ("2" and "3") in the same cell as E. F, Average evoked mitochondrial- Ca^{2+} response before (solid black) and after 30-min treatment with 10 μM Ru360 (dashed green), 2 μM Ru360 (solid green), or 10 μM isradipine (gray) (3-5 dpf, $n \geq 9$ cells per treatment). Error bars in D are min and max; in F the shaded area denotes SEM. Scale bar = 500 nm in C, 5 μm in B and 2 μm in E and E'.

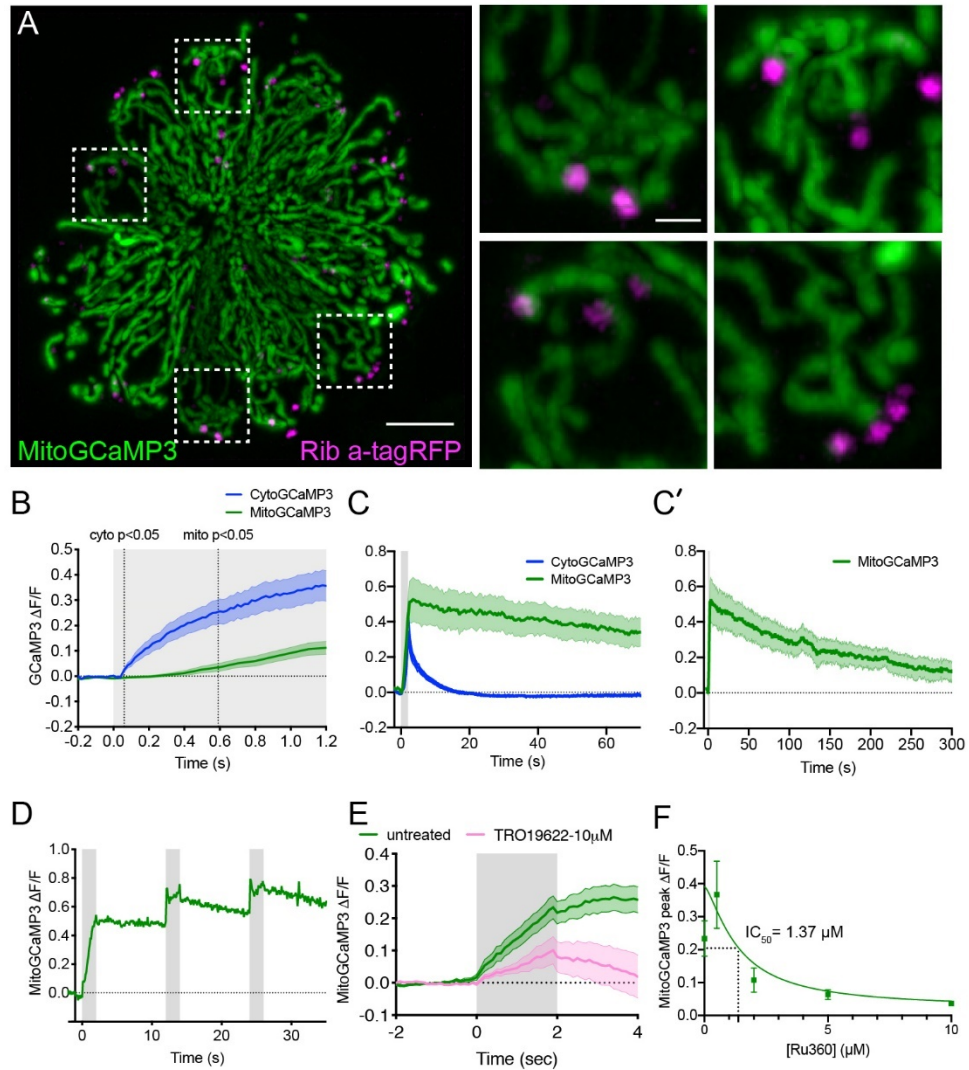
Mitochondrial-Ca²⁺ uptake at ribbons is MCU and Cav1.3 dependent

In zebrafish hair cells, robust rises in mitochondrial-Ca²⁺ have been reported during mechanical stimulation (Pickett et al., 2018). Due to the proximity of the mitochondria to the ribbon, we predicted that rises in mitochondrial-Ca²⁺ levels during mechanical stimulation could be related to presynapse-associated rises in Ca²⁺.

To test this prediction, we used a fluid-jet to mechanically stimulate hair cells and evoke presynaptic activity. During stimulation, we used MitoGCaMP3 to monitor mitochondrial-Ca²⁺ in lateral-line hair cells. As previously reported, we observed robust mitochondrial-Ca²⁺ uptake during stimulation (Figure 2.1E-F, Figure 2.3A-A’). We examined the subcellular distribution of MitoGCaMP3 signals over time and observed an increase in MitoGCaMP3 (ΔF) signals that initiated near ribbons (Figure 2.1E, ΔF). During the latter part of the stimulus, and even after the stimulus terminated, the MitoGCaMP3 signals propagated apically, away from the ribbons (Example, Figure 2.1E’-E’’, regions 1-3, $\Delta F/F_0$). We characterized the time-course of MitoGCaMP3 signals with regards to onset kinetics and return to baseline. During a 2-s stimulus, we detected a significant rise in MitoGCaMP3 signals 0.6 s after stimulus onset (Figure 2.2B, $\Delta F/F_0$). Interestingly, after the stimulus terminated, MitoGCaMP3 levels took approximately 5 min to return to baseline (Figure 2.2C-C’, $\Delta F/F_0$). Despite this long time-course of recovery to baseline, we were still able to evoke additional rises in MitoGCaMP3 signal 10 s after stimulation (Figure 2.2D, $\Delta F/F_0$). As previously reported, the kinetics of MitoGCaMP3 signals in hair-cell mitochondria were quite different from signals observed using cytosolic GCaMP3 (CytoGCaMP3) in hair cells (Pickett et al., 2018). Compared to MitoGCaMP3 signals, CytoGCaMP3 signals had faster onset kinetics and a faster return to baseline (Figure 2.2B-C,

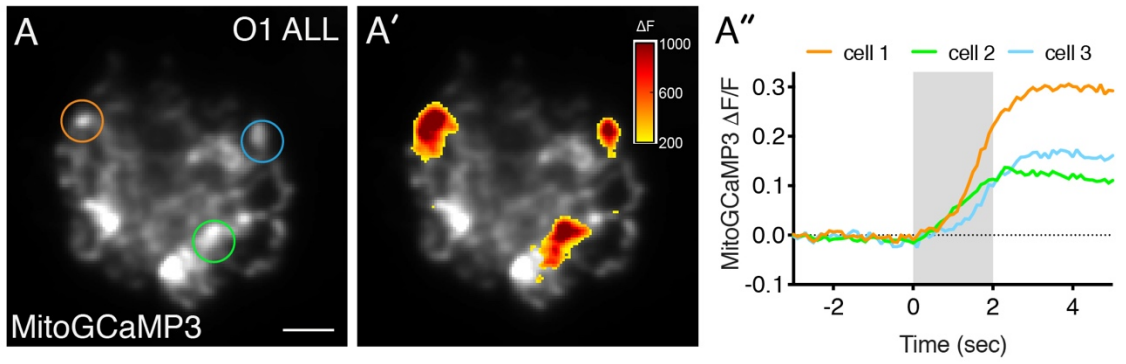
time to rise: 0.06 s, post-stimulus return-to-baseline: 12 s). These differences in kinetics indicate that mitochondrial- Ca^{2+} loading operates over slower timescales compared to the cytosolic compartment. It also confirms that hair-cell stimulation can initiate long lasting increases in mitochondrial- Ca^{2+} .

Figure 2.2. The time course of mechanically-evoked mitochondrial- Ca^{2+} signals are longer-lasting than cytosolic- Ca^{2+} signals and is additive.



A, Airyscan confocal image of a live neuromast expressing MitoGCaMP3 (mitochondria) and Ribeye a-tagRFP (ribbons) at 6 dpf. Insets show the base of 4 individual hair cells from the neuromast in A (dashed white boxes). B, Average cytosolic-Ca²⁺ (blue) and mitochondrial-Ca²⁺ (green) $\Delta F/F$ GCaMP3 signals during the onset of a 2-s stimulus. Mitochondrial-Ca²⁺ signals rise with a delay compared to cytosolic-Ca²⁺ signals, 3-6 dpf, n \geq 18 cells. C-C', Average cytosolic-Ca²⁺ and mitochondrial-Ca²⁺ $\Delta F/F$ GCaMP3 signals during and after a 2-s stimulation shows that cytosolic-Ca²⁺ signals return to baseline shortly after stimulation (C), while mitochondrial-Ca²⁺ remains elevated up to 5 min after stimulation (C-C'), 3-6 dpf, n \geq 7 cells. D, A series of 3, evoked 2-s stimuli initiated at: t = 0-2, 12-14 and 24-26 s. A rise in MitoGCaMP3 can be detected during each stimulus, prior to MitoGCaMP3 signals returning to baseline. E, 10 μ M of the VDAC inhibitor TRO 19622 partially blocks evoked MitoGCaMP3 signals, 5 dpf, n = 15 cells. F, A dose response curve indicates that Ru360 blocks evoked MitoGCaMP3 signals with an IC₅₀ value of 1.37 μ M at 5 dpf, n \geq 9 cells per dose. Error in panel B-C', E and F represent SEM. Scale bar = 5 μ m in A and 2 μ m in inset.

Figure 2.3. Mitochondrial- Ca^{2+} uptake occurs in anterior lateral-line hair cells.



A, A live Image of an anterior-lateral line (ALL) neuromast viewed top-down, expressing the mitochondrial- Ca^{2+} sensor MitoGCaMP3 at 5 dpf. A' shows the spatio-temporal dynamics of evoked mitochondrial- Ca^{2+} signals during a 2-s stimulation. The MitoGCaMP3 signals during the stimulation (ΔF) are indicated by the heatmap overlaid onto the baseline grayscale image. A'', Temporal traces of evoked mitochondrial- Ca^{2+} signals were generated from 3 regions denoted by 3 circles in A. Scale bar = 5 μm in A.

To verify that MitoGCaMP3 signals reflect Ca^{2+} entry into mitochondria, we applied Ru360, an antagonist of the mitochondrial- Ca^{2+} uniporter (MCU). The MCU is the main pathway for rapid Ca^{2+} entry into the mitochondrial matrix (Matlib et al., 1998). We found that stimulus-evoked MitoGCaMP3 signals were blocked in a dose-dependent manner after a 30-min treatment with Ru360 (Figure 2.1F, Figure 2.2F; $\text{IC}_{50} = 1.37 \mu\text{M}$). We confirmed these results by applying TRO 19622, an antagonist of the voltage-dependent anion channel (VDAC). VDAC enables transport of ions including Ca^{2+} across the outer mitochondrial membrane (Figure 1.5; Schein et al., 1976; Shoshan-Barmatz and Gincel, 2003). We observed that similar to the MCU antagonist Ru360, a 30-min treatment with the VDAC antagonist TRO 19622 also impaired stimulus-evoked MitoGCaMP3 signals (10 μM TRO 19622, Figure 2.2E). Due to the initiation of mitochondrial- Ca^{2+} near ribbons, we examined whether $\text{Ca}_v1.3$ -dependent presynaptic- Ca^{2+} influx was the main source of Ca^{2+} entering the mitochondria. To examine $\text{Ca}_v1.3$ channel contribution to mitochondrial- Ca^{2+} uptake, we applied isradipine, a $\text{Ca}_v1.3$ channel antagonist. Similar to blocking the MCU and VDAC, blocking $\text{Ca}_v1.3$ channels eliminated all stimulus-evoked MitoGCaMP3 signals at the base of the cell (Figure 2.1F).

Previous work in zebrafish-hair cells demonstrated that isradipine specifically blocks $\text{Ca}_v1.3$ channels without impairing mechanotransduction (Zhang et al., 2018). For our current study we confirmed that Ru360 and TRO 19622 specifically impaired synaptic mitochondrial- Ca^{2+} uptake without altering mechanotransduction. We measured apical, mechanically-evoked Ca^{2+} signals in hair bundles before and after a 30-min treatment with 10 μM Ru360 or TRO 19622. Neither compound blocked mechanotransduction evoked Ca^{2+} influx (Figure 2.5A-B'). Overall, our MitoGCaMP3 functional imaging indicates that in hair

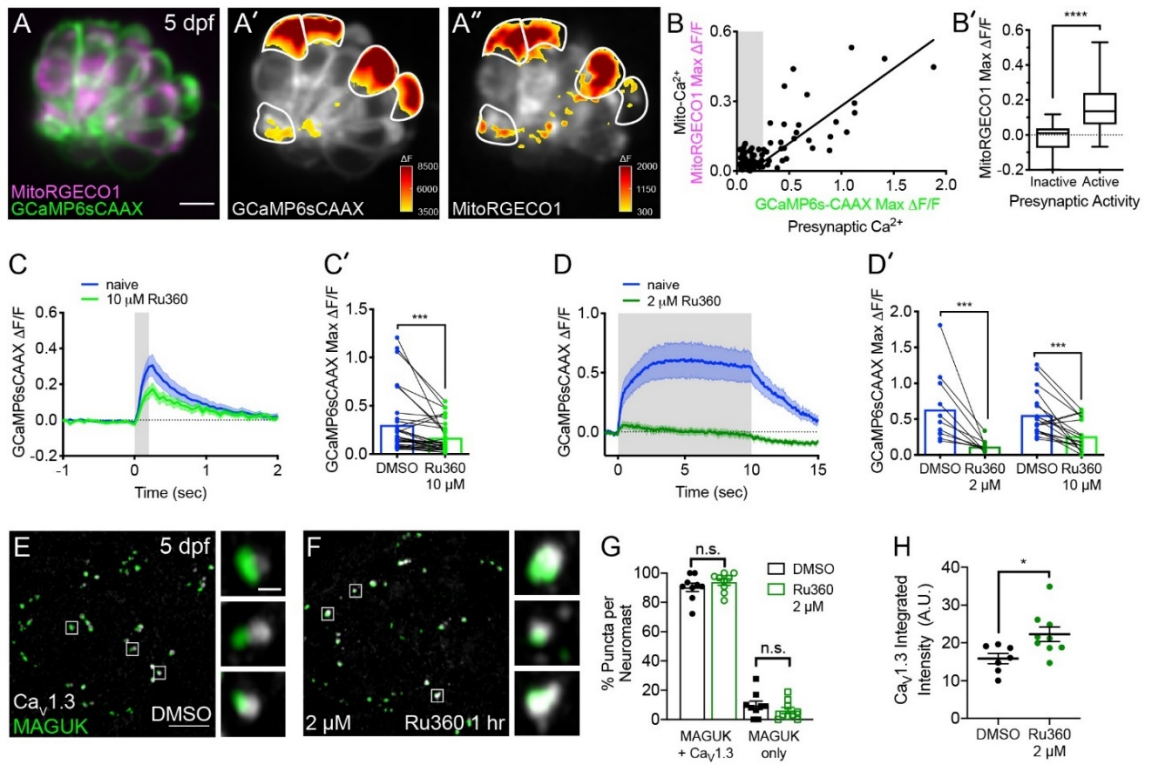
cells, evoked mitochondrial- Ca^{2+} uptake initiates near ribbons and this uptake is dependent on MCU, VDAC and $\text{Ca}_v1.3$ channel function.

Mitochondrial- Ca^{2+} uptake occurs in cells with presynaptic- Ca^{2+} influx

Interestingly, we observed that mitochondrial- Ca^{2+} uptake was only present in ~40 % of cells (Examples, Figure 2.4A' and Figure 2.3A-A''; n = 10 neuromasts, 146 cells). This observation is consistent with previous work demonstrating that only ~30 % of hair cells within each neuromast cluster have presynaptic Ca^{2+} signals and are synaptically active (Zhang et al., 2018). Because presynaptic- Ca^{2+} signals initiate near mitochondria, it is probable that mitochondrial- Ca^{2+} uptake occurs only in hair cells with synaptic activity.

To test whether evoked mitochondrial- Ca^{2+} uptake occurred exclusively in cells with presynaptic- Ca^{2+} influx, we performed two-color functional imaging. We used a double transgenic approach that utilized a membrane-localized GCaMP6s (GCaMP6sCAAX; green) to measure presynaptic Ca^{2+} signals at the base of hair cells (Jiang et al., 2017; Sheets et al., 2017), and we concurrently used MitoRGECO1 (red) to examine mitochondrial- Ca^{2+} signals (Figure 2.4A-B'). Our two-color imaging approach revealed a strong correlation between the magnitude of the GCaMP6sCAAX and MitoRGECO1 signals (Figure 2.4B, $R^2 = 0.77$, $p < 0.0001$; n = 136 cells). We found that in presynaptically active hair cells the median MitoRGECO1 signals were 100 % larger than presynaptically silent hair cells (Figure 2.4B'). Together these results suggest that robust mitochondrial- Ca^{2+} uptake occurs specifically in hair cells with evoked presynaptic- Ca^{2+} influx.

Figure 2.4. Mitochondrial- Ca^{2+} uptake can impact presynaptic Ca^{2+} signals.



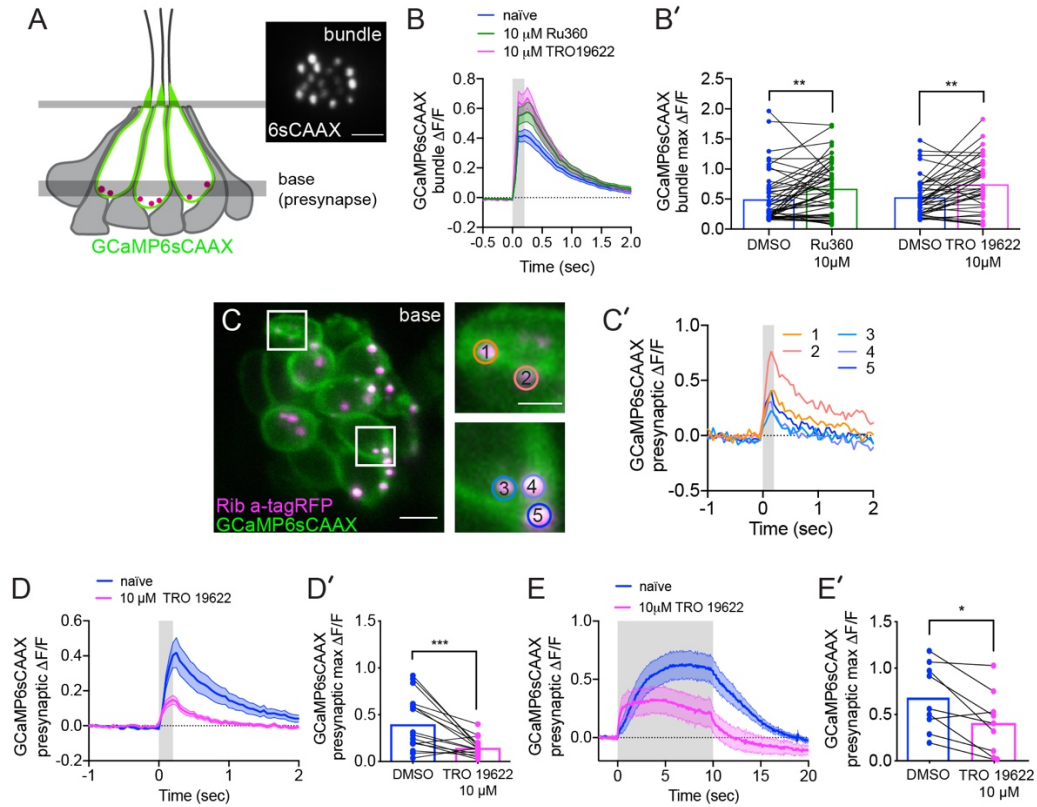
A, A live Image of a neuromast viewed top-down, expressing the presynaptic-Ca²⁺ sensor GCaMP6sCAAX (green) and mitochondrial-Ca²⁺ sensor MitoRGECO1 (magenta) at 5 dpf. A'-A'', GCaMP6sCAAX (A') and MitoRGECO1 (A'') signals (ΔF) from baseline during a 2-s stimulation are indicated by the heatmaps and occur in the same cells (white outline). B, Scatter plot with linear regression of peak presynaptic- and mitochondrial-Ca²⁺ response for individual cells at 4-5 dpf, n = 136 cells. Gray background in graph denotes presynaptic-Ca²⁺ signals below 0.25, a threshold used as a cutoff for presynaptic activity (below inactive, above active). B', Plot of mitochondrial-Ca²⁺ responses segregated based on the activity threshold in B. C-D', Presynaptic-Ca²⁺ response (example in Figure 2.5C-C') averaged per cell before (blue) and after a 30-min treatment with 10 μ M Ru360 (light green) or 2 μ M Ru360 (dark green), n \geq 10 cells per treatment. C and D show averaged traces while C' and D' show before-and-after dot plots of the peak response per cell. E-F, Representative images of mature neuromasts (5 dpf) immunostained with Cav1.3 (white, Ca²⁺ channels) and MAGUK (green, postsynapses) after a 1-hr incubation in 0.1 % DMSO (E) or 2 μ M Ru360 (F). G-H, Scatter plots show percentage of postsynapses that pair with Cav1.3-channel clusters (Cav1.3 + MAGUK) and orphan postsynapses (MAGUK only) (G). The integrated intensity of Cav1.3-channel immunolabel at presynapses is lower in control compared to treatment group (H), n \geq 7 neuromasts per treatment. Whiskers on plots in B' represent min and max; the shaded area in plots C and D and the error bars in C', D' and G-H denotes SEM. Mann-Whitney U test was used in B'; Wilcoxon matched-pairs signed-rank test was used in C' and D'. Welch's unequal variance *t*-test was used in G-H. **p* < 0.05, ****p* < 0.001, *****p* < 0.0001. Scale bar = 5 μ m in A and E.

Blocking mitochondrial-Ca²⁺ entry impairs presynaptic Ca²⁺ signals in mature hair cells

Although we observed mitochondrial-Ca²⁺ uptake specifically in hair cells with active Ca²⁺ channels, the impact of mitochondrial-Ca²⁺ uptake on the function of hair-cell synapses was unclear. Based on previous studies in neurons and bipolar-cell ribbon synapses (Billups and Forsythe, 2002; Chouhan et al., 2010; Kwon et al., 2016; Levy et al., 2003; Zenisek and Matthews, 2000), we reasoned that mitochondria may be important to remove excess Ca²⁺ or to provide ATP for hair-cell neurotransmission.

To determine if mitochondrial-Ca²⁺ uptake impacted presynaptic function, we assayed evoked presynaptic-Ca²⁺ signals by monitoring GCaMP6sCAAX signals adjacent to ribbons as described previously (Sheets et al., 2017; Zhang et al., 2018). We examined GCaMP6sCAAX signals in mature hair cells at 5-6 dpf when neuromast organs are largely mature (Kindt et al., 2012; McHenry et al., 2009; Metcalfe, 1985; Murakami et al., 2003; Santos et al., 2006). Using this approach, we assayed presynaptic GCaMP6sCAAX signals before and after a 30-min application of the MCU antagonist Ru360 (Figure 2.4C-D'). We found that during short, 200-ms stimuli, GCaMP6sCAAX signals at ribbons were reduced after complete MCU block (10 μ M Ru360, Figure 2.4C-C'). Reduction of GCaMP6sCAAX signals were further exacerbated during sustained 10-s stimuli, even when the MCU was only partially blocked (2 μ M Ru360, Figure 2.4D-D'). A similar reduction in GCaMP6sCAAX signals were observed after a 30-min application of the VDAC inhibitor TRO 19622 (Figure 2.5D-E', 10 μ M TRO 19622). These results suggest that in mature hair cells, evoked mitochondrial-Ca²⁺ uptake is critical for presynaptic-Ca²⁺ influx, especially during sustained stimulation.

Figure 2.5. Hair-cell bundle mechanotransduction Ca^{2+} signals and presynaptic Ca^{2+} signals during MCU and VDAC block.



A, Illustration of a neuromast and the imaging planes used to study the mechanotransduction in hair-bundles and the presynaptic-Ca²⁺ influx at ribbons. Localization of the membrane-localized Ca²⁺ sensor GCaMP6sCAAX shown in green. Inset in A shows an example top-down view of GCaMP6sCAAX bundle plane (6sCAAX) at 5 dpf. B-B', Bundle-Ca²⁺ signals before (blue) and after a 30-min treatment with 10 μ M Ru360 (green) or 10 μ M TRO 19622 (magenta), $n \geq 39$ bundles per treatment. Average traces are shown in B while dot plots of the peak response per bundle are shown in B'. C, Double-transgenic hair cells expressing GCaMP6sCAAX (at presynaptic membranes) and Ribeye a-tagRFP (labels ribbons) at 5 dpf. Example cells in presynaptic imaging plane are boxed in white and duplicated in right insets. C', Example cells show evoked presynaptic-Ca²⁺ signals at ribbons during a 0.2-s stimulation. Circles 1-5 (1.3 μ m diameter) in insets in C denote regions at ribbons used to generate the temporal traces of presynaptic-Ca²⁺ signals at each ribbon in C'. Similarly-colored traces of presynaptic-Ca²⁺ signals originate from different presynapses of the same cell. D-E', Presynaptic-Ca²⁺ signals averaged per cell before (blue) and after a 30-min 10 μ M TRO 19622 (magenta), $n \geq 9$ cells per treatment. D and E show averaged traces while D' and E' show before-and-after treatment dot plots of the peak response per cell. Error in panel B-B', D-E' represent SEM. A Wilcoxon matched-pairs signed-rank test was used in B', D' and E'. * $p < 0.05$, ** $p < 0.01$, *** $p < 0.001$. Scale bar = 5 μ m in A and C and 2 μ m in C inset.

Evoked mitochondrial-Ca²⁺ uptake is important for mature synapse integrity and cell health

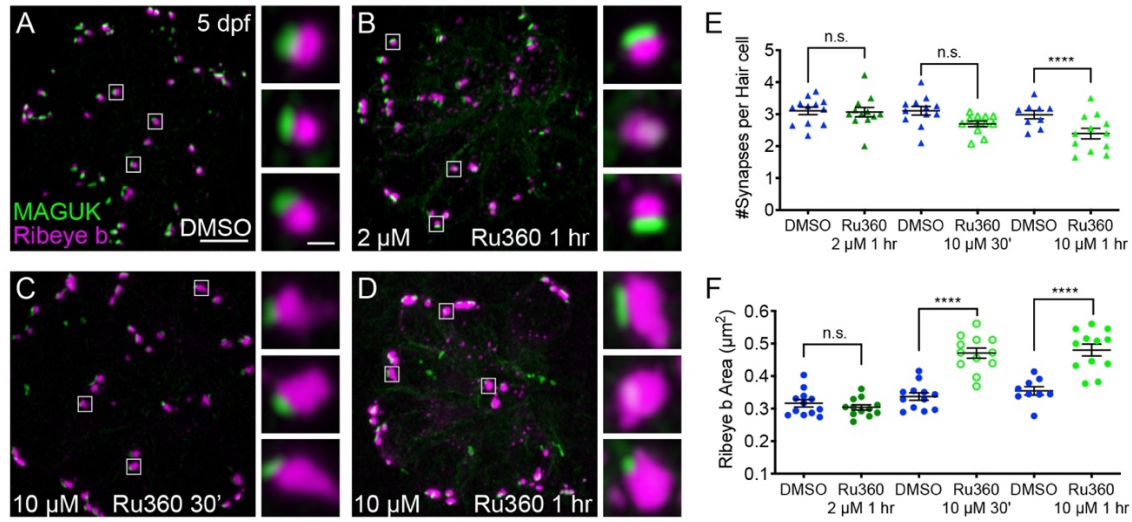
MCU block could impair presynaptic-Ca²⁺ influx through several mechanisms. It could impair the biophysical properties of Cav1.3 channels, for example, through Ca²⁺-dependent inactivation (Platzer et al., 2000; Schnee and Ricci, 2003). MCU block could also impact Cav1.3-channel localization. In addition, mitochondrial-Ca²⁺ has been implicated in synapse dysfunction and cell death (Esterberg et al., 2014; Vos et al., 2010; Wang et al., 2019), and MCU block could be pathological. To distinguish between these possibilities, we assessed whether synaptic components or hair-cell numbers were altered after MCU block with Ru360.

To quantify ribbon-synapse morphology after MCU block, we immunostained mature-hair cells (5 dpf) with Cav1.3, Ribeye b and MAGUK antibodies to label Cav1.3 channels, presynaptic ribbons and postsynaptic densities (MAGUK) respectively. We first applied 2 μM Ru360 for 1 hr, a concentration that partially reduces evoked mitochondrial-Ca²⁺ uptake (See Figure 2.1F) yet is effective at reducing sustained presynaptic-Ca²⁺ influx (See Figure 2.4D-D'). At this dose, Ru360 had no impact on hair cell or synapse number (Figure 2.6E). We also observed no morphological change in ribbon or postsynapse size (Figure 2.6F, Figure 2.7C, Figure 2.8). After the 1-hr 2 μM Ru360 treatment, Cav1.3 clusters were still present at synapses, but the channels were at a significantly higher density compared to controls (Figure 2.4E-H). These findings indicate that in mature hair cells, partial MCU block may impair presynaptic function by increasing Cav1.3 channel density.

We also tested a higher dose of Ru360 (10 μM) that completely blocks evoked mitochondrial-Ca²⁺ uptake (See Figure 2.1F). Interestingly, a 30-min or 1-hr 10 μM Ru360

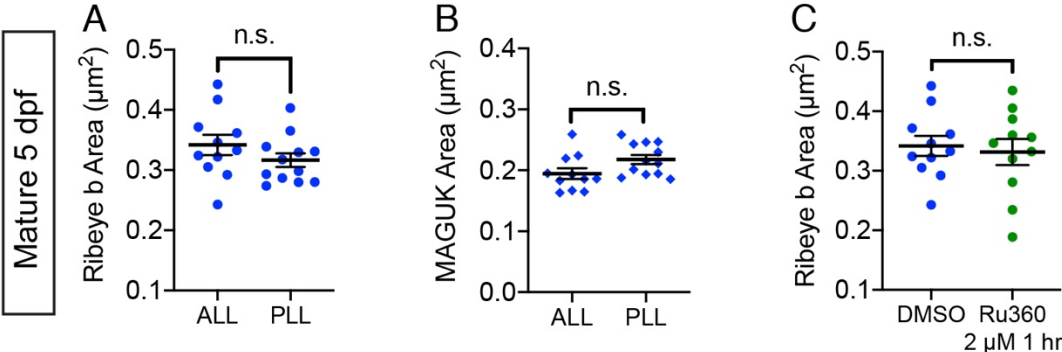
treatment had a progressive impact on synapse and cellular integrity. After a 30-min treatment with 10 μ M Ru360 we did not observe significantly fewer complete synapses per hair cell or fewer hair cells compared to controls (Figure 2.6E; hair cells per neuromast, control: 16.3, 30-min 10 μ M Ru360: 15.5; $p = 0.5$). But after the 30-min treatment, ribbons were significantly larger (Figure 2.6F). The effects of MCU block became more pathological after a 1-hr, 10 μ M Ru360 treatment. After 1-hr, there were both fewer hair cells per neuromast (Hair cells per neuromast, control: 18.1, 1-hr 10 μ M Ru360: 12.0; $p > 0.0001$) and fewer synapses per hair cell (Figure 2.6E). Similar to 30-min treatments with Ru360, after 1 hr, ribbons were also significantly larger (Figure 2.6F). Neither 30-min nor 1-hr 10 μ M Ru360 treatment altered postsynapse size (Figure 2.8). Overall, our results indicate that in mature hair cells, partial block of mitochondrial- Ca^{2+} uptake may impair presynaptic function by altering $\text{Ca}_v1.3$ channel clustering, without seemingly altering other gross pre- or post-synaptic morphology. Complete block of mitochondrial- Ca^{2+} uptake is pathological; it impairs presynaptic function, alters presynaptic morphology, and results in a loss of synapses and hair-cells.

Figure 2.6. Mitochondrial-Ca²⁺ is important for ribbon size and synapse integrity in mature hair cells.



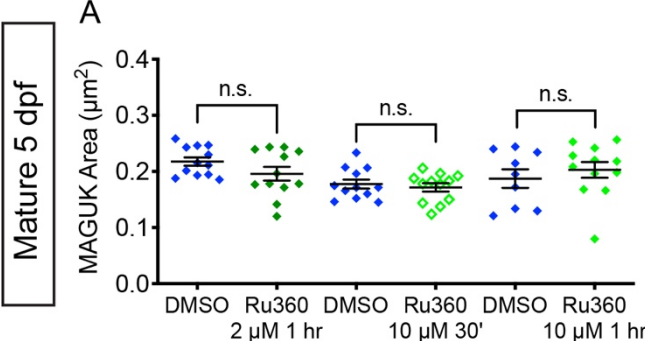
A-D, Representative images of mature neuromasts (5 dpf) immunostained with Ribeye b (magenta, ribbons) and MAGUK (green, postsynapses) after a 1-hr 0.1 % DMSO (A), a 1-hr 2 μ M Ru360 (B), a 30-min 10 μ M Ru360 (C), or a 1-hr 10 μ M Ru360 (D) treatment. Insets show 3 example synapses (white squares). E-F, Scatter plots show synapse counts (E), and ribbon area (F) in controls and in treatment groups. Ribbon areas, synapse numbers, and hair-cell counts are unaffected after a 1-hr 2 μ M Ru360 treatment. Ribbon areas are larger without significant loss of synapses or hair cells after a 30-min treatment with 10 μ M Ru360 (F). After a 1-hr 10 μ M Ru360 treatment there is an increase in ribbon area and a decrease in synapse (E) and hair-cell counts. $N \geq 9$ neuromasts per treatment. Error bars in E-F represent SEM. An unpaired *t*-test was used in E and a Welch's unequal variance *t*-test was used in F. **** $p < 0.0001$. Scale bar = 5 μ m in A, and 2 μ m in inset.

Figure 2.7. Ribbon and postsynapse size in mature ALL neuromasts.



A-B, Scatter plots show that ribbon areas (A) and postsynaptic density areas (B) within the same fish are similar between mature anterior lateral-line (ALL) and posterior lateral-line (PLL) neuromasts. C, Scatter plots show ribbon areas in controls and after a 1-hr treatment with 2 μ M Ru360 are similar in mature hair cells within the ALL. Ribbon sizes of untreated anterior lateral-line hair cells are from the same dataset in A and C, $n \geq 10$ neuromasts per treatment; error bars represent SEM; and a Welch's unequal variance *t*-test was used for comparisons.

Figure 2.8. MCU block does not impact postsynapse size in mature hair cells.



A, Quantification of postsynapse size assayed by MAGUK immunolabel in mature neuromasts indicate the treatments with 2 μ M Ru360 and 10 μ M Ru360 do not significantly alter postsynapse size compared to controls, $n \geq 9$ neuromasts per treatment at 5 dpf. Error bars represent SEM. A Welch's unequal variance *t*-test was used for comparisons.

MCU and Cav1.3 channel activities regulate subcellular Ca²⁺ homeostasis

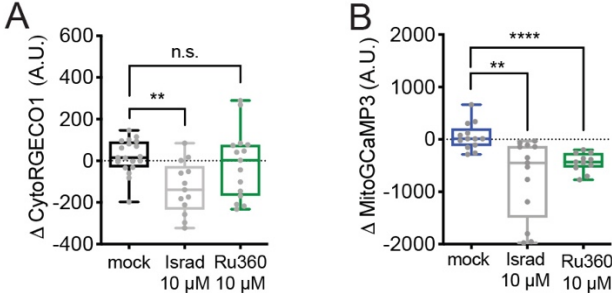
Overall our results indicate that blocking the loading of Ca²⁺ into mitochondria impairs presynaptic-Ca²⁺ influx, leading to a loss of synapse integrity, and can be cytotoxic. But how do the presynaptic- and mitochondrial-Ca²⁺ signals interact to affect synapse function and cell health? One possibility is that mitochondrial-Ca²⁺ uptake disrupts presynaptic-Ca²⁺ influx, synapse structure and cell health by perturbing cytosolic-Ca²⁺ levels.

To examine resting cytosolic-Ca²⁺ levels in hair cells, we examined the fluorescence signal change of the cytosolic-Ca²⁺ indicator RGECO1 (CytoRGECO1) before and after a 30-min pharmacological manipulation of Cav1.3 or MCU channels (Figure 3.7A-C). We observed that treatment with the Cav1.3 channel antagonist isradipine decreased resting CytoRGECO1 fluorescence (Figure 2.9A). However, treatment with MCU blocker Ru360 did not significantly shift resting CytoRGECO1 fluorescence levels (Figure 2.9A). These data suggest that, unlike Cav1.3 channel function, MCU function and associated mitochondrial-Ca²⁺ uptake does not play a critical role in buffering steady state cytosolic-Ca²⁺ levels.

Alternatively, it is possible that rather than impacting cytosolic-Ca²⁺ levels, both Cav1.3 and MCU activity are required to load and maintain Ca²⁺ levels within the mitochondria. In this scenario, mitochondrial-Ca²⁺ levels could be a signal that regulates ribbon size. To test this possibility, we used MitoGCaMP3 to examine resting mitochondrial-Ca²⁺ levels before and after modulating Cav1.3 or MCU channel function (Figure 2.9B). We observed that blocking Cav1.3 channels with isradipine or the MCU with Ru360 decreased resting MitoGCaMP3 fluorescence. Our resting MitoGCaMP3 measurements indicate that the effects of Cav1.3 channel and MCU activity converge to

regulate mitochondrial- Ca^{2+} levels. When either of these channels are blocked, the resting levels of mitochondrial- Ca^{2+} decrease. Therefore, change in mitochondrial- Ca^{2+} levels may be the determining factor in disrupting presynaptic- Ca^{2+} influx, synapse structure and cell health.

Figure 2.9. Cytosolic-Ca²⁺, mitochondrial-Ca²⁺ baseline measurements in mature hair cells.



A, RGECO1 measuring baseline cytosolic-Ca²⁺ before and after a 30-min mock treatment (0.1 % DMSO), or after a 10 μM isradipine, or 10 μM Ru360 treatment. Isradipine decreased cytosolic-Ca²⁺ over the treatment period, but Ru360 did not alter cytosolic-Ca²⁺. B, MitoGCaMP3 measuring baseline mitochondrial-Ca²⁺ before and after a 30-min mock treatment (0.1 % DMSO) or after a 10 μM isradipine, or 10 μM Ru360 treatment. Both isradipine and Ru360 decreased mitochondrial-Ca²⁺ over the treatment period. All plots are box-and-whiskers plot that show median, min and max. N ≥ 9 neuromasts per treatment. All measurements were made in mature hair cells at 5-6 dpf. A one-way Brown-Forsythe ANOVA with Dunnett's T3 post hoc was used to calculate the difference in A-B, ***p* < 0.01, *****p* < 0.0001.

Discussion

In this study, we determined in a physiological setting how mitochondrial- Ca^{2+} influences hair-cell presynapse function. In mature hair cells, evoked $\text{Ca}_v1.3$ -channel- Ca^{2+} influx drives Ca^{2+} into mitochondria. Evoked mitochondrial- Ca^{2+} uptake is important to sustain presynaptic Ca^{2+} responses and maintain synapse integrity. Our study reveals an intriguing mechanism that couples presynaptic activity with mitochondrial- Ca^{2+} to regulate the presynaptic function and stability of a synapse.

Role of evoked mitochondrial- Ca^{2+} uptake in mature hair cells

Sensory hair cells are metabolically demanding cells—both apical mechanotransduction and basal neurotransmission are energy demanding processes (Shin et al., 2007; Spinelli et al., 2012). Therefore, it is likely that hair-cell mitochondria play important roles in both of these functional domains. In mammalian auditory hair cells, mitochondrial- Ca^{2+} uptake has been observed to buffer Ca^{2+} beneath mechanosensory hair bundles (Beurg et al., 2010; Fettiplace and Nam, 2019). Blocking this uptake prolonged evoked Ca^{2+} rises in hair bundles. This work suggested that apical mitochondria, along with the plasma membrane Ca^{2+} -ATPase (PMCA) contribute to cytosolic- Ca^{2+} clearance to maintain optimal mechanotransduction (Beurg et al., 2010). Although the focus of our present study was on the synapse, we also found that blocking mitochondrial- Ca^{2+} uptake using Ru360 (MCU antagonist) or TRO 19622 (VDAC antagonist) increased mechanosensitive Ca^{2+} responses in zebrafish lateral-line hair bundles (Figure 2.5A-B'). In the future it will be extremely interesting to explore the role apical mitochondria play in mechanotransduction.

In the presynaptic region of hair cells, the link between mitochondrial- Ca^{2+} uptake and neurotransmission are less clear. Studies of synapses in various neuronal subtypes have demonstrated that mitochondria play multiple roles to maintain neurotransmission including ATP production, Ca^{2+} buffering and signaling, and neurotransmitter synthesis (reviewed in Kann and Kovács, 2007; Vos et al., 2010). Study of synaptic mitochondria at ribbon synapses in retinal-bipolar cells found that evoked mitochondrial- Ca^{2+} uptake was sporadic and did not significantly contribute to the time course of presynaptic- Ca^{2+} responses or Ca^{2+} clearance (Zenisek and Matthews, 2000). This work concluded that mitochondria may contribute indirectly to Ca^{2+} clearance from the synaptic terminal by providing ATP to fuel the PMCA. In our current study on basal, synaptic mitochondria we found that in mature zebrafish-hair cells, mitochondrial- Ca^{2+} uptake was critical for presynaptic- Ca^{2+} influx. Even partial block of evoked mitochondrial- Ca^{2+} uptake was sufficient to impair presynaptic- Ca^{2+} influx, especially during sustained stimuli (Figure 2.4C-D', Figure 2.5D-E'). Interestingly, our work suggests that mitochondrial- Ca^{2+} uptake may not buffer cytosolic- Ca^{2+} as MCU block did not alter cytosolic- Ca^{2+} levels (Figure 2.9).

Instead our work indicates that mitochondrial- Ca^{2+} may be important to maintain $\text{Ca}_v1.3$ -channel density (Figure 2.4E-H). We found that after partial MCU block, loss of sustained presynaptic- Ca^{2+} responses coincided with an increase in $\text{Ca}_v1.3$ -channel density at the presynapse (Figure 2.4C-H). This result is difficult to interpret as the majority of studies on $\text{Ca}_v1.3$ channels in hair cells focus on activity changes after a decrease or loss of $\text{Ca}_v1.3$ -channel clustering. For example, in Ribeye-depleted zebrafish hair cells $\text{Ca}_v1.3$ channels failed to cluster (Lv et al., 2016). In addition, when ribbons were enlarged in zebrafish-hair cells, $\text{Ca}_v1.3$ -channel density was reduced (Sheets et al., 2017). In these studies, after a loss or reduction of $\text{Ca}_v1.3$ -channel clustering, presynaptic Ca^{2+} signals were increased. Therefore, it

is possible that an increase in $\text{Ca}_v1.3$ -channel density could incur the opposite effect and decrease presynaptic Ca^{2+} responses. An increase in $\text{Ca}_v1.3$ -channel density could enhance Ca^{2+} -dependent inactivation among tightly clustered $\text{Ca}_v1.3$ channels. In hair cells, $\text{Ca}_v1.3$ channels exhibit reduced Ca^{2+} dependent inactivation (Koschak et al., 2001; Platzer et al., 2000; Song et al., 2003; Xu and Lipscombe, 2001). This reduction is thought to be important to transmit sustained sensory stimulation (Kollmar et al., 1997). Alternatively, an increase in $\text{Ca}_v1.3$ -channel density could be a compensatory strategy to boost presynaptic activity after MCU block and impaired presynaptic- Ca^{2+} influx. If channel density is not responsible for impaired presynaptic function, mitochondrial- Ca^{2+} uptake could be critical to produce energy for other cellular tasks to maintain neurotransmission. Additional work is necessary to fully understand how evoked mitochondrial- Ca^{2+} uptake functions to sustain presynaptic- Ca^{2+} influx in mature zebrafish hair cells.

Role of mitochondrial- Ca^{2+} in hair cell death and synapse integrity

In addition to impacting presynaptic function, our work found that in mature hair cells, complete MCU block can be pathological (Figure 2.6E). This pathology has parallels in recent work on noise-induced hearing. This work demonstrated measurable changes in ribbon morphology and synapse number following noise insult (Jensen et al., 2015; Kujawa and Liberman, 2009; Liberman and Liberman, 2015). For example, in auditory inner hair cells within the high frequency region of the mouse cochlea, ribbons were enlarged immediately after noise, followed later by synapse loss (Liberman and Liberman, 2015). This pathology is reminiscent of our 1-hr pharmacological treatments that completely block the MCU in mature zebrafish-hair cells (Figure 3E-F). After this treatment, we observed a reduction in the number of hair cells and synapses, and an increase in ribbon size. Overall,

these studies and our own data in mature hair cells support the association between mitochondrial- Ca^{2+} and the MCU with pathological processes associated with noise-exposure.

In further support of this idea, recent work in mice has investigated the role of the MCU in noise-related hearing loss (Wang et al., 2019). This work demonstrated that pharmacological block or a loss of function mutation in MCU protected against synapse loss in auditory inner hair cells after noise exposure. Although this result is counter to our observed results where complete MCU block reduces synapse number (Figure 2.6E), it highlights an association between mitochondrial- Ca^{2+} , noise exposure and synapse integrity. It is possible that these differences can be explained by transitory versus chronic alterations in mitochondrial- Ca^{2+} homeostasis. These differences may be resolved by studying hair cells in a zebrafish MCU knock out. In the future it will be interesting to examine both mitochondrial- Ca^{2+} uptake and ribbon morphology during noise exposure and aging where synapses may be damaged.

Materials and Methods

Zebrafish husbandry and genetics

Adult *Danio rerio* (zebrafish) were maintained under standard conditions. Larvae 5 to 7 days post-fertilization (dpf) were maintained in E3 embryo medium (in mM: 5 NaCl, 0.17 KCl, 0.33 CaCl_2 and 0.33 MgSO_4 , buffered in HEPES pH 7.2) at 28°C. All husbandry and

experiments were approved by the NIH Animal Care and Use program under protocol #1362-13. Transgenic zebrafish lines used in this study include: *Tg(myo6b:GCaMP6s-CAAX)^{idc1}* (Jiang et al., 2017), *Tg(myo6b:GCaMP3)^{w78Tg}* (Esterberg et al., 2013), *Tg(myo6b:mitoGCaMP3)^{w119Tg}* (Esterberg et al., 2014), and *Tg(myo6b:ribeye a-tagRFP)^{idc11Tg}* (Sheets, 2017). Experiments were performed using Tübingen or TL wildtype strains.

Cloning and transgenic fish production

To create transgenic fish, plasmid construction was based on the *tol2*/Gateway zebrafish kit developed by the lab of Chi-Bin Chien at the University of Utah (Kwan et al., 2007). These methods were used to create *Tg(myo6b:mitoRGECO1)^{idc12Tg}* transgenic line. *mitoRGECO1* was cloned into the middle entry vector pDONR221 using the primers listed in Table 2.1. For mitochondrial matrix targeting, the sequence of cytochrome C oxidase subunit VIII (Rizzuto et al., 1989) was added to the N-terminus of RGECO1. Vectors p3E-polyA and pDestTol2CG2 were recombined with p5E *myosinVIb* (*myo6b*) and our engineered plasmids to create *myo6b:mitoRGECO1*. To generate transgenic fish, DNA clones (25-50 ng/ μ l) were injected along with *tol2* transposase mRNA (25-50 ng/ μ l) into zebrafish embryos at the single-cell stage.

Table 2.1. Primers used to generate *Tg(myo6b:mitoRGECO1)^{idc12Tg}*

Designation	Source or reference	Identifiers	Additional information
RGECO1 FWD1	This paper	PCR primers	[ATGTCCGTCCTGACGCC GCTGCTGCTGCGGGGCT TGACAGGCTCGGCCCGG CGGCTCCCAGTGCCGCG CGCCAAGATCCATTCGT TGGGGGATCCA]- GTCGACTCTTCACGTCG TAAGTG; Made by IDT.
RGECO1 REV1	This paper	PCR primers	CTACTTCGCTGTCATCAT TTGTACAAACTC; Made by IDT.
RGECO1 attB FWD2	This paper	PCR primers	GGGGACAAGTTTGTACA AAAAAGCAGGCTGCCAC CATGTCCGTCCTGACGC CGC; Made by IDT.
RGECO1 attB REV2	This paper	PCR primers	GGGGACCACTTTGTACA AGAAAGCTGGGTGCTAC TTCGCTGTCATCATTTGT ACAAACTC; Made by IDT.

Pharmacological treatment of larvae for immunohistochemistry

For pharmacological studies, zebrafish larvae were exposed to compounds diluted in E3 with 0.1 % DMSO (Isradipine (Sigma-Aldrich, St. Louis, MO), Ru360 (Millipore, Burlington, MA), TRO 19622 (Cayman Chemical, Ann Arbor, MI)) for 30 min or 1 hr at the concentrations indicated. E3 with 0.1 % DMSO were used as control solutions. Dosages of isradipine, Ru360, and TRO 19622 did not confer excessive hair-cell death or synapse loss unless stated. After exposure to the compounds, larvae were quickly sedated on ice and transferred to fixative.

In vivo imaging of evoked Ca^{2+} signals

To measure evoked Ca^{2+} signals in hair cells, larvae were paralyzed with α -bungarotoxin and immersed in neuronal buffer solution (in mM: 140 NaCl, 2 KCl, 2 CaCl_2 , 1 MgCl_2 and 10 HEPES, pH 7.3). Larvae were imaged using a Bruker Swept-field confocal microscope, with a Nikon CFI Fluor 60x 1.0 NA water immersion objective. A 488 nm laser was used to excite MitoGCaMP3 and a dual bandpass 488/561 nm filter set, and a Rolera EM-C2 CCD camera (QImaging) was used to detect signals. To stimulate lateral-line hair cells, a fluid-jet was used as previously described to deliver a saturating stimulus (Lukasz and Kindt, 2018).

To measure presynaptic GCaMP6sCAAX signals at ribbons, images were acquired with 1 x 1 binning using a 35 μm slit at 50 Hz in a single plane containing presynaptic ribbons (Figure 2.5C-C'). Ribbons were marked in live hair cells using the *Tg(myo6b:ribeye a-tagRFP)^{idc11Tg}* transgenic line (Figure 2.5C). Ribbons were located relative to GCaMP6s signals by acquiring a 2-color Z-stack of 5 planes every 1 μm at the base of the hair cells. To

correlate presynaptic GCaMP6sCAAX signals with MitoRGECO1 signals in hair cells, 2-color imaging was performed. Images were acquired in a single plane with 2 x 2 binning at 10 Hz with a 70 μ M slit. MitoGCaMP3 signals were acquired at 10 Hz in Z-stacks of 5 planes 1 μ m apart with 2 x 2 binning and a 70 μ M slit. High speed imaging along the Z-axis was accomplished by using a piezoelectric motor (PICMA P-882.11-888.11 series, Physik Instrumente GmbH, Karlsruhe, Germany) attached to the objective to allow rapid imaging at a 50 Hz frame rate yielding a 10 Hz volume rate. Due to the slow mitochondrial-Ca²⁺ return to baseline after stimulation (~5 min), we waited a minimum of 5 min before initiating a new evoked GCaMP6sCAAX or MitoGCaMP3 acquisition. To examine mechanotransduction, GCaMP6sCAAX signals were measured in apical hair bundles (Figure 2.5A-B'). Apical GCaMP6sCAAX signals were acquired in a single plane at 1 x 1 binning with a 35 μ M slit at 20 Hz. For pharmacological treatment, acquisitions were made prior to drug treatment and after a 30-min incubation in the pharmacological agent. Any neuromasts with cell death after pharmacological treatment were excluded from our analyses.

Electron microscopy

Larvae were prepared for electron microscopy as described previously (Sheets, 2017). Transverse serial sections (~60 nm thin sections) were used to section through neuromasts. Samples were imaged on a JEOL JEM-2100 electron microscope (JEOL Inc., Tokyo, Japan). The distance from the edge of a ribbon density to the edge of the nearest mitochondrion was measured (n = 17 ribbons). A subset of measurements was taken from more than one ribbon within a hair cell. At 81 % of ribbons, a mitochondrion could be clearly identified within 1 μ m of a ribbon (17 out of 21 ribbons). All distances and perimeters were measured in FIJI (Schindelin et al., 2012).

Immunofluorescence staining and Airyscan imaging

Whole larvae were fixed with 4 % paraformaldehyde in PBS at 4°C for 3.5-4 hr as previously described (Zhang et al., 2018). Fixative was washed out with 0.01 % Tween in PBS (PBST) in 4 washes, 5 min each. Larvae were then washed for 5 min with H₂O. The H₂O was thoroughly removed and replaced with ice-cold acetone and placed at -20°C for 5 min for 5 dpf larvae, followed by a 5-min H₂O wash. The larvae were then washed for 4 x 5 min in PBST, then incubated in block overnight at 4°C in blocking solution (2 % goat serum, 1 % bovine serum albumin, 2 % fish skin gelatin in PBST). Primary and secondary antibodies were diluted in blocking solution. Primary antibodies and their respective dilutions are: Ribbon label: Mouse anti-Ribeye b IgG2a, 1:10,000 (Sheets et al., 2011); PSD label: Mouse anti-pan-MAGUK IgG1, 1:500 (MABN72, MilliporeSigma, Burlington, MA); Hair-cell label: Rabbit anti-Myosin VIIa, 1:1000 (#25-6790, Proteus BioSciences Inc., Ramona, CA); Cav1.3 channel label: Rabbit anti-Cav1.3a, 1:500 (Sheets et al., 2012). Larvae were incubated in primary antibody solution for 2 hr at room temperature. After 4 x 5 min washes in PBST to remove the primary antibodies, diluted secondary antibodies were added and samples were incubated for 2 hr at room temperature. Secondary antibodies and their respective dilution are as follows: goat anti-mouse IgG2a, Alexa Fluor 488, 1:1000; goat anti-rabbit IgG (H+L) Alexa Fluor 546, 1:1000; goat anti-mouse IgG1 Alexa Fluor 647, 1:1000 (Thermo Fisher Scientific, Waltham, MA). Secondary antibodies were washed out with PBST for 3 x 5 min, followed by a 5-min wash with H₂O. Larvae were mounted on glass slides with Prolong Gold Antifade Reagent (Invitrogen, Carlsbad, CA) using No. 1.5 coverslips.

Prior to Airyscan imaging, live samples were immobilized in 2 % low-melt agarose in tricaine (0.03 %) in cover-glass bottomed dishes. Live and fixed samples were imaged on an inverted Zeiss LSM 780 laser-scanning confocal microscope with an Airyscan attachment (Carl Zeiss AG, Oberkochen, Germany) using an 63x 1.4 NA oil objective lens. The median (\pm median absolute deviation) lateral and axial resolution of the system was measured at 198 ± 7.5 nm and 913 ± 50 nm (full-width at half-maximum), respectively. The acquisition parameters were adjusted using the control sample such that pixels for each channel reach at least 1/10 of the dynamic range. The Airyscan Z-stacks were processed with Zeiss Zen Black software v2.1 using 3D filter setting of 7.0. Experiments were imaged with the same acquisition settings to maintain consistency between comparisons.

Quantification and Statistical Analysis

Analysis of Ca²⁺ signals, processing, and quantification

To quantify changes in baseline Ca²⁺ and NAD(H) homeostasis, images were processed in FIJI. For our measurements we quantified the fluorescence in the basal-most 8 μ m (4 planes) to avoid overlap between cells. The basal planes were max Z-projected, and a 24.0 μ m (RGECO1) or 26.8 μ m (MitoGCaMP3) circular region of interest (ROI) was drawn over the neuromast to make intensity measurements. To correct for photobleaching, a set of mock-treated control neuromasts were imaged during every trial. These mock treatments were used to normalize the post-treatment intensity values.

To quantify the magnitude of evoked changes in Ca²⁺, images were processed in FIJI. Images in each time series were aligned using Stackreg (Thevenaz et al., 1998). For

evoked MitoRGECO1, MitoGCaMP3, CytoGCaMP3 and two-color GCaMP6sCAAX and MitoRGECO1 signals, Z-stacks were max z-projected, and a 5 μm diameter circular ROI was drawn over each hair cell to make intensity measurements. For ribbon-localized measurements, GCaMP6sCAAX signals were measured within 1.34 μm round ROIs at individual ribbons, and intensity change at multiple ribbons per cell were averaged. For measurements of mechanotransduction, GCaMP6sCAAX signals were measured within 1.34 μm round ROIs at individual hair bundles, and intensity change in multiple bundles per neuromast were averaged.

To plot evoked changes in Ca^{2+} , we subtracted the baseline (F_0 , signal during the pre-stimulus period) was subtracted from each timepoint acquired. Then each timepoint was divided by F_0 to generate the relative change in fluorescent signal from baseline or $\Delta F/F_0$. Quantification of evoked Ca^{2+} signals were made on max $\Delta F/F_0$ measurements. Cells with presynaptic Ca^{2+} activity are defined by max $\Delta F/F_0$ of > 0.05 for MitoRGECO1 and MitoGCaMP3, and max $\Delta F/F_0 > 0.25$ for GCaMP6sCAAX for a 2-s stimulation. The method to obtain and overlay the spatial signal distribution of evoked signals as heat maps has been previously described (Lukasz and Kindt, 2018). We first computed the baseline image (F_0 or reference image) by averaging the images over the pre-stimulus period. Then the F_0 was subtracted from each image acquired, to represent the relative change in fluorescent signal from baseline or ΔF . The ΔF signal images during the stimulus period were binned, scaled and encoded by color maps with red indicating an increase in signal intensity.

Image processing and quantification of synapse morphology

To quantify synapse morphology and pairing, images were first processed in ImageJ (NIH), and then synapses were paired using Python (Python Software Foundation) in the Spyder Scientific Environment (MIT). In ImageJ, each Airyscan Z-stack was background subtracted using rolling-ball subtraction. Z-stacks containing the MAGUK channel were further bandpass filtered to remove details smaller than 6 px and larger than 20 px. A duplicate of the Z-stack was normalized for intensity. This duplicated Z-stack was used to identify individual ribbon and MAGUK using the Simple 3D Segmentation of ImageJ 3D Suite (Ollion et al., 2013). Local intensity maxima, identified with 3D Fast Filter, and 3D watershed were used to separate close-by structures. The centroid for each identified ribbon and MAGUK was obtained using 3D Manager and were used to identify complete synapses. The max Z-projection of the segmented Z-stack was used to generate a list of 2D objects as individual ROIs corresponding to each punctum. This step also included a minimum size filter, Ribeye: $0.08 \mu\text{m}^2$, MAGUK $0.04 \mu\text{m}^2$. For quantification of extrasynaptic Ribeye b puncta, the minimum size filter was not applied. The 2D puncta ROI were applied over the max Z-projection of the original Z-stack which has only been processed with background subtraction. This step measures the intensity of the antibody label. Centroid and intensity information were exported as a CSV spreadsheet (macro is available on <https://github.com/wonghc/ImageJ-ribbon-synapse-quantification>).

In Python, the 3D centroid coordinates for each ribbon punctum was measured against the coordinates of every post-synaptic MAGUK punctum to find the MAGUK punctum within a threshold distance. This threshold was calculated by taking the 2D area of the Ribeye and MAGUK punctum measured in the max Z-projection to calculate an approximate radius by dividing by π and taking the square root. The two radii were then summed to get the threshold. Puncta that were not paired were excluded from later statistical

analyses of synaptic ribbon and postsynaptic MAGUK puncta. Hair cell and synapse count were confirmed manually. Hair cell counts were performed with myosin VIIa antibody label in treatments where synapse or cell numbers were reduced.

Statistics

Statistical analyses and data plots were performed with Prism 8 (Graphpad, San Diego, CA). Values of data with error bars on graphs and in text are expressed as mean \pm SEM unless indicated otherwise. All experiments were performed on a minimum of 2 animals, 6 neuromasts (posterior lateral-line neuromasts L1-L4 or anterior lateral-line neuromasts O1 and O2 (Figure 2.3 and 2.7)), on 2 independent days. For 3 and 5 dpf larvae each neuromast represents analysis from 8-12 hair cells; 24-36 synapses and 14-18 hair cells; 42-54 synapses respectively. All replicates are biological. Based on the variance and effect sizes reported previously and measured in this study, these numbers were adequate to provide statistical power to avoid both Type I and Type II error (Sheets et al., 2012; Zhang et al., 2018). No animals or samples were excluded from our analyses unless control experiments failed—in these cases all samples were excluded. No randomization or blinding was used for our animal studies. Where appropriate, data was confirmed for normality using a D'Agostino-Pearson normality test and for equal variances using a F test to compare variances. Statistical significance between two conditions was determined by either an unpaired t -test, an unpaired Welch's unequal variance t-test, a Mann-Whitney U test or a Wilcoxon matched-pairs signed-rank test as appropriate. For comparison of multiple conditions, a Brown-Forsythe with Dunnett's T3 post hoc or a Brown-Forsythe and Welch ANOVA with Holm-Sidak's post hoc were used as appropriate. To calculate the IC50 for Ru360 block of evoked MitoGCaMP3 signals a dose response curve was plotted using 0, 0.5,

2, 5 and 10 μM Ru360. A non-linear fit with four parameters and a variable slope was performed to calculate an IC50 of 1.37 μM .

Acknowledgements

This work was supported by National Institute on Deafness and Other Communication Disorders Intramural Research Program Grant 1ZIADC000085-01 to K.S.K. and ZICDC000081 to R.S.P. and Y.-X.W. We would like to thank Daria Lukasz, Katie Drerup, Paul Fuchs and Doris Wu for their support and thoughtful comments on the manuscript.

K.S.K. and I designed all experiments. I performed all experiments and quantification of results except those pertaining to transmission electron microscopy (performed by R.S.P. and Y.-X.W.) and some immunostaining (performed by A.J.B). K.S.K. and I wrote and edited the manuscript.

Chapter 3: Spontaneous mitochondrial-Ca²⁺ uptake modulates ribbon synapse formation

*Hiu-tung C. Wong^{1,2}, Qinxiang Zhang¹, Alisha J. Beir¹, Ronald S. Petralia³, Ya-Xian Wang³, and
Katie S. Kind¹*

Affiliations

¹Section on Sensory Cell Development and Function, NIDCD/National Institutes of Health, Bethesda, MD 20892 USA

²National Institutes of Health-Johns Hopkins University Graduate Partnership Program, NIDCD/National Institutes of Health, Bethesda, MD 20892 USA

³Advanced Imaging Core, NIDCD/National Institutes of Health, Bethesda, MD 20892, USA

Work presented in Chapter 3 was published in eLife, volume 8, 2019, page e48914. DOI: 10.7554/eLife.48914. Licensed under Creative Commons Attribution (CC BY 4.0) / Figure 3.1 and relevant paragraphs added to original.

Abstract

Sensory hair cells in the ear utilize specialized ribbon synapses. These synapses are defined by electron-dense presynaptic structures called ribbons, composed primarily of the structural protein Ribeye. Previous work has shown that influx of Ca^{2+} through voltage-gated $\text{Ca}_v1.3$ channels is critical for hair-cell synapse function and can impede ribbon formation. We show that in developing hair cells, there are spontaneous rises in presynaptic- Ca^{2+} that are reliant on $\text{Ca}_v1.3$ channels. These spontaneous rises in presynaptic- Ca^{2+} coincide with mitochondrial- Ca^{2+} uptake. Spontaneous mitochondrial- Ca^{2+} loading lowers cellular NAD^+/NADH redox and downregulates ribbon formation. Direct application of NAD^+ or NADH increase or decrease ribbon formation respectively, possibly acting through the NAD(H) -binding domain on Ribeye. Our results present a mechanism where presynaptic- and mitochondrial- Ca^{2+} couple for proper presynaptic formation.

Introduction

In the inner ear and retina, sensory neurotransmission relies on specialized ribbon synapses. These specialized synapses have a unique presynaptic density called “ribbons”, that facilitate rapid and sustained vesicle release (reviewed in: Matthews and Fuchs, 2010). The size and morphology of ribbons varies between species and sensory epithelia (Schmitz, 2009) and these variations are thought to reflect the specific encoding requirements of a given sensory cell (Matthews and Fuchs, 2010). Currently the fundamental mechanism that regulates ribbon size is not known.

Sensory hair cells in auditory, vestibular and lateral-line systems use ribbon synapses to encode information sensory stimuli. In hair cells, one known way to regulate ribbon size is through its main structural component Ribeye (Schmitz et al., 2000). Perhaps unsurprisingly, previous work has shown that overexpression or depletion of Ribeye in hair cells can increase or decrease ribbon size respectively (Becker et al., 2018; Jean et al., 2018; Lv et al., 2016; Sheets, 2017; Sheets et al., 2011). Ribeye is a splice variant of the transcriptional co-repressor Carboxyl-terminal binding protein 2 (CtBP2) – a splice variant that is unique to vertebrate evolution (Schmitz et al., 2000). Ribeye contains a unique A-domain and a B-domain that is nearly identical to full-length CtBP2. The B-domain contains a nicotinamide adenine dinucleotide (NAD⁺, NADH or NAD(H)) binding site (Magupalli et al., 2008; Schmitz et al., 2000). NAD(H) redox is linked to mitochondrial metabolism (Srivastava, 2016). Because CtBP2 is able to bind and detect NAD⁺ and NADH levels, it is thought to function as a metabolic biosensor (Stankiewicz et al., 2014). For example, previous work has demonstrated that changes in NAD(H) redox can impact CtBP oligomerization and its transcriptional activity (Fjeld et al., 2003; Thio et al., 2004). Interestingly, *in vitro* work has

shown that both NAD^+ and NADH can also promote interactions between Ribeye domains (Magupalli et al., 2008). Whether NAD^+ or NADH can impact Ribeye interactions and ribbon formation has not been confirmed *in vivo*.

In hair cells, studies have shown that presynaptic Ca^{2+} may also impact ribbon formation. Neurotransmission at hair-cell ribbon synapses requires the presynaptic- Ca^{2+} channel $\text{Ca}_v1.3$ (Brandt et al., 2003; Kollmar et al., 1997; Sidi, 2004). Hair-cell depolarization opens $\text{Ca}_v1.3$ channels, resulting in a spatially restricted increase of Ca^{2+} at presynaptic ribbons that triggers vesicle fusion. *In vivo* work in zebrafish hair cells found that increasing or decreasing Ca^{2+} influx through $\text{Ca}_v1.3$ channels during development led to the formation of smaller or larger ribbons respectively (Sheets et al., 2012).

Studies in mammals have also shown that presynaptic Ca^{2+} and $\text{Ca}_v1.3$ channels also play an important role during inner-ear development. In mammals, prior to hearing onset, auditory hair cells fire spontaneous Ca^{2+} action potentials (Eckrich et al., 2018; Marcotti et al., 2003; Tritsch et al., 2007, 2010). In mammalian hair cells, these Ca^{2+} action potentials are $\text{Ca}_v1.3$ -dependent and are thought to be important for synapse and circuit formation. In support of this idea, in mouse knockouts of $\text{Ca}_v1.3$, auditory outer hair cells have reduced afferent innervation and synapse number (Ceriani et al., 2019). Mechanistically, how $\text{Ca}_v1.3$ -channel activity regulates ribbon size and innervation is not known.

In neurons, work has shown that presynaptic activity and mitochondrial- Ca^{2+} can couple together to influence cellular bioenergetics, including NAD(H) redox homeostasis (reviewed in: Kann and Kovács, 2007; Llorente-Folch et al., 2015). Based on these studies, we hypothesized that Ca^{2+} influx through $\text{Ca}_v1.3$ channels may regulate mitochondrial- Ca^{2+} , which in turn could regulate NAD(H) redox. Changes to cellular bioenergetics and NAD(H) redox could function to control Ribeye interactions and ribbon formation.

To study the impact of mitochondrial- Ca^{2+} and NAD(H) redox on ribbon synapse formation, we examined hair cells in the lateral-line system of larval zebrafish. This system is advantageous because it contains hair cells with easy access for *in vivo* pharmacology, and imaging cellular morphology and function. Within the lateral-line, hair cells are arranged in clusters called neuromasts. The hair cells and ribbon synapses in each cluster form rapidly between 2 to 3 days post-fertilization (dpf) (Kindt et al., 2012; McHenry et al., 2009; Metcalfe, 1985; Murakami et al., 2003; Santos et al., 2006). Thus, this system can be used to study mitochondrial- Ca^{2+} and NAD(H) redox in developing hair cells.

Using this sensory system, we find that in developing hair cells spontaneous rises in presynaptic Ca^{2+} drive mitochondrial- Ca^{2+} uptake. Blocking these spontaneous changes in Ca^{2+} leads to the formation of larger ribbons. Using a redox biosensor, we demonstrate that specifically in developing hair cells, decreasing mitochondrial- Ca^{2+} levels increases the NAD^+/NADH redox ratio. Furthermore, we show that application of NAD^+ or NADH can promote the formation of larger or smaller ribbons respectively. Overall, our results suggest that in hair cells presynaptic- Ca^{2+} influx and mitochondrial- Ca^{2+} uptake couple in hair cells to impact ribbon formation.

Results

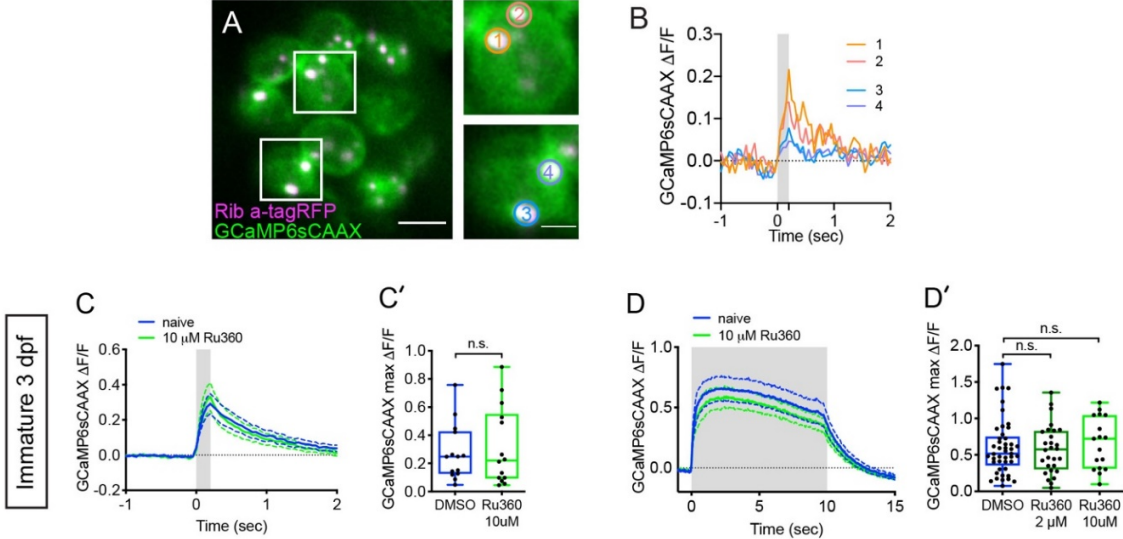
Blocking mitochondrial- Ca^{2+} entry does not impair presynaptic- Ca^{2+} signals in immature hair cells

In previous work, we found that MCU block impaired evoked-presynaptic- Ca^{2+} influx. But it was not clear whether mitochondrial- Ca^{2+} uptake also impacts presynapse function of immature hair-cell synapses. We reasoned that mitochondria may be similarly

important to remove excess Ca^{2+} or provide ATP for hair-cell neurotransmission in the immature hair cell.

To determine if mitochondrial- Ca^{2+} uptake impacted presynaptic function, we assayed evoked presynaptic- Ca^{2+} signals by monitoring GCaMP6sCAAX signals adjacent to ribbons as described previously (Figure 2.4C-D', 2.5C-E'; Sheets et al., 2017; Zhang et al., 2018). We examined GCaMP6sCAAX signals in immature hair cells at 3 dpf when neuromast organs and hair cells are developing (Kindt et al., 2012; McHenry et al., 2009; Metcalfe, 1985; Murakami et al., 2003; Santos et al., 2006). Using this approach, we assayed presynaptic GCaMP6sCAAX signals before and after a 30-min application of the MCU antagonist Ru360 (Figure 2.4C-D'). We found that for both short 200-ms stimuli and sustained 10-s stimuli, GCaMP6sCAAX signals at ribbons were unaffected by partial or complete MCU block (Figure 3.1C-D'). These results suggest that, unlike in mature hair cells, evoked mitochondrial- Ca^{2+} uptake is dispensable for presynaptic- Ca^{2+} influx in immature hair cells.

Figure 3.1. Mitochondrial- Ca^{2+} uptake does not impact presynaptic Ca^{2+} signals in immature hair cells.



A, Double-transgenic hair cells expressing GCaMP6sCAAX (at presynaptic membranes) and Ribeye a-tagRFP (labels ribbons) at 3 dpf. Example cells in presynaptic imaging plane are boxed in white and duplicated in right insets. C', Example cells show evoked presynaptic-Ca²⁺ signals at ribbons during a 0.2-s stimulation. Circles 1-4 (1.3 μm diameter) in insets in A denote regions at ribbons used to generate the temporal traces of presynaptic-Ca²⁺ signals at each ribbon in B. Similarly-colored traces of presynaptic-Ca²⁺ signals originate from different presynapses of the same cell. C-D', Presynaptic-Ca²⁺ response averaged per cell before (blue) and after a 30-min treatment with 10 μM Ru360 (light green) or 2 μM Ru360 (dark green), n ≥ 13 cells per treatment. C and D show averaged traces while C' and D' show before-and-after dot plots of the peak response per cell.

Spontaneous presynaptic and mitochondrial-Ca²⁺ influx pair in developing hair cells

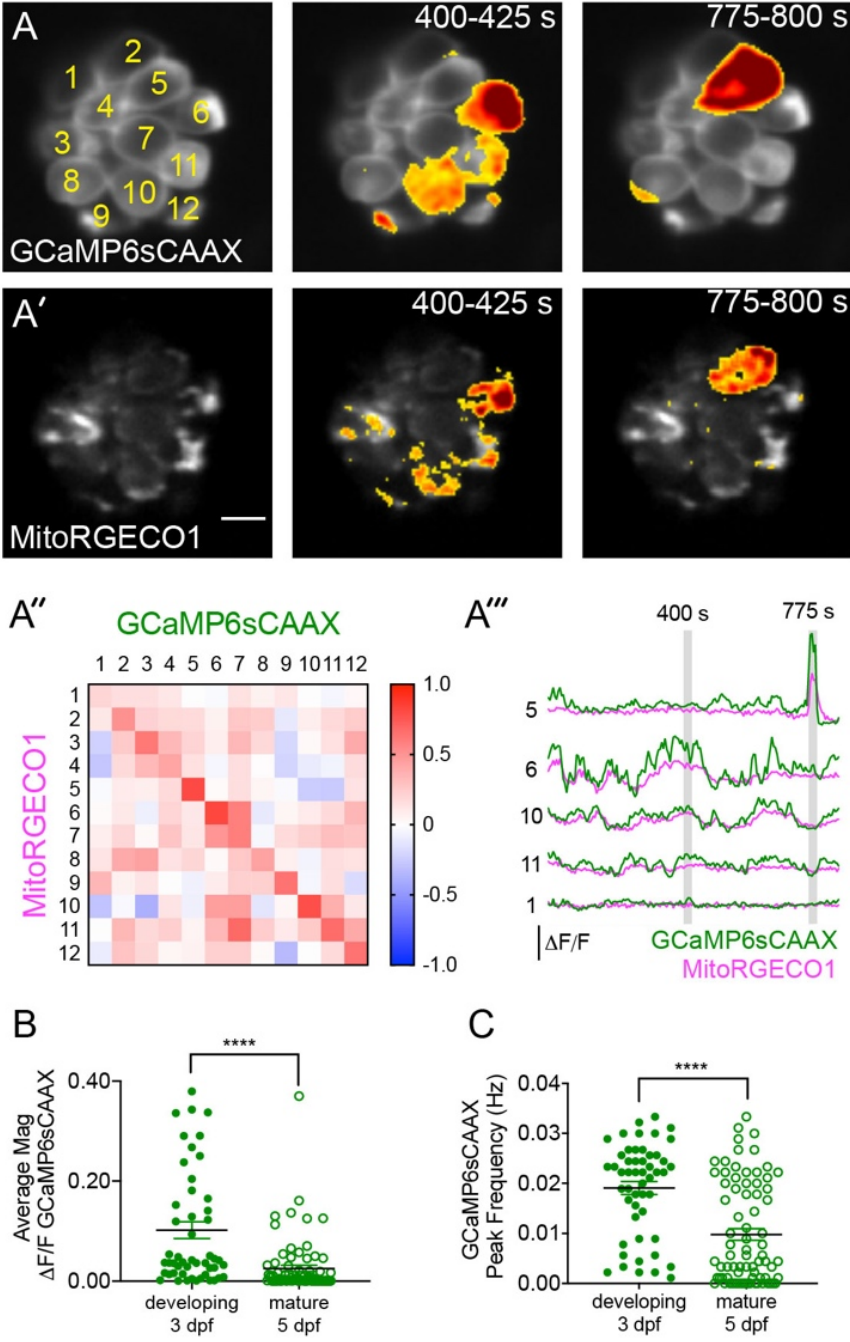
Numerous studies have demonstrated that mammalian hair cells have spontaneous presynaptic-Ca²⁺ influx during development (Eckrich et al., 2018; Holman et al., 2019; Marcotti et al., 2003; Tritsch et al., 2007, 2010). Therefore, we predicted that similar to mammals, spontaneous presynaptic-Ca²⁺ uptake may be a feature of development. Furthermore, we predicted that spontaneous mitochondrial-Ca²⁺ uptake may correlate with instances of spontaneous presynaptic-Ca²⁺ influx.

First, we tested whether spontaneous presynaptic-Ca²⁺ signals were a feature of developing hair cells. In zebrafish neuromasts, hair cells are rapidly added between 2-3 dpf, but by 5-6 dpf relatively fewer cells are added and the hair cells and the organs are largely mature (Kindt et al., 2012; McHenry et al., 2009; Metcalfe, 1985; Murakami et al., 2003; Santos et al., 2006). Therefore, we examined the magnitude and frequency of spontaneous, presynaptic GCaMP6sCAAX signals in developing (3 dpf) and mature (5 dpf) hair cells. We found that in developing hair cells, spontaneous GCaMP6sCAAX signals occurred with larger magnitudes and more frequency compared to those in mature hair cells (Figure 3.2B-C). Our spontaneous GCaMP6sCAAX imaging demonstrates that similar to mammals, spontaneous presynaptic Ca²⁺ activity is a feature of developing zebrafish hair cells.

Next, we tested whether spontaneous mitochondrial-Ca²⁺ uptake and presynaptic-Ca²⁺ influx was correlated. For this analysis we concurrently imaged GCaMP6sCAAX and MitoRGECO1 signals in the same cells for 15 mins to measure presynaptic- and mitochondrial-Ca²⁺ responses respectively. We found that spontaneous presynaptic-Ca²⁺ influx was often associated with spontaneous mitochondrial-Ca²⁺ uptake (Example, Figure

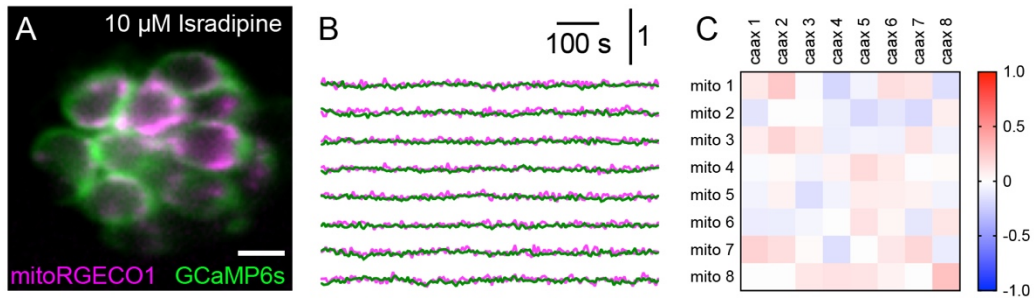
3.2A-A”). Overall, we observed a high correlation between the rise and fall of these two signals within individual cells (Figure 3.2A”-A”). Both of these signals and their correlation were abolished by application of the Cav1.3-channel antagonist isradipine (Figure 3.3). Together these experiments indicate that spontaneous presynaptic- and mitochondrial-Ca²⁺ signals are correlated.

Figure 3.2. Spontaneous presynaptic-Ca²⁺ influx is linked with Mitochondrial-Ca²⁺ uptake.



A-A', A live Image of a neuromast viewed top-down, expressing the presynaptic-Ca²⁺ sensor GCaMP6sCAAX (A) and mitochondrial-Ca²⁺ sensor MitoRGECO1 (A') at 3 dpf. Example GCaMP6sCAAX (A') and MitoRGECO1 (A') signals during two 25-s windows within a 900-s acquisition are indicated by the ΔF heatmaps and occur in the same cells. A'', A heatmap of Pearson correlation coefficients comparing GCaMP6sCAAX and MitoRGECO1 signals from the cells in A-A'. A''', Example GCaMP6sCAAX (green) MitoRGECO1 (magenta) traces during the 900-s acquisition from the 5 cells numbered in A, also see Video 2. B, Scatter plot showing the average magnitude of GCaMP6sCAAX signals in developing and mature hair cells, n = 6 neuromasts per age. C, Scatter plot showing frequency of GCaMP6sCAAX events in developing and mature hair cells, n = 6 neuromasts. Error bars in B-C represent SEM. A Mann-Whitney U test was used in B and C. **** $p < 0.0001$. Scale bar = 5 μm in A'.

Figure 3.3. Spontaneous presynaptic and mitochondrial- Ca^{2+} signals are abolished by $\text{Cav}1.3$ channel antagonist isradipine.



A, A live Image of a neuromast viewed top-down, expressing the presynaptic-Ca²⁺ sensor GCaMP6sCAAX (green) and mitochondrial-Ca²⁺ sensor MitoRGECO1 (magenta) at 6 dpf.

B, Representative GCaMP6sCAAX (green) and MitoRGECO1 (magenta) traces during a 900-s continuous image acquisition in the absence of stimuli and 10 μ M isradipine. C, There is no correlation between GCaMP6sCAAX and MitoRGECO1 signals within each cell in the presence of isradipine.

Spontaneous mitochondrial-Ca²⁺ uptake regulates ribbon formation

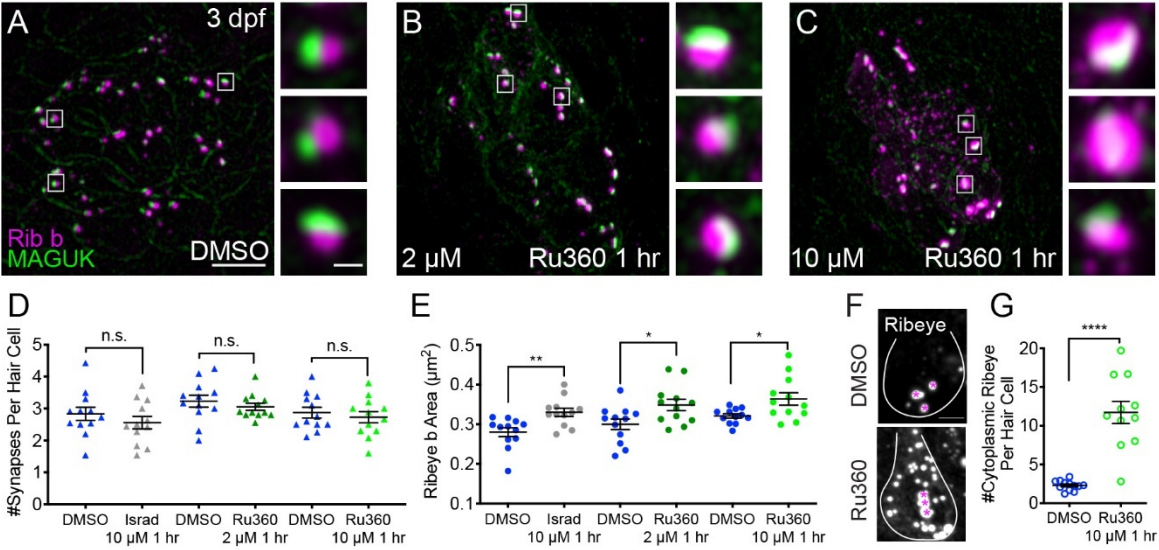
Although mitochondrial-Ca²⁺ uptake did not affect presynaptic-Ca²⁺ influx in immature hair cells, spontaneous mitochondrial-Ca²⁺ uptake may play a role at developing ribbons. Previous work in zebrafish demonstrated that Cav1.3 channel activity plays a role in regulating ribbon size specifically during development (Sheets et al., 2012). This work found that a transient, 1-hr pharmacological block of Cav1.3 channels increased ribbon size, while Cav1.3 channel agonists decreased ribbon size (Figure 3.4E; Sheets et al., 2012).

Interestingly, this Ca²⁺-dependent regulation of ribbon size is most impactful in the developing hair cells. This developmental time window coincides with the strongest and most frequent bouts of spontaneous presynaptic- and mitochondrial-Ca²⁺ activity in the immature hair cells (Figure 3.2). Therefore, spontaneous presynaptic- and mitochondrial-Ca²⁺ activities could function together to control ribbon size in developing hair cells.

To characterize the role of spontaneous mitochondrial-Ca²⁺ uptake on ribbon size, we applied the MCU antagonist Ru360 to developing hair cells (3 dpf). After this treatment, we quantified ribbon synapse morphology by immunostaining hair cells to label presynaptic ribbons and postsynaptic densities. After a 1-hr application of 2 μ M Ru360 to block the MCU, we observed a significant increase in ribbon size in developing hair cells (Figure 3.4A-B, E, Figure 3.5C). In contrast, this same treatment did not impact ribbon size in mature hair cells (Figure 2.6F, Figure 2.7C). We also applied a higher concentration of Ru360 (10 μ M) to developing hair cells for 1 hr. In developing hair cells, after a 1-hr 10 μ M Ru360 treatment, we also observed a significant increase in ribbon size (Figure 3.4A, C, E). Unlike in mature hair cells (Figure 2.6), in developing hair cells, these concentrations of the MCU antagonist did not alter the number of hair cells nor the number of synapses per hair cell (Figure 3.4D);

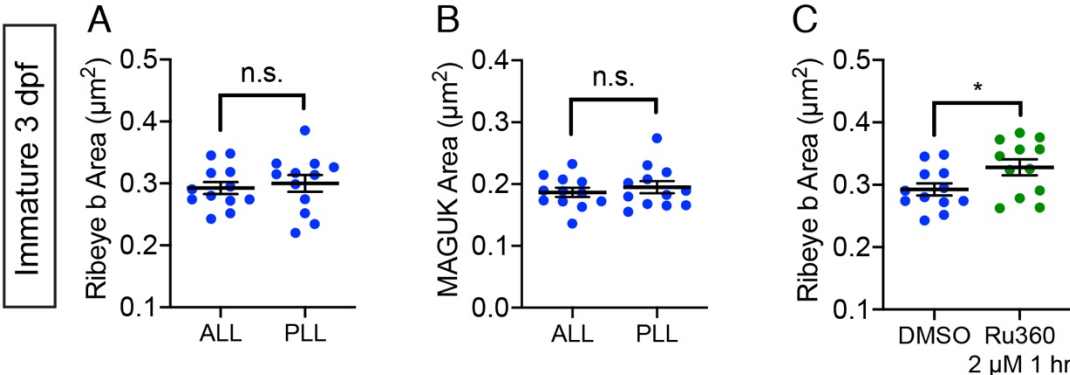
Hair cells per neuromast, control: 9.0, 1-hr 10 μ M Ru360: 8.8, $p = 0.3$). All morphological changes were restricted to the ribbons, as MCU block did not alter the size of the postsynapse (Figure 3.6).

Figure 3.4. Mitochondrial-Ca²⁺ regulates ribbon formation.



A-C, Representative images of immature neuromasts (3 dpf) immunostained with Ribeye b (magenta, ribbons) and MAGUK (green, postsynapses) after a 1-hr 0.1 % DMSO (A), 2 μ M Ru360 (B) or 10 μ M Ru360 (C) treatment. Insets show 3 representative synapses (white squares) for each treatment. D-E, Scatter plot show quantification of synapse number (D), and ribbon area (E) in controls and in treatment groups. F, Side-view of 2 hair cells (white outline) shows synaptic ribbon (3 magenta asterisks in each cell) and extrasynaptic Ribeye b aggregates after a 1-hr 0.1 % DMSO or 10 μ M Ru360 treatment. G, Quantification of extrasynaptic Ribeye puncta. $N \geq 12$ neuromasts per treatment. Error bars in D-E and G represent SEM. An unpaired t -test was used in D and a Welch's unequal variance t -test was used in D-E and G, $*p < 0.05$, $**p < 0.01$, $****p < 0.0001$. Scale bar = 5 μ m in A, 2 μ m in insets and F.

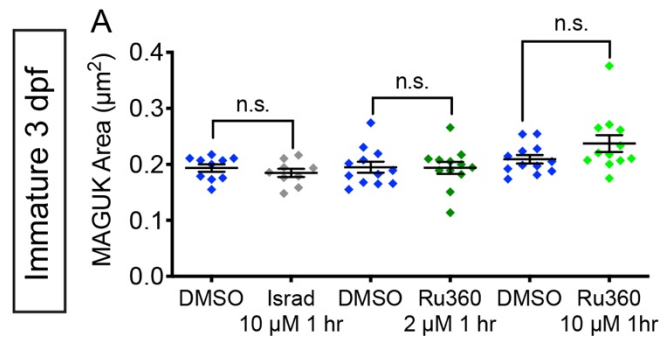
Figure 3.5. Ribbon and postsynapse size in immature ALL neuromasts.



A-B, Scatter plots show that ribbon areas (A) and postsynaptic density areas (B) within the same fish are similar between immature anterior lateral-line (ALL) and posterior lateral-line (PLL) neuromasts. C, Scatter plots show ribbon areas in controls and after a 1-hr treatment with 2 μ M Ru360 are larger in immature hair cells within the ALL. Ribbon sizes of untreated anterior lateral-line hair cells are from the same dataset in A and C, $n \geq 10$ neuromasts per treatment; error bars represent SEM; and a Welch's unequal variance *t*-test was used for comparisons. * $p < 0.05$.

In addition to larger ribbons, at higher concentrations of Ru360 (10 μ M), we also observed an increase in cytosolic, non-synaptic Ribeye aggregates (Figure 3.4F, G). Previous work in zebrafish reported both larger ribbons and cytosolic aggregates of Ribeye in $Ca_v1.3a$ -deficient hair cells (Sheets et al., 2011). These parallel phenotypes indicate that spontaneous presynaptic- Ca^{2+} influx and mitochondrial- Ca^{2+} uptake may couple to shape ribbon size. Our results suggest that during development, spontaneous Ca^{2+} entry through both $Ca_v1.3$ and MCU channels continuously regulate ribbon formation; blocking the Ca^{2+} channels increases Ribeye aggregation and ribbon size.

Figure 3.6. MCU and Cav1.3 block do not impact postsynapse size.



A, Quantification of postsynapse size assayed by MAGUK immunolabel in mature neuromasts indicate the treatments with 10 μ M isradipine, 2 μ M Ru360 and 10 μ M Ru360 do not significantly alter postsynapse size compared to controls, $n \geq 9$ neuromasts per treatment. Error bars represent SEM. A Welch's unequal variance *t*-test was used for comparisons.

MCU and Cav1.3 channel activities regulate subcellular Ca²⁺ homeostasis

Our results indicate that spontaneous-Ca²⁺ influx through Cav1.3 channels and subsequent loading of Ca²⁺ into mitochondria regulates ribbon size in developing hair cells. But how do these two Ca²⁺ signals converge to regulate ribbon size? It is possible that mitochondria could buffer Ca²⁺ during spontaneous presynaptic activity and function to decrease resting levels of cytosolic Ca²⁺; cytosolic-Ca²⁺ levels could be a signal that regulates ribbon size. To examine resting cytosolic-Ca²⁺ levels in hair cells, we examined the fluorescence signal change of the cytosolic-Ca²⁺ indicator RGECO1 (CytoRGECO1) before and after a 30-min pharmacological manipulation of Cav1.3 or MCU channels (Figure 3.7A-C).

We observed that treatment with the Cav1.3 channel antagonist isradipine and agonist Bay K8644 decreased and increased resting CytoRGECO1 fluorescence respectively (Figure 3.7A). However, treatment with MCU blocker Ru360 did not significantly shift resting CytoRGECO1 fluorescence levels (Figure 3.7A). These data suggest that, unlike Cav1.3 channel function, MCU function and associated mitochondrial-Ca²⁺ uptake does not play a critical role in buffering steady state cytosolic-Ca²⁺ levels in developing hair cells.

Alternatively, it is possible that rather than impacting cytosolic-Ca²⁺ levels, both Cav1.3 and MCU activity are required to load and maintain Ca²⁺ levels within the mitochondria. In this scenario, mitochondrial-Ca²⁺ levels could be a signal that regulates ribbon size. To test this possibility, we used MitoGCaMP3 to examine resting mitochondrial-Ca²⁺ levels before and after modulating Cav1.3 or MCU channel function (Figure 3.7B). We observed that blocking Cav1.3 channels with isradipine or the MCU with Ru360 decreased resting MitoGCaMP3 fluorescence. Conversely, Cav1.3 channel agonist

Bay K8644 increased resting MitoGCaMP3 fluorescence. These results were consistent in mature hair cells as well (Figure 2.9B). Our resting MitoGCaMP3 measurements indicate that the effects of Cav1.3 channel and MCU activity converge to regulate mitochondrial-Ca²⁺ levels. When either of these channels are blocked, the resting levels of mitochondrial-Ca²⁺ decrease. Therefore, if presynaptic-Ca²⁺ influx and mitochondrial-Ca²⁺ regulate ribbon size through a similar mechanism, they may act through mitochondrial- rather than cytosolic-Ca²⁺ homeostasis.

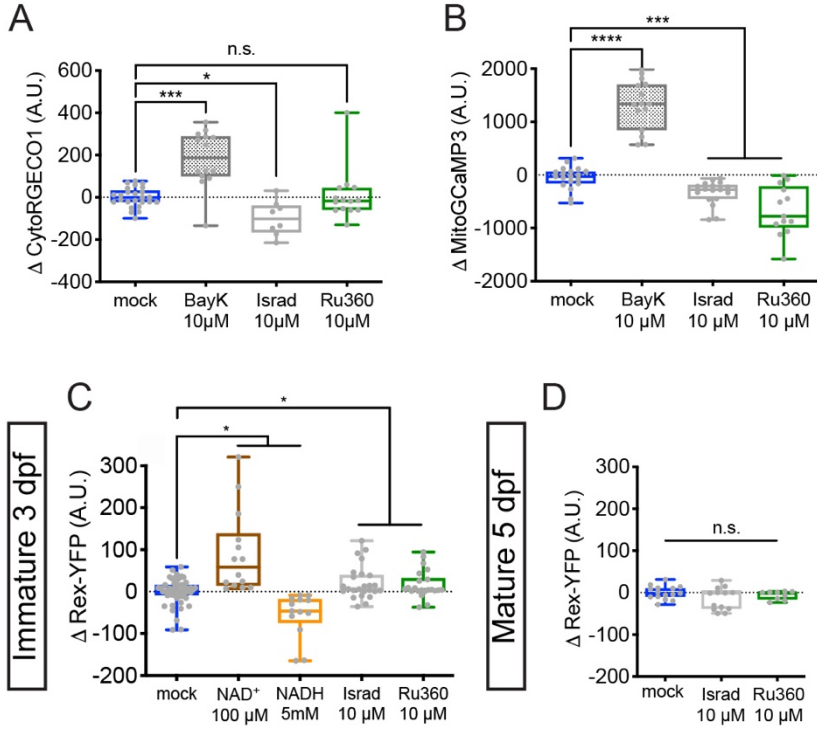
Mitochondrial-Ca²⁺ levels regulate NAD(H) redox in developing hair cells

If mitochondrial-Ca²⁺ levels signal to regulate ribbon size, how is this signal transmitted from the mitochondria to the ribbon? An ideal candidate is via NAD(H) homeostasis. Ribeye protein, the main component of ribbons contains a putative NAD(H) binding site. Because mitochondria regulate NAD(H) redox homeostasis (Jensen-Smith et al., 2012), we reasoned that there may be a relationship between mitochondrial-Ca²⁺ levels, NAD(H) redox, and ribbon size.

To examine NAD(H) redox, we created a stable transgenic line expressing Rex-YFP, a fluorescent NAD⁺/NADH ratio biosensor in hair cells. We verified the function of the Rex-YFP biosensor in our *in vivo* system by exogenously applying NAD⁺ or NADH for 30 min. We found that incubation with 100 μM NAD⁺ increased while 5 mM NADH decreased Rex-YFP fluorescence; these intensity changes are consistent with an increase and decrease in the NAD⁺/NADH ratio respectively (Figure 3.7C). Next, we examined if Cav1.3 and MCU channel activities impact the NAD⁺/NADH ratio. We found that 30-min treatments with either a Cav1.3 or MCU channel antagonist increased the NAD⁺/NADH ratio (increased Rex-YFP fluorescence) in developing hair cells (Figure 3.7C). Interestingly, similar

30-min treatments did not alter Rex-YFP fluorescence in mature hair cells (Figure 3.7D). Together, our baseline MitoGCaMP3 and Rex-YFP measurements indicate that during development, $Ca_v1.3$ and MCU channel activities normally function to increase mitochondrial- Ca^{2+} and decrease the $NAD^+/NADH$ ratio. Overall, this work provides strong evidence that links NAD(H) redox and mitochondrial- Ca^{2+} with ribbon formation.

Figure 3.7. Cytosolic-Ca²⁺, mitochondrial-Ca²⁺ and NAD⁺/NADH redox baseline measurements.



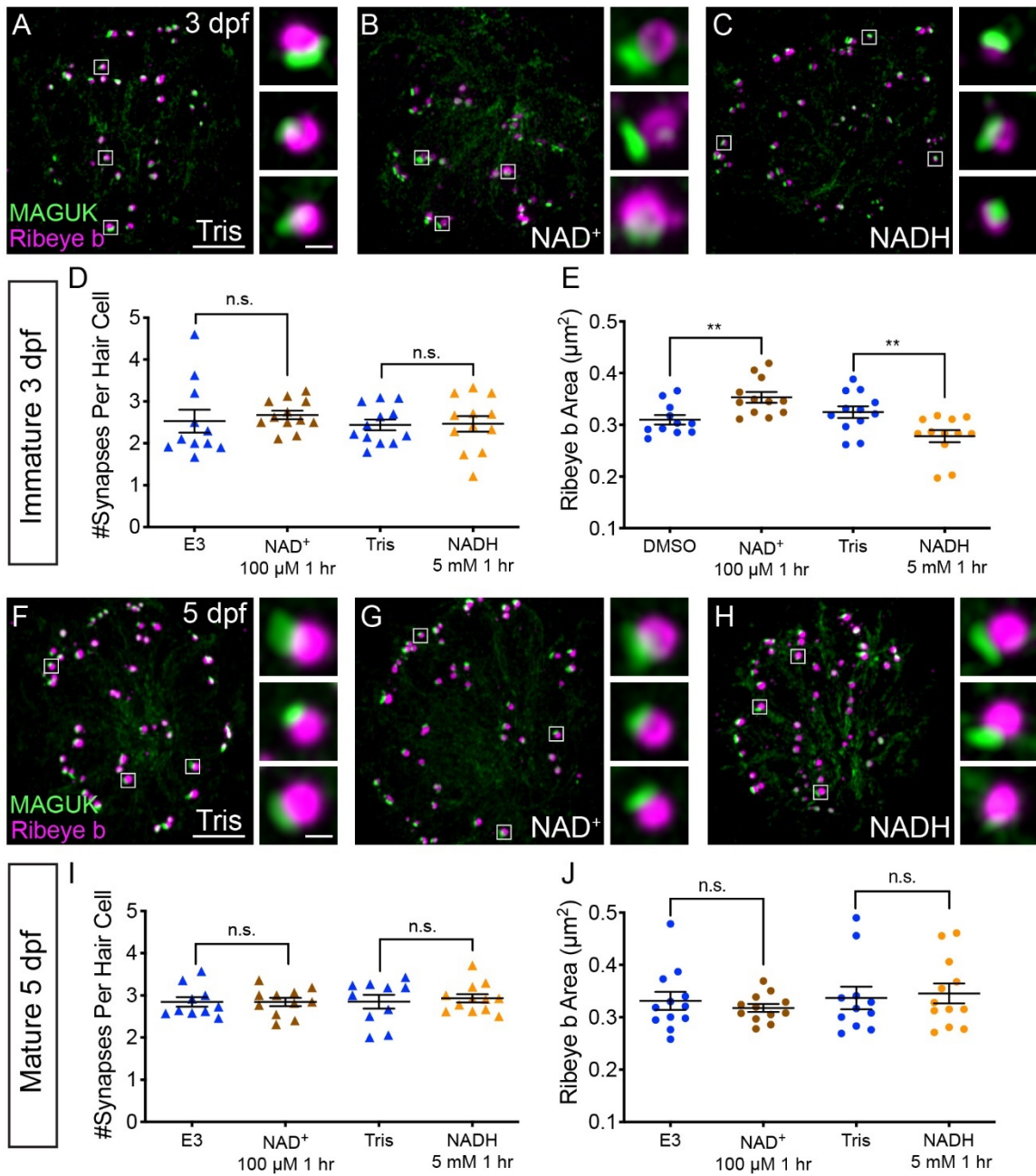
A, RGECO1 baseline measurements before and after a 30-min mock treatment (0.1 % DMSO) or after a 30-min 10 μ M Bay K8644 (BayK), 10 μ M isradipine, or 10 μ M Ru360 treatment in immature hair cells. B, MitoGCaMP3 baseline measurements before and after a 30-min mock treatment (0.1 % DMSO) or after a 10 μ M BayK, 10 μ M isradipine, or 10 μ M Ru360 treatment in immature hair cells. C-D, Rex-YFP baseline measurements before and after 30-min mock treatment (0.1 % DMSO) or after a 30 min 100 μ M NAD⁺, 5 mM NADH, 10 μ M isradipine, or 10 μ M Ru360 treatment, in immature (C) and mature (D) hair cells. All plots are box-and-whiskers plot that show median, min and max. $N \geq 9$ neuromasts per treatment. A one-way Brown-Forsythe ANOVA with Dunnett's T3 post hoc was used to calculate the difference in A-B, and a one-way Brown-Forsythe and Welch ANOVA with Holm-Sidak's post hoc was used in C-D, $*p < 0.05$, $***p < 0.001$, $****p < 0.0001$. Horizontal lines in B-D indicate that both conditions had similar p values compared to mock treatment.

NAD⁺ and NADH directly influence ribbon formation

Our Rex-YFP measurements suggest that in developing hair cells, Cav1.3 and MCU Ca²⁺ activities normally function to decrease the NAD⁺/NADH ratio; furthermore, these activities may function to restrict ribbon size. Conversely, blocking these activities increases the NAD⁺/NADH ratio and may increase ribbon size. If the NAD⁺/NADH ratio is an intermediate step between Cav1.3 and MCU channel activities and ribbon formation, we predicted that more NAD⁺ or NADH would increase or decrease ribbon size respectively. To test this prediction, we treated developing hair cells with exogenous NAD⁺ or NADH.

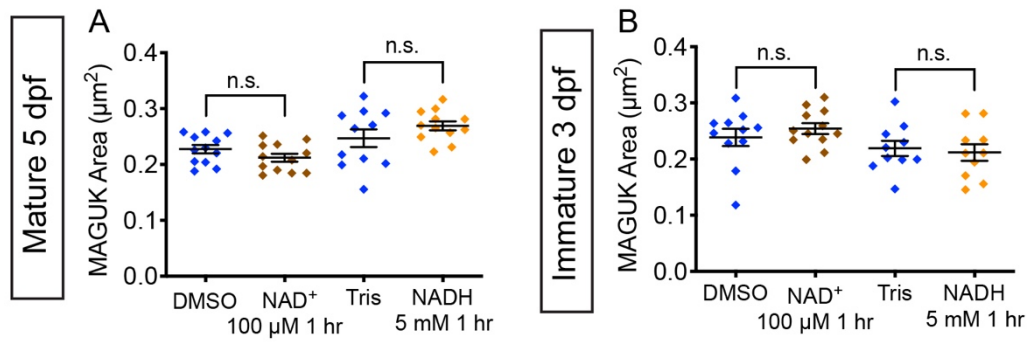
After a 1-hr treatment with 100 μM NAD⁺, we found that the ribbons in developing hair cells were significantly larger compared to controls (Figure 3.8A-B, E). In contrast, after a 1-hr treatment with 5 mM NADH, ribbons were significantly smaller compared to controls (Figure 3.8A, C, E). Neither exogenous NAD⁺ nor NADH were able to alter ribbon size in mature hair cells (Figure 3.8F-H, J). These concentrations of NAD⁺ and NADH altered neither the number of synapses per hair cell nor postsynapse size in developing or mature hair cells (Figure 3.8D, I, Figure 3.9). These results suggest that in developing hair cells, NAD⁺ promotes while NADH inhibits Ribeye-Ribeye interactions or Ribeye localization to the ribbon. Overall these results support the idea that during development, the levels of NAD⁺ and NADH can directly regulate ribbon size *in vivo*.

Figure 3.8. NAD^+ and NADH directly influence ribbon formation.



Representative images of immature (A-C, 3 dpf) and mature (G-H, 5 dpf) neuromasts immunostained with Ribeye b (magenta, ribbons) and MAGUK (green, postsynapses) after a 0.1 % Tris-HCl (A, F), 100 μ M NAD⁺ (B, G) or 5 mM NADH treatment (C, H). Insets show 3 example synapses (white squares). D-E and I-J, Scatter plots show synapse count (D, I) and ribbon area (E, J) in controls and treatments groups. $N \geq 10$ neuromasts per treatment. Error bars in B-C represent SEM. An unpaired *t*-test was used for comparisons in D and I and a Welch's unequal variance *t*-test was used for comparisons in E and J, $**p < 0.01$. Scale bar = 5 μ m in A and F, 2 μ m in insets.

Figure 3.9. NAD⁺ and NADH treatment do not impact postsynapse size.



Quantification of postsynapse size assayed by MAGUK immunolabel in mature (A) and immature (B) neuromasts indicate the treatment with 100 μM NAD^+ and 5 mM NADH do not significantly alter postsynapse size compared to controls, $n \geq 9$ neuromasts per treatment. Error bars represent SEM. A Welch's unequal variance t -test was used for comparisons.

Discussion

In this study, we determined in a physiological setting how mitochondrial- Ca^{2+} influences presynapse function and formation in developing hair cells. In developing hair cells mitochondrial- Ca^{2+} uptake is not critical for evoked presynapse activity. Instead, in developing hair cells, spontaneous $\text{Ca}_v1.3$ channel Ca^{2+} influx drives Ca^{2+} into mitochondria. These spontaneous Ca^{2+} activities regulate presynaptic ribbon size. Elevated mitochondrial- Ca^{2+} levels rapidly lower the NAD^+/NADH ratio and downregulate ribbon formation. Furthermore, during development, NAD^+ and NADH can directly increase and decrease ribbon formation respectively. Our study reveals an intriguing mechanism that couples presynaptic activity with mitochondrial- Ca^{2+} to regulate the formation of a presynaptic structure.

Functional significance of ribbon size

Our work outlines how during development, spontaneous presynaptic activity controls the size of ribbons. When either presynaptic- Ca^{2+} influx or mitochondrial- Ca^{2+} uptake was perturbed, ribbons were significantly larger (Figure 3.4A-C, E; Sheets et al., 2012). But why regulate ribbon size?

Previous work has reported variations in ribbon size and shape among hair-cell types and species (Moser et al., 2006). In many instances ribbon size is correlated with functional properties of the synapse. For example, in the mammalian vestibular system, the ribbons of type II dimorphic hair cells in the striolar region are larger than those in the extrastriolar region (Lysakowski and Goldberg, 1997). Functionally, afferents that innervate hair cells with larger ribbons in the striolar region have lower rates of spontaneous activity compared

to afferents that innervate hair cells in the extrastriolar region (Eatock et al., 2008; Goldberg et al., 1984; Risner and Holt, 2006). Similarly, in the mammalian auditory system, ribbon size is correlated with differences in afferent activity. Inner hair cells are populated by ribbons with a range of sizes, each of which is innervated by a unique afferent fiber. Compared to larger ribbons, smaller ribbons within inner hair cells are innervated by afferent fibers with higher thresholds of activation and lower rates of spontaneous activity (Furman et al., 2013; Kalluri and Monges-Hernandez, 2017; Liberman and Liberman, 2015; Liberman et al., 2011, 1990; Merchan-Perez and Liberman, 1996; Song et al., 2016; Yin et al., 2014). Interestingly, in mice, differences in ribbon size can be distinguished just after the onset of hearing (Liberman and Liberman, 2016). This timing suggests that similar to our data (Figure 3.2, 3.4), activity during development may help determine ribbon size.

Previous work in the zebrafish-lateral line has also examined how ribbon size impacts synapse function (Sheets, 2017). This work overexpressed Ribeye in zebrafish hair cells to dramatically enlarge ribbons. Functionally, compared to controls, hair cells with enlarged ribbons were associated with afferent neurons with lower spontaneous activity (Sheets et al., 2017). Furthermore, the onset encoding, or the timing of the first afferent spike upon stimulation, was significantly delayed in hair cells with enlarged ribbons. Together, both studies in zebrafish and mammals indicate that ribbon size can impact the functional properties of the synapse. Based on these studies, we predict that the alterations to ribbon size we observed in our current study would impact functional properties of the synapse in a similar manner. For example, pharmacological treatments that enlarge ribbons (Figure 3.4: MCU channel block; Figure 3.8: exogenous NAD^+) would also lower spontaneous spiking in afferents and delay onset encoding.

Ribeye and CtBP localization at synapses

In this study, we found that NAD(H) redox state had a dramatic effect on ribbon formation. NAD⁺ promotes while NADH reduces ribbon size (Figure 3.8). The main component of ribbons is Ribeye. Ribeye has two domains, a unique A-domain and a B-domain that contains an NAD(H) binding domain (Schmitz et al., 2000). *In vitro* work on isolated A- and B-domains has shown that both NAD⁺ and NADH can affect interactions between A- and B-domains as well as B-domain interactions (Magupalli et al., 2008). In the context of ribbons, the B-domain has been shown to concentrate at the interface between the ribbon and the membrane opposing the postsynapse (Sheets et al., 2014). Therefore, promoting B-domain homodimerization may act to seed larger ribbons at the presynapse. In this scenario, NAD⁺ and NADH could increase and decrease B-domain homodimerization to impact ribbon size. We also observed an increase in cytosolic Ribeye aggregates after MCU block (Figure 3.4F-G). Therefore, it is alternatively possible that NAD⁺ and NADH could impact interactions between A- and B-domains more broadly. NAD(H) redox could alter Ribeye interactions and alter the overall accumulation or separation of Ribeye within aggregates or at the presynapse.

Work in zebrafish has characterized lateral-line hair cells largely depleted of full-length Ribeye (Lv et al., 2016). When viewed using TEM, ribbons in Ribeye-depleted hair cells are strikingly transparent, suggesting that full-length Ribeye is required for the characteristic electron-dense structure of ribbons. Although these ribbons are smaller compared to controls, they are still able to tether vesicles near the active zone. Ribeye-depleted hair cells could be used to test whether mitochondrial-Ca²⁺ and NAD(H) redox regulate ribbons size by impacting Ribeye interactions. If full-length Ribeye and its NAD(H)

binding domain are the site of regulation, we predict that Ribeye-depleted hair cells will be unaffected by perturbations in mitochondrial- Ca^{2+} and NAD(H).

Regardless of the exact mechanism, the effect of presynaptic activity, mitochondrial- Ca^{2+} and related changes in NAD(H) redox homeostasis may extend beyond the sensory ribbon synapse. Ribeye is a splice variant of the transcriptional co-repressor CtBP2 (Schmitz et al., 2000). While the A-domain is unique to Ribeye, the B-domain is nearly identical to CtBP2 minus the nuclear localization sequence (NLS) (Hübler et al., 2012). In vertebrates, the CtBP family also includes CtBP1 (Chinnadurai, 2007). CtBP proteins are expressed in both hair cells and the nervous system, and there is evidence that both CtBP1 and CtBP2 may act as scaffolds at neuronal synapses (Hübler et al., 2012; tom Dieck et al., 2005). Interestingly, in cultured neurons, it has been shown that synaptic activity is associated with both an increase in CtBP1 localization at the presynapse as well as a decrease in the NAD^+/NADH ratio (Ivanova et al., 2015). In our *in vivo* study, we also found that the NAD^+/NADH ratio was lower in developing hair cells with presynaptic activity (Figure 3.7C). But in contrast to *in vitro* work on CtBP1 in cultured neurons, we found that Ribeye localization to the presynapse and ribbon size were reduced when the NAD^+/NADH ratio was lowered (Figure 3.8A-C). It is unclear why presynaptic activity regulates Ribeye localization differently from that of CtBP1. Ribeye and CtBP1 behavior may differ due to the divergent function of their N-terminal domains. Synaptic localization may also be influenced by external factors, such as the cell type in which the synapse operates, whether the study is performed *in vitro* or *in vivo*, as well as the maturity of the synapse. Overall, both studies demonstrate that the presynaptic localization of CtBP family members CtBP1 and Ribeye can be influenced by synaptic activity and NAD(H) redox state.

Role of spontaneous mitochondrial-Ca²⁺ uptake in developing hair cells

In addition to a role in synapse function, mitochondria have been studied in the context of cellular metabolism and cell death (Devine and Kittler, 2018; Tait and Green, 2013; Vakifahmetoglu-Norberg et al., 2017). Our work suggests that mitochondria may play distinct roles in these processes in developing and mature hair cells. We found that mitochondria spontaneously take up Ca²⁺ at the presynapse during hair-cell development (Figure 3.2B-C). Blocking presynaptic- and mitochondrial-Ca²⁺ activities rapidly decreased the NAD⁺/NADH ratio and altered ribbon size in developing hair cells (Figure 3.4, 3.7, 3.8). However, in mature hair cells, blocking these activities was pathological and did not influence NAD(H) redox (Figure 3.7C).

Some insight into these differences can be inferred from cardiac myocytes where the relationship between mitochondrial-Ca²⁺ and NAD(H) redox has been extensively studied. Similar to our results in developing hair cells, in cardiac myocytes, mitochondrial-Ca²⁺ drives cellular metabolism, which reduces NAD⁺ to NADH (Bertero and Maack, 2018). In cardiac myocytes NADH is oxidized to NAD⁺ when the MCU is blocked. These results are consistent with the changes in NAD(H) redox we observed in developing, but not mature hair cells. Instead, after complete MCU block in mature hair cells, we observed a loss of hair cells and synapses, and an increase in ribbon size (Figure 2.6). This outcome may be more similar to what occurs in heart failure or after extended MCU block—in cardiac myocytes, the production of oxidized NAD⁺ quickly leads to energetic deficits, oxidative stress and ultimately the generation of reactive oxygen species (ROS) (Bertero and Maack, 2018). This is consistent with work in many cell types where mitochondrial-Ca²⁺ loading is associated with pathological processes such as ROS production, cell death and synapse loss (Cai and

Tammineni, 2016; Court and Coleman, 2012; DiMauro and Schon, 2008; Esterberg et al., 2013, 2014; Sheng and Cai, 2012). Therefore, in mature hair cells, it is possible that after MCU block, changes in NAD(H) redox quickly become pathological. Recent work has suggested that younger hair cells may be more resilient to ototoxins, perhaps because they have not yet accumulated an excess of mitochondria oxidation (Pickett et al., 2018). This could explain why complete MCU block alters NAD(H) redox without any observable pathological consequence in developing hair cells. In the future it will be exciting to use zebrafish to explore how mitochondrial- Ca^{2+} influx is impacted by pathological treatments such as age, noise and ototoxins.

Although studies have demonstrated that there are spontaneous presynaptic- Ca^{2+} signals in developing mammalian hair cells (Marcotti et al., 2003; Tritsch et al., 2010), these Ca^{2+} signals have not been reported in zebrafish hair cells. Currently, no studies have investigated what happens downstream of spontaneous presynaptic- Ca^{2+} signals in hair cells. Our work highlights the mitochondria as a downstream signaling organelle that can couple presynaptic activity to ribbon formation. In the future, zebrafish will be a useful model to further explore the origin and role of these Ca^{2+} signals.

Materials and Methods

Zebrafish husbandry and genetics

Zebrafish husbandry and genetics

Adult *Danio rerio* (zebrafish) were maintained under standard conditions. Larvae 2 to 6 days post-fertilization (dpf) were maintained in E3 embryo medium (in mM: 5 NaCl, 0.17 KCl, 0.33 CaCl₂ and 0.33 MgSO₄, buffered in HEPES pH 7.2) at 28°C. All husbandry and experiments were approved by the NIH Animal Care and Use program under protocol #1362-13. Transgenic zebrafish lines used in this study include: *Tg(myo6b:GCaMP6s-CAAX)^{idc1}* (Jiang et al., 2017), *Tg(myo6b:RGECO1)^{no10Tg}* (Maeda et al., 2014), *Tg(myo6b:mitoGCaMP3)^{w119Tg}* (Esterberg et al., 2014), and *Tg(myo6b:ribeye a-tagRFP)^{idc11Tg}* (Sheets, 2017). Experiments were performed using Tübingen or TL wildtype strains.

Cloning and transgenic fish production

To create transgenic fish, plasmid construction was based on the tol2/Gateway zebrafish kit developed by the lab of Chi-Bin Chien at the University of Utah (Kwan et al., 2007). *Tg(myo6b:mitoRGECO1)^{idc12Tg}* was created as described in chapter 2 (see Materials and Methods, “Cloning and transgenic fish production”). The same method was used to create *Tg(myo6b:Rex-YFP)^{idc13Tg}* transgenic line. *Rex-YFP* was cloned into the middle entry vector pDONR221 using the primers listed in Table 3.1. Vectors p3E-polyA and pDestTol2CG2 were recombined with p5E-*myosinVIb* (*myo6b*) and our engineered plasmids to create *myo6b:REX-YFP*. To generate transgenic fish, DNA clones (25-50 ng/μl) were injected along with *tol2* transposase mRNA (25-50 ng/μl) into zebrafish embryos at the single-cell stage.

Table 3.1. Primers used to generate *Tg(myo6b:Rex-YFP)^{idc13Tg}*

Designation	Source or reference	Identifiers	Additional information
Rex-YFP attB FWD	This paper	PCR primers	GGGGACAAGTTTGTACA AAAAAGCAGGCTCCGCC ACCATGAAGGTCCCCGA AGCG; Made by Integrated DNA Technologies (IDT).
Rex-YFP attB REV	This paper	PCR primers	GGGGACCACTTTGTACA AGAAAGCTGGGTGTCAC CCCATCATCTCTCCCG

Pharmacological treatment of larvae for immunohistochemistry

For pharmacological studies, zebrafish larvae were exposed to compounds diluted in E3 with 0.1 % DMSO (Isradipine, Bay K8644, NAD⁺ (Sigma-Aldrich, St. Louis, MO), Ru360 (Millipore, Burlington, MA), TRO 19622 (Cayman Chemical, Ann Arbor, MI) or Tris-HCl (NADH (Cayman Chemical, Ann Arbor, MI)) for 30 min or 1 hr at the concentrations indicated. E3 with 0.1 % DMSO or Tris-HCl were used as control solutions. In solution at pH 7.0-7.3, NADH oxidizes into NAD⁺ by exposure to dissolved oxygen. To mitigate this, NADH was dissolved immediately before use and was exchanged with a freshly dissolved NADH solution every half hour. Dosages of isradipine, Ru360, Bay K8644, TRO 19622, NAD⁺ and NADH did not confer excessive hair-cell death or synapse loss unless stated. After exposure to the compounds, larvae were quickly sedated on ice and transferred to fixative.

***In vivo* imaging of baseline Ca²⁺ and NAD(H) redox**

To prepare larvae for imaging, larvae were immobilized as previously described (Kindt et al, 2012). Briefly, larvae were anesthetized with tricaine (0.03 %) in E3 and pinned to a chamber lined with Sylgard 184 Silicone Elastomer (Dow Corning, Midland, MI). Larvae were injected with 125 μM α-bungarotoxin (Tocris, Bristol, UK) into the pericardial cavity to induce paralysis. Tricaine was rinsed off the larvae and replaced with fresh E3.

For baseline measurements of Rex-YFP and CytoRGECO1 fluorescence, larvae were imaged using an upright Nikon ECLIPSE Ni-E motorized microscope (Nikon Inc., Tokyo, Japan) in widefield mode with a Nikon 60x 1.0 NA water-immersion objective, an

480/30 nm excitation and 535/40 nm emission filter set or 520/35 nm excitation and 593/40 nm emission filter set, and an ORCA-D2 camera (Hamamatsu Photonics K.K., Hamamatsu City, Japan). Acquisitions were taken at 5 Hz, in 15 plane Z-stacks every 2 μm . For baseline measurements of MitoGCaMP3, larvae were imaged using a Bruker Swept-field confocal microscope (Bruker Inc., Billerica, MA), with a Nikon CFI Fluor 60x 1.0 NA water-immersion objective. A Rolera EM-C2 CCD camera (QImaging, Surrey, Canada) was used to detect signals. Acquisitions were taken using a 70 μm slit at a frame rate of 10 Hz, in 26 plane Z-stacks every 1 μm . MitoGCaMP3 baseline intensity varied dramatically in controls between timepoints. To offset this variability, we acquired and averaged the intensity of 4 Z-stacks per time point. For all baseline measurements transgenic larvae were first imaged in E3 with 0.1 % DMSO or 0.1 % Tris-HCl as appropriate. Then larvae were exposed to pharmacological agents for 30 min and a second acquisition was taken. Any neuromasts with cell death after pharmacological or mock treatment were excluded from our analyses.

***In vivo* imaging of evoked Ca^{2+} signals**

To measure evoked Ca^{2+} signals in hair cells, larvae were immobilized in a similar manner as described for baseline measurements. After α -bungarotoxin paralysis, larvae were immersed in neuronal buffer solution (in mM: 140 NaCl, 2 KCl, 2 CaCl_2 , 1 MgCl_2 and 10 HEPES, pH 7.3). Evoked Ca^{2+} measurements were acquired using the Bruker Swept-field confocal system described above. To stimulate lateral-line hair cells, a fluid-jet was used as previously described to deliver a saturating stimulus (Lukasz and Kindt, 2018).

To measure presynaptic GCaMP6sCAAX signals at ribbons, images were acquired with 1 x 1 binning using a 35 μm slit at 50 Hz in a single plane containing presynaptic

ribbons (Figure 2.5C-C'). Ribbons were marked in live hair cells using the *Tg(myo6b:ribeye a-tagRFP)^{idc11Tg}* transgenic line (Figure 2.5C). Ribbons were located relative to GCaMP6s signals by acquiring a 2-color Z-stack of 5 planes every 1 μm at the base of the hair cells. To correlate presynaptic GCaMP6sCAAX signals with MitoRGECO1 signals in hair cells, 2-color imaging was performed. Images were acquired in a single plane with 2 x 2 binning at 10 Hz with a 70 μM slit. MitoGCaMP3 signals were acquired at 10 Hz in Z-stacks of 5 planes 1 μm apart with 2 x 2 binning and a 70 μM slit. High speed imaging along the Z-axis was accomplished by using a piezoelectric motor (PICMA P-882.11-888.11 series, Physik Instrumente GmbH, Karlsruhe, Germany) attached to the objective to allow rapid imaging at a 50 Hz frame rate yielding a 10 Hz volume rate. Due to the slow mitochondrial- Ca^{2+} return to baseline after stimulation (~ 5 min), we waited a minimum of 5 min before initiating a new evoked GCaMP6sCAAX or MitoGCaMP3 acquisition. To examine mechanotransduction, GCaMP6sCAAX signals were measured in apical hair bundles (Figure 2.5A-B'). Apical GCaMP6sCAAX signals were acquired in a single plane at 1 x 1 binning with a 35 μM slit at 20 Hz. For pharmacological treatment, acquisitions were made prior to drug treatment and after a 30-min incubation in the pharmacological agent. Any neuromasts with cell death after pharmacological treatment were excluded from our analyses.

***In vivo* imaging of spontaneous Ca^{2+} signals**

To measure spontaneous Ca^{2+} signals in hair cells, larvae were prepared in a similar manner as described for evoked Ca^{2+} measurements. Spontaneous Ca^{2+} measurements were acquired using the Bruker Swept-field confocal system described above. To measure spontaneous presynaptic GCaMP6sCAAX signals, images were acquired with 2 x 2 binning with a 70 μm slit at 0.33 Hz in a single plane for 900 s. For acquisition of two-color

spontaneous presynaptic GCaMP6sCAAX and MitoRGECO1 signals images were acquired with 2 x 2 binning with a 70 μ m slit at 0.2 Hz in a single plane for 900 s.

Immunofluorescence staining and Airyscan imaging

Whole larvae were fixed with 4 % paraformaldehyde in PBS at 4°C for 3.5-4 hr as previously described (Zhang et al., 2018). Fixative was washed out with 0.01 % Tween in PBS (PBST) in 4 washes, 5 min each. Larvae were then washed for 5 min with H₂O. The H₂O was thoroughly removed and replaced with ice-cold acetone and placed at -20°C for 3 min for 3 dpf and 5 min for 5 dpf larvae, followed by a 5-min H₂O wash. The larvae were then washed for 4 x 5 min in PBST, then incubated in block overnight at 4°C in blocking solution (2 % goat serum, 1 % bovine serum albumin, 2 % fish skin gelatin in PBST).

Primary and secondary antibodies were diluted in blocking solution. Primary antibodies and their respective dilutions are: Ribbon label: Mouse anti-Ribeye b IgG2a, 1:10,000 (Sheets et al., 2011); PSD label: Mouse anti-pan-MAGUK IgG1, 1:500 (MABN72, MilliporeSigma, Burlington, MA); Hair-cell label: Rabbit anti-Myosin VIIa, 1:1000 (#25-6790, Proteus BioSciences Inc., Ramona, CA); Ca_v1.3 channel label: Rabbit anti-Ca_v1.3a, 1:500 (Sheets et al., 2012). Larvae were incubated in primary antibody solution for 2 hr at room temperature. After 4 x 5 min washes in PBST to remove the primary antibodies, diluted secondary antibodies were added and samples were incubated for 2 hr at room temperature. Secondary antibodies and their respective dilution are as follows: goat anti-mouse IgG2a, Alexa Fluor 488, 1:1000; goat anti-rabbit IgG (H+L) Alexa Fluor 546, 1:1000; goat anti-mouse IgG1 Alexa Fluor 647, 1:1000 (Thermo Fisher Scientific, Waltham, MA). Secondary antibodies were washed out with PBST for 3 x 5 min, followed by a 5-min wash with H₂O. Larvae were

mounted on glass slides with Prolong Gold Antifade Reagent (Invitrogen, Carlsbad, CA) using No. 1.5 coverslips.

Prior to Airyscan imaging, live samples were immobilized in 2 % low-melt agarose in tricaine (0.03 %) in cover-glass bottomed dishes. Live and fixed samples were imaged on an inverted Zeiss LSM 780 laser-scanning confocal microscope with an Airyscan attachment (Carl Zeiss AG, Oberkochen, Germany) using an 63x 1.4 NA oil objective lens. The median (\pm median absolute deviation) lateral and axial resolution of the system was measured at 198 ± 7.5 nm and 913 ± 50 nm (full-width at half-maximum), respectively. The acquisition parameters were adjusted using the control sample such that pixels for each channel reach at least 1/10 of the dynamic range. The Airyscan Z-stacks were processed with Zeiss Zen Black software v2.1 using 3D filter setting of 7.0. Experiments were imaged with the same acquisition settings to maintain consistency between comparisons.

Quantification and Statistical Analysis

Analysis of Ca²⁺ and NAD(H) signals, processing, and quantification

To quantify changes in baseline Ca²⁺ and NAD(H) homeostasis, images were processed in FIJI. For our measurements we quantified the fluorescence in the basal-most 8 μ m (4 planes) to avoid overlap between cells. The basal planes were max Z-projected, and a 24.0 μ m (Rex-YFP and RGECO1) or 26.8 μ m (MitoGCaMP3) circular region of interest (ROI) was drawn over the neuromast to make intensity measurements. To correct for

photobleaching, a set of mock-treated control neuromasts were imaged during every trial. These mock treatments were used to normalize the post-treatment intensity values.

To quantify the magnitude of evoked changes in Ca^{2+} , images were processed in FIJI. Images in each time series were aligned using Stackreg (Thevenaz et al., 1998). For evoked MitoRGECO1, MitoGCaMP3, CytoGCaMP3 and two-color GCaMP6sCAAX and MitoRGECO1 signals, Z-stacks were max z-projected, and a 5 μm diameter circular ROI was drawn over each hair cell to make intensity measurements. For ribbon-localized measurements, GCaMP6sCAAX signals were measured within 1.34 μm round ROIs at individual ribbons, and intensity change at multiple ribbons per cell were averaged. For measurements of mechanotransduction, GCaMP6sCAAX signals were measured within 1.34 μm round ROIs at individual hair bundles, and intensity change in multiple bundles per neuromast were averaged.

To plot evoked changes in Ca^{2+} , we subtracted the baseline (F_0 , signal during the pre-stimulus period) was subtracted from each timepoint acquired. Then each timepoint was divided by F_0 to generate the relative change in fluorescent signal from baseline or $\Delta F/F_0$. Quantification of evoked Ca^{2+} signals were made on max $\Delta F/F_0$ measurements. Cells with presynaptic Ca^{2+} activity are defined by max $\Delta F/F_0$ of > 0.05 for MitoRGECO1 and MitoGCaMP3, and max $\Delta F/F_0 > 0.25$ for GCaMP6sCAAX for a 2-s stimulation. The method to obtain and overlay the spatial signal distribution of evoked signals as heat maps has been previously described (Lukasz and Kindt, 2018). We first computed the baseline image (F_0 or reference image) by averaging the images over the pre-stimulus period. Then the F_0 was subtracted from each image acquired, to represent the relative change in fluorescent signal from baseline or ΔF . The ΔF signal images during the stimulus period

were binned, scaled and encoded by color maps with red indicating an increase in signal intensity.

To quantify the average magnitude and frequency of spontaneous Ca^{2+} changes in GCaMP6sCAAX signals, images were processed in Matlab R2014b (Mathworks, Natick, MA) and ImageJ (NIH, Bethesda, MD). First, images in each time series were aligned in ImageJ using Stackreg (Thevenaz et al., 1998). To measure the average magnitude during the 900 s GCaMP6sCAAX image acquisition, a 5 μm diameter circular ROI was drawn over each hair cell and a raw intensity value was obtained from each time point. Then, in Matlab, the raw traces were bleach corrected. Next, the corrected intensity values were normalized as $\Delta F/F_0$. For spontaneous Ca^{2+} signals F_0 is defined as the bottom 15th percentile of fluorescence values (Babola et al., 2018). Then, values of $\Delta F/F_0$ of less than 10 % were removed. These values were considered to be noise and our threshold value for a true signal. A 10 % threshold was determined by imaging spontaneous GCaMP6CAAX signals in the presence of isradipine where no signals were observed (Figure 3.3). The averaged magnitude of spontaneous activity per cell was obtained by dividing the integral/sum of GCaMP6sCAAX signals ($\Delta F/F_0 > 10\%$) during the whole recording period by 300 (300 frames in 900 s). The frequency of GCaMP6sCAAX signals was defined as the average number of peaks per second during the whole recording period.

Image processing and quantification of synapse morphology

To quantify synapse morphology and pairing, images were first processed in ImageJ, and then synapses were paired using Python (Python Software Foundation, Wilmington, DE) in the Spyder Scientific Environment (MIT, Cambridge, MA). In ImageJ, each Airyscan Z-stack was background subtracted using rolling-ball subtraction. Z-stacks containing the

MAGUK channel were further bandpass filtered to remove details smaller than 6 px and larger than 20 px. A duplicate of each Z-stack was normalized for intensity. This duplicated Z-stack was used to identify individual ribbon and MAGUK using the Simple 3D Segmentation of ImageJ 3D Suite (Ollion et al., 2013). Local intensity maxima, identified with 3D Fast Filter, and 3D watershed were used to separate close-by structures. The centroids for each identified ribbon and MAGUK puncta were obtained using 3D Manager and these coordinates were used to identify complete synapses. The max Z-projection of the segmented Z-stack was used to generate a list of 2D objects as individual ROIs corresponding to each punctum. This step also included a minimum size filter: Ribeye: $0.08 \mu\text{m}^2$, MAGUK: $0.04 \mu\text{m}^2$. For quantification of extrasynaptic Ribeye b puncta, the minimum size filter was not applied. The 2D puncta ROI were applied over the max Z-projection of the original Z-stack processed only with background subtraction. This step measures the intensity of the antibody label. Centroid and intensity information were exported as a CSV spreadsheet (macro is available on <https://github.com/wonghc/ImageJ-ribbon-synapse-quantification>).

In Python, the 3D centroid coordinates for each ribbon punctum were measured against the coordinates of every post-synaptic MAGUK punctum to find the MAGUK punctum within a threshold distance. This threshold was calculated by taking the 2D area of the Ribeye and MAGUK punctum measured in the max Z-projection to calculate an approximate radius by dividing by π and taking the square root. The two radii were then summed to get the threshold. Puncta that were not paired were excluded from later statistical analyses of synaptic ribbon and postsynaptic MAGUK puncta. To quantify the amount of Cav1.3 immunolabel at ribbons, 2D ROIs generated from the Ribeye label to generate ribbon areas were applied to a max Z-projection of the Cav1.3 immunolabel. The integrated

intensity of Ca_v1.3 immunolabel was measured within each ROI. The number of hair cells, synapses per cell, and Ca_v1.3 clusters per PSD were counted manually. Hair-cell counts were assayed with Myosin VIIa antibody label in treatments when synapse or cell numbers were reduced. Due to slight variability between clutches and immunostains we only compared experimental data taken from the same clutch, immunostain and imaging session.

Statistics

Statistical analyses and data plots were performed with Prism 8 (Graphpad, San Diego, CA). Values of data with error bars on graphs and in text are expressed as mean \pm SEM unless indicated otherwise. All experiments were performed on a minimum of 2 animals, 6 neuromasts (posterior lateral-line neuromasts L1-L4 or anterior lateral-line neuromasts O1 and O2 (Figure 3.5)), on 2 independent days. For 3 and 5 dpf larvae each neuromast represents analysis from 8-12 hair cells; 24-36 synapses and 14-18 hair cells; 42-54 synapses respectively. All replicates are biological. Based on the variance and effect sizes reported previously and measured in this study, these numbers were adequate to provide statistical power to avoid both Type I and Type II error (Sheets et al., 2012; Zhang et al., 2018). No animals or samples were excluded from our analyses unless control experiments failed—in these cases all samples were excluded. No randomization or blinding was used for our animal studies. Where appropriate, data was confirmed for normality using a D'Agostino-Pearson normality test and for equal variances using a F test to compare variances. Statistical significance between two conditions was determined by either an unpaired *t*-test, an unpaired Welch's unequal variance *t*-test, a Mann-Whitney U test or a Wilcoxon matched-pairs signed-rank test as appropriate. For comparison of multiple conditions, a Brown-Forsythe with Dunnett's T3 post hoc or a Brown-Forsythe and Welch

ANOVA with Holm-Sidak's post hoc were used as appropriate. To calculate the IC₅₀ for Ru360 block of evoked MitoGCaMP3 signals a dose response curve was plotted using 0, 0.5, 2, 5 and 10 μM Ru360. A non-linear fit with four parameters and a variable slope was performed to calculate an IC₅₀ of 1.37 μM.

Acknowledgements

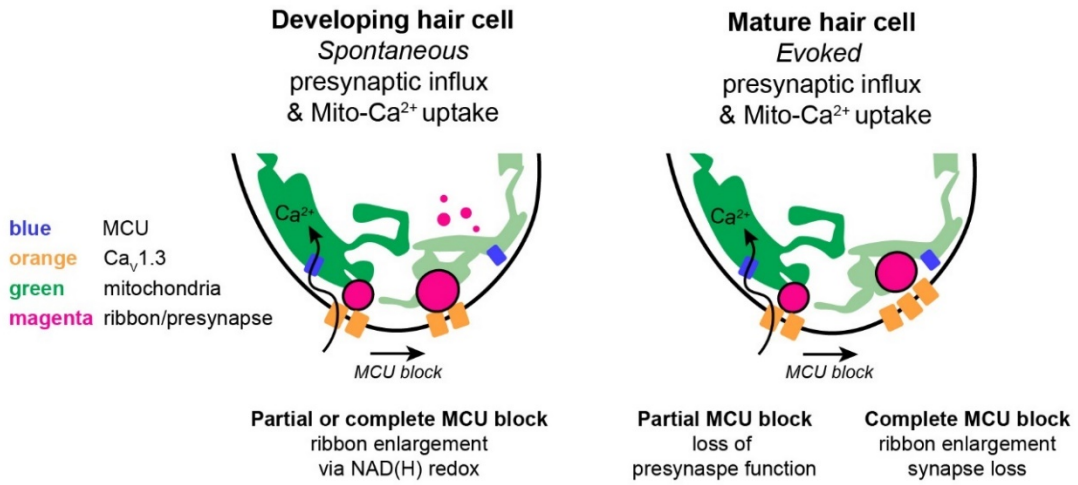
This work was supported by National Institute on Deafness and Other Communication Disorders Intramural Research Program Grant 1ZIADC000085-01 to K.S.K.. We would like to thank Daria Lukasz, Katie Drerup, Paul Fuchs and Doris Wu for their support and thoughtful comments on the manuscript.

K.S.K. and I designed all experiments. I performed all experiments and quantification of results except those pertaining to the change in spontaneous presynaptic Ca²⁺ activity between immature and mature hair cells (designed by K.S.K. and Q.Z. and performed by Q.Z.) and some immunostaining (performed by A.J.B). K.S.K. and I wrote and edited the manuscript.

Chapter 4: Conclusion

Sensory hair cells are critical for communication, the enjoyment of music, and proper balance. The hair cell ribbon synapse is an essential component of hair cell function. It is required for the release of neurotransmitter in order to relay auditory and vestibular signals to the innervating neuron and ultimately the brain. Despite decades of studies, how hair cell ribbon synapses form and how these synapses function is still uncertain. In this thesis, I determined in a physiological setting how mitochondrial- Ca^{2+} influences hair-cell presynapse function and presynapse formation (Figure 4.1).

Figure 4.1. Schematic model of mitochondrial- Ca^{2+} activity and function in developing and mature hair cells.



A, Summary of how in ribbon size is impacted when mitochondrial Ca^{2+} uniporter (MCU, blue) is blocked in the developing hair cell. In the developing hair cell spontaneous presynaptic- Ca^{2+} influx is correlated with and mitochondrial- Ca^{2+} uptake. Blocking mitochondrial- Ca^{2+} uptake also modulates NAD(H) redox, which increases ribbon formation. B, Summary of synaptopathic changes when MCU is blocked in the mature hair cell. Stimulus-evoked mitochondrial- Ca^{2+} uptake is dependent on presynaptic- Ca^{2+} influx. Blocking mitochondrial- Ca^{2+} uptake can adversely affect synaptic function by decreasing the presynaptic- Ca^{2+} influx which triggers synaptic vesicle exocytosis. Blocking mitochondrial- Ca^{2+} uptake also adversely affect the maintenance of presynapse structures, where synapse numbers decrease.

At neuronal presynapses, studies have shown that mitochondrial- Ca^{2+} uptake can modulate evoked presynaptic Ca^{2+} signals and therefore neurotransmission (Devine and Kittler, 2018). In hair cells, the relationship between mitochondrial- Ca^{2+} uptake and presynapse function in hair cells was unclear. Using *in vivo* Ca^{2+} imaging, I examined the spatio-temporal characteristics of evoked presynaptic- and mitochondrial- Ca^{2+} signals. Using this approach, I observed robust mitochondrial Ca^{2+} influx occurring concurrently with evoked presynaptic- Ca^{2+} influx. Furthermore, mitochondria located near to the presynapse had the most rapid and intense Ca^{2+} uptake. Using pharmacological approaches, I demonstrated that evoked mitochondrial- Ca^{2+} uptake at the presynapse is $\text{Ca}_v1.3$ -channel dependent. Interestingly, I found that evoked mitochondrial- Ca^{2+} uptake is important to sustain evoked presynaptic Ca^{2+} responses. Overall these results have revealed mitochondrial- Ca^{2+} uptake as a new way to regulate presynaptic activity in hair cells. Identifying new ways to regulate presynaptic- Ca^{2+} influx is critical for understanding hair cell synaptic transmission, and ultimately hearing and balance. In addition to regulating presynapse function, my work also indicates that mitochondrial- Ca^{2+} levels may be important for maintenance of synaptic architecture. I found that after prolonged block of mitochondrial- Ca^{2+} uptake, there was a loss of synapse integrity. Therefore, it is possible that mitochondrial- Ca^{2+} also may play a role in pathological processes that lead to synapse and hearing loss. In general, these findings represent an example of mitochondria acting on non-neuronal synapse function and maintenance.

Although mitochondrial- Ca^{2+} uptake has been implicated in synapse function in neurons, less is known about the role that mitochondrial Ca^{2+} plays in synapse development. These studies indicate that in developing mouse auditory and vestibular hair cells, spontaneous $\text{Ca}_v1.3$ -dependent Ca^{2+} influx may play an important role in synapse and circuit

formation (Beutner and Moser, 2001; Glowatzki and Fuchs, 2002; Holman et al., 2019; Kros et al., 1998; Marcotti et al., 2003; Sendin et al., 2014; Tritsch and Bergles, 2010; Tritsch et al., 2007, 2010). My work revealed that in developing zebrafish hair cells, there is also spontaneous $\text{Ca}_v1.3$ -dependent Ca^{2+} influx at the presynapse. Further, my work demonstrates that these spontaneous presynaptic signals coincide with spontaneous mitochondrial- Ca^{2+} uptake. Intriguingly, blocking either spontaneous presynaptic- Ca^{2+} influx or mitochondrial- Ca^{2+} uptake impacts ribbon formation (Sheets et al., 2012). Block of either of these activities leads to the formation of larger ribbons. Overall this result indicates that mitochondrial- Ca^{2+} can regulate presynapse formation in developing hair cells. In contrast to zebrafish neuromast, mammalian inner ear is structurally and functionally more complex, containing several mitochondria-rich, highly energetic cell-types. Results from this work highlight that hair cell mitochondria may be themselves an important contributor to inner ear development. Differences in mitochondrial distribution among cells with ribbon synapses, such as between hair cells and retinal photoreceptors and bipolar cells, may reveal further mechanistic insights in ribbon synapse development.

My work also illuminated a downstream process that connects spontaneous presynaptic- or mitochondrial- Ca^{2+} influx with ribbon formation. This process involved the mitochondrial metabolic intermediate, NAD(H). NAD(H) is relevant to ribbons because the main ribbon component, Ribeye protein, contains a NAD(H) binding domain. My work showed that spontaneous presynaptic- and mitochondrial- Ca^{2+} influx lower the NAD^+/NADH ratio to restrict ribbon assembly. Overall, this work outlines an intriguing mechanism that couples spontaneous presynaptic activity with mitochondrial- Ca^{2+} to regulate the formation of a presynaptic structure. This mechanism is fundamentally meaningful because the involvement of NAD^+/NADH ratio homeostasis suggests that

during development, spontaneous presynaptic activity in hair cells can drive metabolic changes (Bogan and Brenner, 2008; Imai, 2009; Li and Sauve, 2015). These metabolic changes can then impact presynapse formation. This mechanism outlines a novel mechanism that describes on a fundamental level how the assembly of presynaptic ribbons is regulated in vivo. The same mechanism may underly the change in ribbon size after noise-damage (Jensen et al., 2015; Kujawa and Liberman, 2009; Liberman and Liberman, 2015; Song et al., 2016), and may be utilized to better understand, prevent and restore the damaged ribbon structure. Proper formation of ribbon synapses also will play an important role in the development of hearing- or balance-restoration therapy based on hair cell regeneration. Better understanding of the structure and formation of the ribbon synapse will contribute to the complete maturation and mechanotransduction function of these newly regenerated hair cells.

Future directions

Overall, this thesis has made significant progress towards understanding the role that mitochondria play at hair cell synapses. This progress prompts new questions. For example, why does mitochondrial Ca^{2+} and cellular metabolism impact ribbon size in developing but not mature hair cells? Additionally, why does block of mitochondrial Ca^{2+} influx impact presynaptic function in mature but not developing hair cells? Along these lines, why does mitochondrial- Ca^{2+} depletion lead to synapse loss and cell death specifically in mature hair cells? These questions highlight just some of the unknowns that must be addressed to understand how the presynapse is affected by mitochondrial Ca^{2+} .

Role of Ribeye NAD(H)-binding domain in presynaptic ribbon formation

In this thesis, I describe how mitochondrial- Ca^{2+} uptake, driven by Cav1.3-dependent Ca^{2+} influx, helps maintain a low NAD^+/NADH ratio to modulate ribbon size during synapse development. I further show that increasing the NAD^+/NADH ratio promotes Ribeye self-aggregation and increases ribbon size. Similarly, NAD^+ or NADH can directly increase or decrease ribbon size. My work concludes that the NAD^+ and NADH ratio acts on Ribeye through its NAD(H) binding domain to regulate Ribeye-Ribeye protein interactions.

Currently, my work has not conclusively demonstrated that NAD^+ and NADH require the Ribeye NAD(H)-binding domain to determine ribbon size. This would require direct manipulation of the NAD(H)-binding domain to assess its importance on ribbon size determination *in vivo*. One way to achieve this manipulation is to generate transgenic zebrafish that express in hair cells an exogenous GFP-tagged Ribeye with a mutated

NAD(H)-binding domain. This transgenic line could be used to visualize the localization of this mutant form of Ribeye and infer the function of NAD(H)-binding domains. It is possible that Ribeye protein lacking an NAD(H)-binding domain would not localize to the presynapse. In addition, this line could be used in conjunction with NAD⁺ or NADH treatment for a comparison between wildtype and mutant Ribeye. The GFP-tagged mutant Ribeye may be unable to respond to NAD⁺ and NADH treatment. In addition to removal of the NAD(H)-binding domain from Ribeye, a transgenic approach also could be used to over-express just the Ribeye NAD(H)-binding domain in hair cells. An excess of Ribeye NAD(H)-binding domain could interfere with or outcompete endogenous Ribeye proteins at the presynapse. Excess Ribeye NAD(H)-binding domain may reduce the amount of endogenous Ribeye protein that localizes to the presynapse, leading to the formation of smaller ribbons.

Alternatively, future research could use genetic manipulations to alter the endogenous NAD(H)-binding domain of Ribeye. Based on my studies, I predict that, in hair cells expressing Ribeye that lacks a NAD(H)-binding domain, ribbons may not be sensitive to alterations in mitochondrial Ca²⁺ or the NAD⁺/NADH ratio, or even fail to anchor to the presynapse during development. Unfortunately, there are two major obstacles for this type of analysis. First, there are two isoforms of *ribeye* in zebrafish, *ribeye a* and *ribeye b*; the NAD(H)-binding domain must be successfully altered in both isoforms. Previously work has successfully lesioned both isoforms of *ribeye* in zebrafish to knockout Ribeye (Lv et al., 2016). In *ribeye a; ribeye b* double knockouts, smaller ribbon-like presynaptic structures still remain. The remaining structure suggests that knockdown is not complete and there may be compensation or splicing around the lesion sites. Second, *ribeye* must be disrupted while preserving *ctbp2*. Ribeye can be separated into a unique A-domain, and a B-domain which is

essentially the transcriptional co-repressor CtBP2. It is the shared B-domain that contains the Ribeye NAD(H)-binding domain. A major hurdle limiting the genetic modification the B-domain of Ribeye is that such modification also disrupts CtBP2 expression. In mammals, CtBP2 protein is an important developmental protein at the organismal level (Hildebrand and Soriano, 2002). To overcome this challenge, it is possible that Ribeye could be genetically altered using a cell-specific or acute knockdown. For example, *ribeye* could be modified in zebrafish hair cells using cell-specific CRISPR-Cas9 gene editing (Ablain et al., 2015). Cell-specific *ribeye* knockout could silence Ribeye/CtBP2 in hair cells, while preserving CtBP2 expression in the rest of the organism. In summary, Ribeye protein lacking a NAD(H) binding domain could be used to study the importance of this domain on synapse assembly and function. Together, manipulating the endogenous Ribeye locus could help determine if the NAD^+/NADH redox ratio specifically regulates Ribeye interactions, and the contribution of the NAD(H)-binding domain.

It is likely that Ribeye-Ribeye interactions and the NAD(H)-binding domain are important for ribbon formation. With regards to ribbon formation, it is also important to understand how mitochondrial- Ca^{2+} and the NAD^+/NADH ratio fit into the series of events that define ribbon formation. Currently the series of events that underlies ribbon formation is unclear. While the sequence of ribbon formation was very well studied in mammals, it is studied as “snapshots in time” and lacks information about the dynamic movement of ribbon proteins. Previous TEM and immunohistochemical studies using mouse hair cells to study ribbon synapse maturation suggests that small ribbon precursors may fuse to form the mature ribbons (Michanski et al., 2019). Ultimately, the ribbons become anchored to the presynaptic membrane. NAD(H)-binding domain may play a role in anchoring Ribeye to the presynapse, based on its localization at the interface of the ribbon and the presynaptic active

zone (Sheets et al., 2014). Additional studies suggest that there may also be a second mode of ribbon synapse maturation where free Ribeye is recruited directly from the cytosol to the ribbon. In support of cytosolic recruitment of Ribeye, previous *in vivo* work has shown that Ribeye proteins can move within and between adjacent ribbons (Chen et al., 2018; Graydon et al., 2017). In general, it is important first to understand the sequence of events that define ribbon formation. Second, the sequence of ribbon formation can serve as a foundation to understand how changes in the NAD^+/NADH ratio affect ribbon size. NAD(H) may regulate ribbon size either by controlling Ribeye anchoring to the presynapse or by regulating the number of extrasynaptic Ribeye puncta that merge with ribbons. One way to test the effect of NAD(H) on Ribeye dynamics in developing hair cells is to use transgenic zebrafish expressing exogenous Ribeye fused to fluorescent proteins. Hair cells expressing fluorescently-labeled Ribeye can be used to record movies of ribbon formation *in vivo*. With sufficient resolution, extrasynaptic Ribeye puncta may be visualized as they migrate from the hair cell midbody towards the base. Ribeye also may be recruited directly from the cytosol to the ribbon, which would become larger without noticeable contribution of extrasynaptic ribbon precursors. Once the sequence of ribbon formation is established in the zebrafish hair cell *in vivo*, ribbon formation may be imaged live while presynaptic- or mitochondrial- Ca^{2+} , or NAD^+/NADH is perturbed. In summary, imaging Ribeye dynamics *in vivo* could better show ribbon formation and the contribution of NAD(H) -binding domains to Ribeye localization.

In addition to Ribeye-Ribeye interactions, NAD(H) redox homeostasis may also impact Ribeye interactions with other presynaptic proteins. To date, only a handful of proteins have been identified in the hair cell ribbon presynapse. One of the most critical presynaptic components is $\text{Cav}1.3$, which requires Ribeye directly for localization to the

presynapse in the zebrafish hair cell (Sheets et al., 2011). Bassoon is a presynaptic protein that likely also could directly interact with Ribeye. Bassoon is required to anchor the ribbon to the presynapse (Buran et al., 2010; Frank et al., 2010; Jing et al., 2013; Khimich et al., 2005; Meyer et al., 2009). In hippocampal neurons, Bassoon interacts with CtBP1, which is homologous to the Ribeye-B domain (Ivanova et al., 2015). It is possible that NAD(H) redox homeostasis may impact Ribeye interactions with Bassoon or Cav1.3 channels to influence ribbon formation.

My work indicates that mitochondrial- Ca^{2+} impacts Cav1.3 channel clustering in mature hair cells (Figure 2.4E-H). While NAD(H) redox did not appear to change when mitochondrial- Ca^{2+} uptake is blocked (Figure 3.7D), it is possible that local changes in NAD(H) redox below indicator detection threshold can directly impact Cav1.3 channel clustering. Immunostaining of Cav1.3 channel after NAD^+ is applied may show a similar change in channel clustering as blocking mitochondrial- Ca^{2+} uptake. Similarly, the localization of Bassoon at ribbon synapses after blocking mitochondrial Ca^{2+} could be assessed with immunostaining.

In addition to Bassoon and Cav1.3, Piccolino was shown to localize to ribbons in zebrafish hair cells and interact with Ribeye in the retinal ribbon. Initial work indicates that Piccolino localization may not be affected by the loss of Ribeye NAD(H) binding (Michanski et al., 2019; Müller et al., 2019). However, other work on retinal ribbons indicates that Piccolino may interact with Ribeye through a PxDLS-motif (Müller et al., 2019). In support of this idea, *in vitro* work on the Ribeye homolog CtBP1 shows that mutation of NAD(H)-binding domain did not affect PxDLS-dependent protein interaction (Madison et al., 2013). Overall, these genetic, immunohistological, and imaging approaches highlight how

the zebrafish hair cell may be used to study ribbon formation in detail. These approaches may be used to investigate how NAD(H) redox homeostasis modulates the composition of the ribbon presynapse through the Ribeye NAD(H)-binding domain.

The role of mitochondrial- Ca^{2+} uptake in hair cells

Ca^{2+} is tightly regulated within cells, and several mechanisms are in place to isolate Ca^{2+} signaling domains. For example, Ca^{2+} that enters the cell does not remain free in the cytosol but instead is quickly bound by cytosolic buffers. Organelles also can regulate Ca^{2+} signaling—my work and others have shown that mitochondria act as a Ca^{2+} buffer for Ca^{2+} clearance at the hair cell stereocilia bundle, and to promote presynaptic- Ca^{2+} influx at the base of the hair cell (Beurg et al., 2010; Boyer et al., 2001; Pickett et al., 2018; Yamoah et al., 1998).

In my thesis work, I characterized mitochondrial- Ca^{2+} stores at the hair cell presynapse and linked this store to ribbon synapse formation and function. My work reveals a new function for mitochondrial- Ca^{2+} uptake in synapse formation, synaptic activity and cell health. It is interesting that mitochondrial- Ca^{2+} plays many important roles and that these roles change during hair cell maturation. In immature hair cells, blocking mitochondrial- Ca^{2+} uptake increases ribbon size during synapse development, and can lead to the formation of extrasynaptic Ribeye-containing puncta. In contrast, blocking mitochondrial- Ca^{2+} uptake in mature hair cells reduces presynaptic- Ca^{2+} influx and leads to synapse and hair cell loss.

It is unclear how, in mature hair cells, presynaptic- Ca^{2+} influx is reduced by blocking mitochondrial- Ca^{2+} uptake. I have shown that loss of mitochondrial Ca^{2+} storage does not decrease presynaptic- Ca^{2+} influx by reducing the Ca^{2+} concentration gradient across the cell

membrane. My work and others have shown that blocking mitochondrial- Ca^{2+} uptake has no effect on cytosolic- Ca^{2+} levels or presynaptic- Ca^{2+} clearance at ribbon synapses (Figure 2.9A, Figure 3.7A; Frank et al., 2009). However, I found that blocking mitochondrial- Ca^{2+} uptake increased $\text{Ca}_v1.3$ clustering at the presynapse. An increase in $\text{Ca}_v1.3$ channel clustering may reduce presynaptic- Ca^{2+} influx through Ca^{2+} -dependent inactivation (Platzer et al., 2000; Schnee and Ricci, 2003). Alternatively, it could be a compensatory strategy to recover presynaptic- Ca^{2+} influx activity after MCU block impaired presynaptic- Ca^{2+} influx through another mechanism. Changes in $\text{Ca}_v1.3$ Ca^{2+} -dependent inactivation kinetics as a result of MCU block may be assessed using patch clamp electrophysiology. For example, exogenous Ca^{2+} buffers may be supplied to the cytosol to compensate for the loss of the mitochondrial- Ca^{2+} store (Haack and Rosenberg, 1994). This approach could help illuminate to what extent $\text{Ca}_v1.3$ channel density couples with presynaptic- Ca^{2+} influx. Alternatively, mitochondrial- Ca^{2+} uptake may be itself an important component of presynaptic- Ca^{2+} activity.

Alternatively, presynaptic- Ca^{2+} uptake may be modulated in a non-cell autonomous manner. My work used pharmacology to block MCU-dependent Ca^{2+} uptake activity in the hair cell mitochondria. However, because the compounds are not cell specific, mitochondrial- Ca^{2+} activity in supporting cells and afferent neurons also may be blocked during the treatment. Supporting cells are glia-like cells that intimately surround and isolate hair cells from one another (Balak et al., 1990; Monzack and Cunningham, 2013; Williams and Holder, 2000). These cells are also thought to be critical for hair cell function and health (Hernández et al., 2006, 2007; Ma et al., 2008; Williams and Holder, 2000). To confirm that mitochondrial- Ca^{2+} uptake in hair cells has cell-autonomous effects on ribbon synapses, the MCU could be genetically disrupted in a cell-specific manner. A cell-specific genetic disruption of MCU could allow the study of long-term loss of mitochondrial- Ca^{2+} uptake.

Alternatively, to achieve cell-specificity, a dominant negative approach could be used to abolish MCU channel function. Previously published work identified a dominant negative form of the human MCU subunit in the conserved Ca^{2+} ion selectivity filter domain WDXXEP (Baradaran et al., 2018; De Stefani et al., 2011). A transgenic zebrafish line could be created, expressing this dominant negative form of the MCU specifically in hair cells. These approaches could help illuminate with greater certainty that the contribution of mitochondrial- Ca^{2+} uptake is in hair cells.

In addition to a role in hair cell function, Ca^{2+} stores are also implicated in hair cell pathology. While investigating the effect of blocking mitochondrial- Ca^{2+} uptake on hair cell synapse, I observed that pharmacologically blocking the MCU leads to synapse and hair cell loss in mature hair cells. However, this treatment was not cytotoxic to immature hair cells. Mitochondrial- Ca^{2+} overload is intimately tied to cell death and synapse loss (Baumgartner et al., 2009; Giorgi et al., 2012; Kakkar and Singh, 2007; Peng and Jou, 2010). Recent work in mice has demonstrated that pharmacological block or a loss of function mutation in MCU protected against synapse loss in auditory inner hair cells after noise exposure (Wang et al., 2019). However, mitochondrial- Ca^{2+} uptake is intimately tied to ROS generation (Adam-Vizi and Starkov, 2010; Jensen-Smith et al., 2012; Owens et al., 2007). A proposed reason for age-dependent sensitivity to cytotoxic conditions is that hair cells incur cumulative ROS damage through mitochondrial- Ca^{2+} uptake (Pickett et al., 2018). Therefore, it is not surprising that blocking mitochondrial- Ca^{2+} uptake is not beneficial in the present work, but instead causes hair cell and synapse loss in an age-dependent manner (Figure 2.6E, 3.4D).

To test if blocking mitochondrial- Ca^{2+} uptake is associated with ROS production in mature hair cells, a fluorescent oxidation reporter dye such as cellROX, or the

mitochondrial-targeted equivalent mitoSOX could be used (Esterberg et al., 2016). These oxidation reporters may be applied in conjunction with pharmacological block of MCU or VDAC to determine if ROS production occurs after blocking mitochondrial- Ca^{2+} uptake. If blocking mitochondrial- Ca^{2+} uptake is cytotoxic through the same mechanism as mitochondrial- Ca^{2+} overload, mitoSOX would show an increase in ROS production. It would be interesting to see if blocking mitochondrial- Ca^{2+} uptake also increases cellROX report of cytosolic ROS. Results from this type of study can provide evidence whether MCU-block induces hair cell death via ROS production.

Alternatively, the cytotoxic effects associated with blocking mitochondrial- Ca^{2+} uptake in mature hair cells could reflect cellular stress due to a reduction in ATP production. At pyramidal cortical neuron presynapses, LKB1 protein loss-of-function reduces mitochondrial- Ca^{2+} uptake (Kwon et al., 2016). Paradoxically, while LKB1 has tumor suppressing functions, loss of LKB1 function leads to hypersensitivity to apoptosis induced by energy stress (Shaw et al., 2004). LKB1 can detect changes in the AMP/ATP ratio to activate AMP-activated protein kinase (AMPK) when ATP levels are low (Hawley et al., 2003; Shaw et al., 2004; Woods et al., 2003). It would be interesting to determine if ATP depletion and AMPK activation are involved in the cytotoxic effects associated with blocking mitochondrial- Ca^{2+} uptake in mature hair cells. This could be examined by using an activator of AMPK (Stefanelli et al., 1998). If AMPK is involved in mature hair cells, an activator of AMPK could rescue Ru360-associated cytotoxicity. Overall this approach could help determine if mitochondrial- Ca^{2+} levels are required to respond to energy stress and promote cellular health of mature hair cells.

While blocking MCU is cytotoxic to mature hair cells, this is not so in developing hair cells. This result suggests that mitochondrial- Ca^{2+} may play different roles in the developing and mature hair cell. This could be because developing hair cells use different cellular metabolism pathways compared to mature hair cells. Proliferating cells and tumors have been shown to metabolize glucose preferentially by fermentation rather than oxidative phosphorylation preferred by differentiated cells (Warburg, 1956). For example, in proliferating thymocytes, the ATP produced from glycolysis can exceed that from oxidative phosphorylation in mitochondria (Guppy et al., 1993; Pfeiffer et al., 2001). While glycolysis produces fewer ATP per glucose molecule than oxidative phosphorylation, glycolysis may overall produce more ATP because the process also generates metabolites that serve as building blocks for cell components needed in cell proliferation (Bauer et al., 2004; DeBerardinis et al., 2008). Therefore, it is possible that developing hair cells also predominantly utilize glycolysis to produce ATP and generate cellular structures needed for maturation. Under this assumption, blocking MCU in developing hair cell may impose less energy stress than in mature cells. In contrast, as mature cells rely on oxidative phosphorylation for ATP production, blocking MCU may lead to energy stress and cytotoxicity.

A shift from glycolysis to oxidative phosphorylation in energy generation could be tested in developing and mature hair cells by disrupting oxidative phosphorylation, for example by acute oxygen deprivation (Manchenkova et al., 2015). Oxidative phosphorylation also may be disrupted by inhibiting the mitochondrial pyruvate carrier (Wiemer et al., 1995). Alternatively, mitochondrial uncouplers could be used to dissipate the proton gradient that drives ATP synthesis at the IMM (Zhang et al., 2008). If mature hair cells have a greater reliance on oxidative phosphorylation compared to developing hair cells, disrupting

oxidative phosphorylation using any of these approaches could lead to higher energy stress, ROS production and cell death. In summary, understanding the changing function of mitochondria will inform our understanding of the transition from developing to mature hair cells. It could help to understand why mature hair cells are more vulnerable to insults and how the maturation process may be replicated in regeneration.

Endoplasmic reticulum Ca²⁺ handling

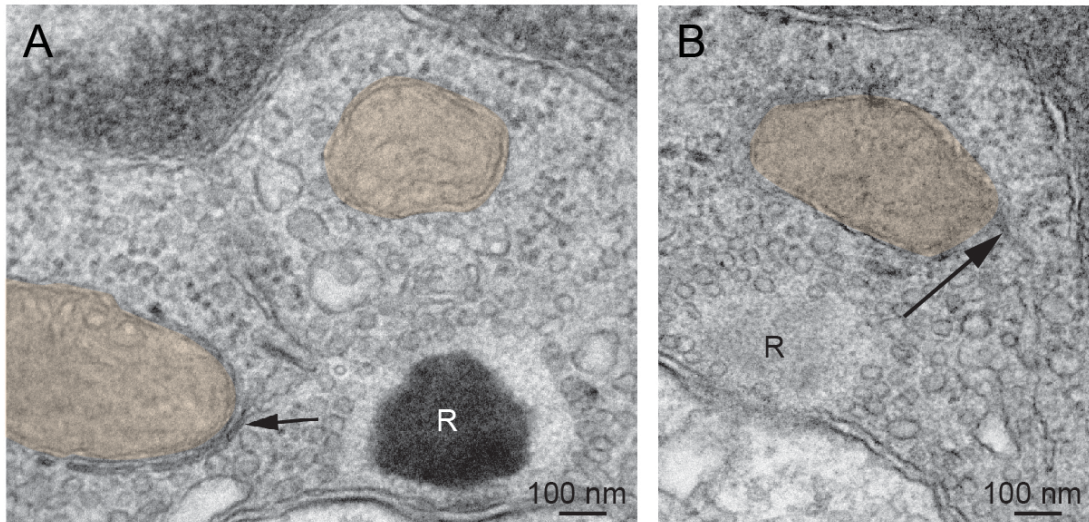
My work and others have shown that mitochondria act as a Ca²⁺ store at the hair cell (Beurg et al., 2010; Boyer et al., 2001; Pickett et al., 2018; Yamoah et al., 1998). In addition to the mitochondria, the endoplasmic reticulum (ER) is another effective Ca²⁺ store. In vertebrate cells, the ER resting Ca²⁺ level can range from 100 μM to 1 mM in various cell types (de la Fuente et al., 2013; Mogami et al., 1998; Solovyova et al., 2002; Vandecaetsbeek et al., 2011; Verkhratsky, 2005; Verkhratsky and Petersen, 2002). Ca²⁺ enters into the ER through the sarco-ER Ca²⁺ ATPase (SERCA) (Vandecaetsbeek et al., 2011). Two related channels, the inositol-1,4,5-*triphosphate* receptor (IP₃R) and ryanodine receptor (RyR) act as intracellular Ca²⁺-release channels to release Ca²⁺ from the ER (Lanner, 2012; Lanner et al., 2010; Mikoshiba, 2015).

In many cell types, the ER forms contacts with mitochondria that allows for exchange of Ca²⁺ between the two organelles (Giacomello and Pellegrini, 2016; Liu and Zhu, 2017; Qi et al., 2015; Wu et al., 2018). Electron and fluorescence micrographs of labeled ER-mitochondrial contacts placed the distance between mitochondria and both smooth and rough ER at contact sites to be around 10 to 30 nm (Cieri et al., 2018; Csordás et al., 1999, 2006; Rizzuto et al., 1998). Contacts between mitochondria and tubular ER structures have also been shown in auditory and vestibular hair cells of gerbils (Cunningham et al., 2000;

Spicer et al., 1999). 3D reconstruction of ER and mitochondria in neuronal axons using focused ion beam-scanning electron microscopy (FIB-SIM) also showed multiple contacts of variable length between these two organelles (Krols et al., 2016). In liver cells, studies found that the length of contact sites and the distance between the two organelles are altered by metabolism (Sood et al., 2014) and apoptosis (Csordás et al., 2006).

In my thesis work, TEM images used to measure the distance between mitochondria and ribbons also showed occasional contacts between mitochondria and ER (examples: Figure 4.2). These contacts could be measured to show the average membrane-to-membrane distance between mitochondria and ER. In zebrafish, hair cell mitochondrial-ER contacts may be further imaged live and in 3D using transgenic fish expressing Förster Resonance Energy Transfer (FRET) sensors or split-GFP proteins on the cytosolic faces of ER and mitochondria (Cieri et al., 2018; Kindt et al., 2012). Using this method, spatio-temporal changes in these contact sites may be measured in the hair cells during development, mechanotransduction or ototoxin-exposure. This is important because, in hair cells, ER may participate in the mitochondrial functions demonstrated in my work through such contact sites.

Figure 4.2. Contacts between mitochondria and ER cisternae.



Example TEM showing hair cell mitochondria (orange) in contact with ER cisternae (arrow) near presynaptic ribbon (R). A, To the left of the ribbon body, a mitochondrion is contacted by a cistern that runs parallel to the OMM. B, The mitochondrion on top of the ribbon body is contacted by a cistern.

Molecular composition of these contact points has been studied by isolating membrane fragments with ER characteristics that strongly associate with the OMM (Lewis and Tata, 1973; Pickett et al., 1980; Shore and Tata, 1977; Wanson et al., 1975). These fragments are often referred to as mitochondria-associated membranes (MAM) (Vance, 2014). MAMs are enriched in ER-resident proteins, including IP₃R and RyR Ca²⁺ channels (reviewed in: Rossi et al., 2019). It has been proposed that these MAMs that compose the ER-mitochondrial contacts are important for shuttling Ca²⁺ between organelles. For example, upon stimulation by IP₃, ER Ca²⁺ is preferentially released to the cytosol near mitochondria, leading to mitochondrial-Ca²⁺ uptake (Rizzuto et al., 1993, 1998). The transitory increase in Ca²⁺ at ER-mitochondrial contact sites drives Ca²⁺ diffusion through VDAC across the OMM and MCU across the IMM (Baughman et al., 2011; De Stefani et al., 2011; Rapizzi et al., 2002). My work demonstrated that mitochondria take up Ca²⁺ spontaneously during development as well as during evoked hair cell synaptic activity in immature and mature hair cells. Based on work in other cell types, it is possible that ER is also involved in this regulation of hair cell synapse function and ribbon formation.

My work showed that, in mature hair cells, mitochondrial-Ca²⁺ uptake enhances presynaptic-Ca²⁺ uptake. Similarly, ER-Ca²⁺ stores have been shown to play a role downstream of hair cell presynaptic-Ca²⁺ influx. In mammalian hair cells, ER is thought to take up Ca²⁺ during presynaptic-Ca²⁺ influx to help maintain a lower basal level of cytosolic-Ca²⁺ (Kennedy, 2002; Tucker and Fettiplace, 1995). ER also has been shown to have Ca²⁺-induced Ca²⁺ release to augment presynaptic-Ca²⁺ influx in hair cells (Castellano-Muñoz and Ricci, 2014; Castellano-Muñoz et al., 2016; Lioudyno et al., 2004). The role of Ca²⁺-induced Ca²⁺ release from ER in evoked presynaptic-Ca²⁺ could be tested by pharmacologically blocking ER-Ca²⁺ release. By measuring evoked presynaptic-Ca²⁺ influx as outlined in my

thesis (Figure 2.4C-D' and 3.1C-D'), the role of ER Ca^{2+} -induced Ca^{2+} release could be assessed by treatment with IP_3R inhibitor 2-aminoethoxydiphenyl borate (Maruyama et al., 1997), or a high dose (around 200 μM) of ryanodine, to blocks RyR (Buck et al., 1992). If ER Ca^{2+} -induced Ca^{2+} release is required to support presynaptic- Ca^{2+} influx, blocking ER- Ca^{2+} efflux would decrease presynaptic- Ca^{2+} signals.

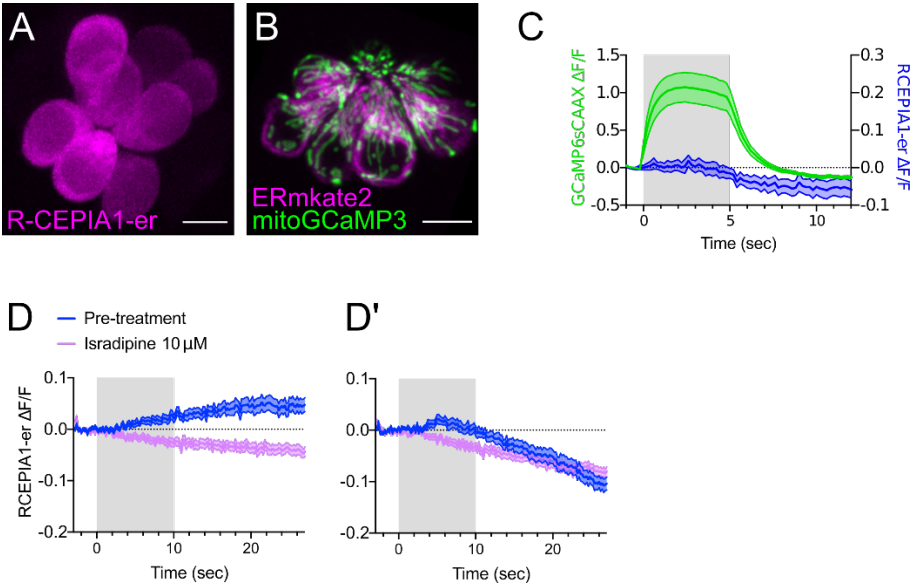
Alternatively, ER may act as a Ca^{2+} buffer to maintain the basal level of cytosolic- Ca^{2+} . In mammalian hair cells, the ER is thought to take up Ca^{2+} during presynaptic- Ca^{2+} influx to help maintain a lower basal level of cytosolic- Ca^{2+} (Kennedy, 2002; Tucker and Fettiplace, 1995). Using similar approaches applied in my thesis work (Figure 2.9A, 3.7A), cytosolic- Ca^{2+} levels could be measured before and after blocking ER- Ca^{2+} influx. If the ER maintain a low basal level of cytosolic- Ca^{2+} , I predict that treatment with SERCA inhibitor thapsigargin to block ER- Ca^{2+} uptake would increase cytosolic- Ca^{2+} (Luo et al., 2000; Thastrup et al., 1990). This result would suggest that ER is an important Ca^{2+} buffer.

In addition to ER and mitochondria acting as distinct Ca^{2+} stores, it is likely that the two organelles can coordinate during synaptic activity. If blocking ER- Ca^{2+} release decreases presynaptic- Ca^{2+} influx, it is possible that both mitochondrial- and ER- Ca^{2+} stores work together in the same pathway. Additionally, mitochondrial- Ca^{2+} uptake could be downstream of ER- Ca^{2+} release, as was shown in aminoglycoside-induced hair cell death in zebrafish (Esterberg et al., 2014). To test if mitochondrial- Ca^{2+} uptake is downstream of ER- Ca^{2+} release during presynaptic activity, evoked mitochondrial- Ca^{2+} signals could be measured while ER- Ca^{2+} release is manipulated. If mitochondrial- Ca^{2+} uptake is downstream of ER- Ca^{2+} -release, blocking or enhancing ER- Ca^{2+} efflux would respectively decrease or increase evoked mitochondrial- Ca^{2+} signals.

The role of the ER during presynaptic- Ca^{2+} influx or mitochondrial- Ca^{2+} uptake in hair cells could be addressed further by using ER-localized Ca^{2+} indicators. An ER-localized Ca^{2+} indicator could be used to verify the effects of pharmacological treatments such as the SERCA, IP_3R and RyR inhibitors discussed above (Buck et al., 1992; Luo et al., 2000; Maruyama et al., 1997; Thastrup et al., 1990). ER- Ca^{2+} flux also may be examined during evoked-presynapse function, as well as during spontaneous- Ca^{2+} uptake that we described in the developing hair cells (Figure 3.2A-A’’). In addition, the ER-localized Ca^{2+} indicator could be used in conjunction with mitochondrial- or presynaptic-localized Ca^{2+} indicators to perform two-color imaging during evoked and spontaneous presynaptic- Ca^{2+} activity.

Compared to other Ca^{2+} domains in the cell, it is challenging to measure the time course of ER Ca^{2+} because ER- Ca^{2+} levels are comparatively very high. ER- Ca^{2+} concentration has been shown to be at least 1000-fold that of cytosolic- Ca^{2+} level (Burdakov et al., 2005). In order to detect changes in Ca^{2+} levels in the high resting Ca^{2+} levels in the ER, genetically-encoded Ca^{2+} indicators have been engineered with much lower affinities for Ca^{2+} to ensure that the indicators do not become saturated by Ca^{2+} within the ER (Suzuki et al., 2014). Preliminarily, in collaboration with Raible lab, we have expressed R-CEPIA, a low affinity ER- Ca^{2+} indicator in zebrafish hair cells. I was able to observe in zebrafish hair cells clear changes in R-CEPIA intensity during and after evoked presynaptic- Ca^{2+} influx (Figure 4.3 C-D’). Additionally, increases in R-CEPIA intensity was abolished with isradipine, which indicated that the Ca^{2+} increase detected by the indicator was $\text{Cav}1.3$ -dependent. Future work using R-CEPIA in neuromast hair cells will help establish whether there is a relationship between presynaptic, ER and mitochondrial- Ca^{2+} influx.

Figure 4.3. ER-localized Ca²⁺ indicator R-CEPIA1-er



A, Airyscan confocal image of 8 live hair cells expressing R-CEPIA1-er in a neuromast at 4 dpf. B, For comparison, Airyscan confocal image of a live neuromast in side-view expressing ERmkate2 (magenta) MitoGCaMP3 (green). C, Average membrane- Ca^{2+} signal rise and ER- Ca^{2+} signal $\Delta F/F$ in a 5-s stimulation shows that synaptic activity is associated with decrease in ER- Ca^{2+} signal, 5 dpf, $n = 9$ cells. D-D', In a 10-s stimulation, 10 μM of the $\text{Ca}_v1.3$ inhibitor isradipine blocks evoked R-CEPIA1-er signals, 5 dpf, $n = 12$ cells. R-CEPIA1 signal decrease in C and during pre-treatment in D' are both preceded by 4 to 6-s of inactivity, the signal of which is abolished by isradipine (D').

Part of my thesis work provides evidence that in mature hair cells, mitochondrial Ca^{2+} is important to maintain synapses and hair cell health. My work showed that complete MCU block disrupts synapse maintenance and is cytotoxic (Chapter 2, Figure 2.6E). It is possible that ER- Ca^{2+} handling also contributes to the observed hair cell vulnerability and synapse loss. In hair cells, it has been shown that Ca^{2+} flows from ER to mitochondria immediately prior to cell death (Esterberg et al., 2014). Similarly, in other cell-types, increased Ca^{2+} release from ER into the mitochondria sensitizes cells to cell death (Nakamura et al., 2000; Pinton et al., 2001). Disruption of the connection between ER and mitochondria is also associated with cell death (Liu and Zhu, 2017), as is a higher number of ER-mitochondria contacts (Csordás et al., 2006). The role ER- Ca^{2+} stores play in hair cell death or synapse loss could be studied using pharmacological block of ER- Ca^{2+} uptake or release. After pharmacologically inhibiting SERCA, IP_3R , or RyR, hair cell and ribbon synapse number can be assessed by immunostaining. If blocking ER- Ca^{2+} influx or release is cytotoxic in a manner similar to blocking MCU, then ribbon synapse and hair cell number would decrease at a sufficient dose. Future research may reveal whether ER- Ca^{2+} stores contribute to hair cell health and synapse maintenance.

In summary, the research described in my thesis has revealed previously unappreciated roles for the mitochondria in immature and mature hair cells. My work has extended our understanding of $\text{Ca}_v1.3$ channel activity-dependence during ribbon development. I identified NAD(H) redox as a potential mechanism regulating ribbon size during development. In mature hair cells, my research has identified new roles for the mitochondria in cell health and in synapse function and maintenance. Overall, my work has contributed to the understanding of hair cell synapse structure, function and formation in relation to mitochondrial function. Better understanding of mitochondria in hair cell

development and function may also provide insight in how to protect, and or rescue auditory or vestibular hair cell from injury.

References

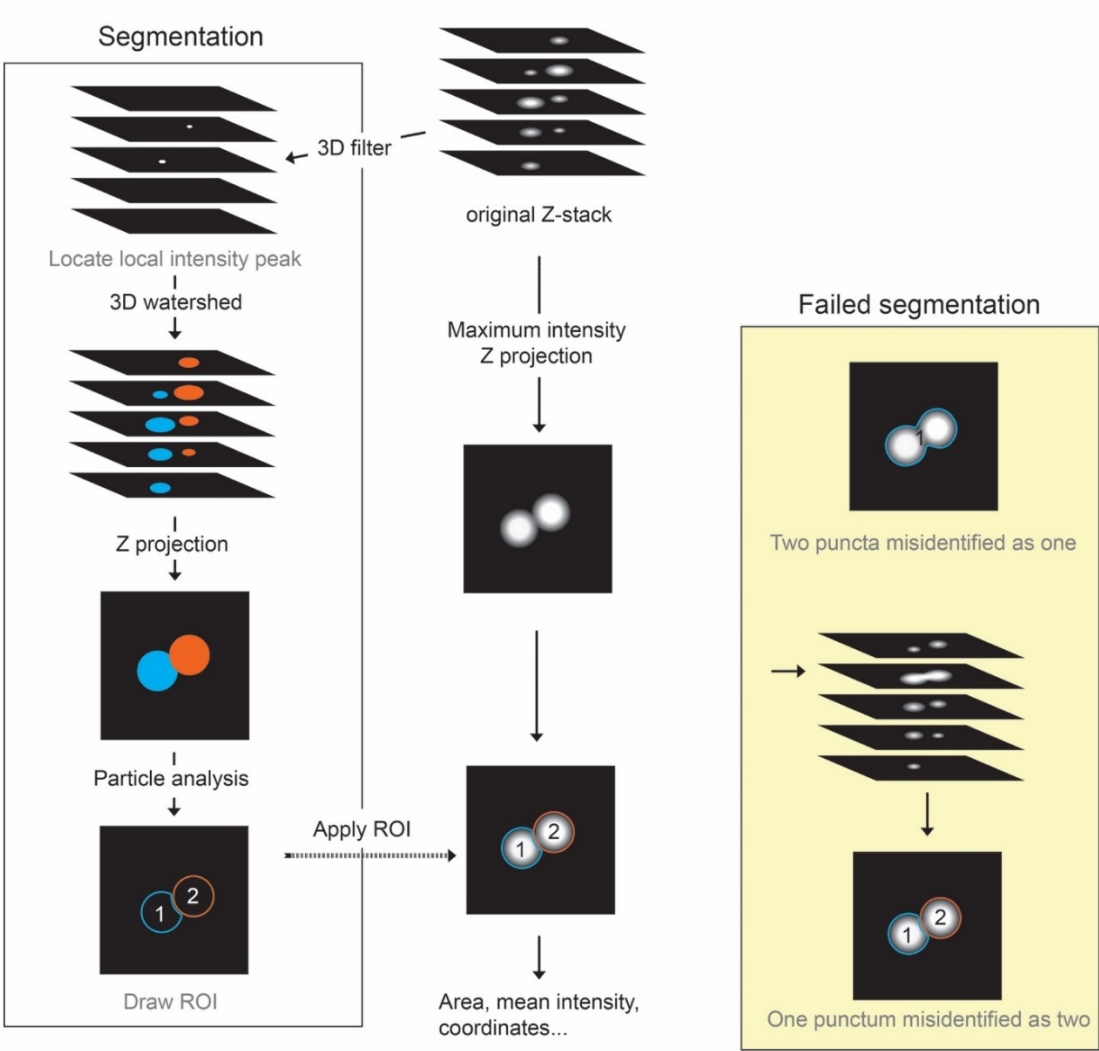
Appendix

A component of this thesis project was to quantify Ribeye puncta size and pair the puncta with postsynaptic density in order to measure only the synapse-associated structures. The Airyscan attachment of the LSM 780 confocal microscope offered increased resolution and therefore details that eluded previously published analysis using simple intensity threshold (Sheets et al., 2012). Because of the increased resolution, closely associated puncta may be resolved, but were not recognized as multiple objects by the analysis. The increase resolution made it challenging to automatically segment Ribeye puncta in a manner similar to manual quantification. I developed a custom image analysis method to properly identify individual Ribeye punctum that were paired with an opposing postsynaptic density.

Image analysis

Using the ImageJ 3D Suite, Simple 3D Segmentation was used to isolate and identify pre- and postsynapses (Figure A1). The location of local maximum intensity was generated to segment the puncta. A separate Z stack of single pixel points was generated using the 3D Fast Filters with the provided input (estimated x, y radius of Ribeye puncta: 8 px, MAGUK: 8 px; estimated z radius: 4). A final segmented Z-stack was generated using 3D Watershed, which took the Z stack containing the segmented puncta generated by Simple 3D Segmentation, and the local maxima Z stack generated by 3D Fast Filters. In this step, a seeds threshold was applied to the local maxima Z stack to disregard maxima generated from background noise. Dim puncta that were not captured by the local maxima detection step were eliminated during 3D watershed step; as such the cuts generated by watershed were applied to the simple segmentation Z stack by transforming the watershed-processed Z stack into edges and then subtracting the edges from the simple segmentation Z-stack. The centroid for every punctum was obtained using 3D Manager to get their x, y,z coordinates, and exported as a spreadsheet. The Z coordinate was matched to the associated area information later. The extra dimension helped better to identify complete synapses. The max Z-projection of the segmented Z stack was used to generate a list of 2D objects as individual regions of interests (ROIs) corresponding to each punctum. This step also included a minimum size filter, Ribeye: $0.08 \mu\text{m}^2$, MAGUK $0.04 \mu\text{m}^2$. The 2D puncta ROI were applied over the max Z projection of the original Z-stack which has only been processed with background subtraction. This step measures the intensity of the antibody label. Coordinate and intensity information were exported as a CSV spreadsheet.

Figure A1. Image analysis scheme for identification and measurement of Ribeye and MAGUK puncta.



To properly segment the labeled puncta, confocal image Z-stack of Ribeye and MAGUK are duplicated and altered to produce a 3D, filled shape of the puncta using 3D Fast Filter and 3D Watershed. Some steps to back-fill puncta that were lost in 3D Fast Filter were omitted for brevity. The 3D filled shape is then Z projected to generate a 2D shape image, which can be used as a mask to create regions of interests (ROIs) representing each Ribeye or MAGUK punctum. The ROIs are applied to the maximum Z-projection of the original Z-stack in order to measure the area, intensity, and coordinate of each punctum. The coordinate of Ribeye and MAGUK coordinates may be used to filter for synaptic structure. This image analysis method aims to reduce two “failed segmentation” scenarios: 1) two puncta that do not touch across the Z-stack but is misidentified as one punctum after Z-projection and 2) dumbbell-shaped object that is misidentified as two puncta.

Bibliography

Ablain, J., Durand, E.M., Yang, S., Zhou, Y., and Zon, L.I. (2015). A CRISPR/Cas9 Vector System for Tissue-Specific Gene Disruption in Zebrafish. *Dev Cell* 32, 756–764.

Ackermann, F., Waites, C.L., and Garner, C.C. (2015). Presynaptic active zones in invertebrates and vertebrates. *EMBO Rep* 16, 923–938.

Adam-Vizi, V., and Starkov, A.A. (2010). Calcium and mitochondrial reactive oxygen species generation: how to read the facts. *J Alzheimers Dis* 20 *Suppl* 2, S413-426.

Ahmed, Z.M., Riazuddin, S., Bernstein, S.L., Ahmed, Z., Khan, S., Griffith, A.J., Morell, R.J., Friedman, T.B., Riazuddin, S., and Wilcox, E.R. (2001). Mutations of the protocadherin gene PCDH15 cause Usher syndrome type 1F. *Am. J. Hum. Genet.* 69, 25–34.

Alagramam, K.N. (2001). Mutations in the novel protocadherin PCDH15 cause Usher syndrome type 1F. *Human Molecular Genetics* 10, 1709–1718.

Alagramam, K.N., Murcia, C.L., Kwon, H.Y., Pawlowski, K.S., Wright, C.G., and Woychik, R.P. (2001). The mouse Ames waltzer hearing-loss mutant is caused by mutation of Pcdh15, a novel protocadherin gene. *Nat Genet* 27, 99–102.

Alpadi, K., Magupalli, V.G., Käppel, S., Köblitz, L., Schwarz, K., Seigel, G.M., Sung, C.-H., and Schmitz, F. (2008). RIBEYE recruits Munc119, a mammalian ortholog of the *Caenorhabditis elegans* protein unc119, to synaptic ribbons of photoreceptor synapses. *J Biol Chem* 283, 26461–26467.

Altrock, W.D., tom Dieck, S., Sokolov, M., Meyer, A.C., Sigler, A., Brakebusch, C., Fässler, R., Richter, K., Boeckers, T.M., Potschka, H., et al. (2003). Functional inactivation of a fraction of excitatory synapses in mice deficient for the active zone protein bassoon. *Neuron* 37, 787–800.

Amsterdam, A., Lin, S., and Hopkins, N. (1995). The *Aequorea victoria* green fluorescent protein can be used as a reporter in live zebrafish embryos. *Dev Biol* 171, 123–129.

Anniko, M. (1983). Cytodifferentiation of cochlear hair cells. *American Journal of Otolaryngology* 4, 375–388.

Anniko, M., Wenngren, B.-I., Wróblewski, R., and Anniko, M. (1988). Aberrant elemental composition of otoconia in the dancer mouse mutant with a semidominant gene causing a morphogenetic type of inner ear defect. *Acta Otolaryngol* 106, 208–212.

Austin, S., Tavakoli, M., Pfeiffer, C., Seifert, J., Mattarei, A., De Stefani, D., Zoratti, M., and Nowikovsky, K. (2017). LETM1-mediated K^+ and Na^+ homeostasis regulates mitochondrial Ca^{2+} efflux. *Front Physiol* 8, 839.

Babola, T.A., Li, S., Gribizis, A., Lee, B.J., Issa, J.B., Wang, H.C., Crair, M.C., and Bergles, D.E. (2018). Homeostatic control of spontaneous activity in the developing auditory system. *Neuron* 99, 511-524.e5.

Balak, K., Corwin, J., and Jones, J. (1990). Regenerated hair cells can originate from supporting cell progeny: evidence from phototoxicity and laser ablation experiments in the lateral line system. *J Neurosci* 10, 2502–2512.

Ballana, E., Morales, E., Rabionet, R., Montserrat, B., Ventayol, M., Bravo, O., Gasparini, P., and Estivill, X. (2006). Mitochondrial 12S rRNA gene mutations affect RNA secondary structure and lead to variable penetrance in hearing impairment. *Biochem Biophys Res Commun* *341*, 950–957.

Baradaran, R., Wang, C., Siliciano, A.F., and Long, S.B. (2018). Cryo-EM structures of fungal and metazoan mitochondrial calcium uniporters. *Nature* *559*, 580–584.

Bauer, D.E., Harris, M.H., Plas, D.R., Lum, J.J., Hammerman, P.S., Rathmell, J.C., Riley, J.L., and Thompson, C.B. (2004). Cytokine stimulation of aerobic glycolysis in hematopoietic cells exceeds proliferative demand. *The FASEB Journal* *18*, 1303–1305.

Baughman, J.M., Perocchi, F., Girgis, H.S., Plovanich, M., Belcher-Timme, C.A., Sancak, Y., Bao, X.R., Strittmatter, L., Goldberger, O., Bogorad, R.L., et al. (2011). Integrative genomics identifies MCU as an essential component of the mitochondrial calcium uniporter. *Nature* *476*, 341–345.

Baumgartner, H.K., Gerasimenko, J.V., Thorne, C., Ferdek, P., Pozzan, T., Tepikin, A.V., Petersen, O.H., Sutton, R., Watson, A.J.M., and Gerasimenko, O.V. (2009). Calcium elevation in mitochondria is the main Ca^{2+} requirement for mitochondrial permeability transition pore (mPTP) opening. *J. Biol. Chem.* *284*, 20796–20803.

Becker, L., Schnee, M.E., Niwa, M., Sun, W., Maxeiner, S., Talaei, S., Kachar, B., Rutherford, M.A., and Ricci, A.J. (2018). The presynaptic ribbon maintains vesicle populations at the hair cell afferent fiber synapse. *ELife* *7*, e30241.

- Bellesis, A.G., Jecrois, A.M., Hayes, J.A., Schiffer, C.A., and Royer, W.E. (2018). Assembly of human C-terminal binding protein (CtBP) into tetramers. *J Biol Chem* 293, 9101–9112.
- Berglund, A.M., and Ryugo, D.K. (1987). Hair cell innervation by spiral ganglion neurons in the mouse. *J Comp Neurol* 255, 560–570.
- Bertero, and Maack (2018). Calcium signaling and reactive oxygen species in mitochondria. *Circulation Research* 122, 1460–1478.
- Beurg, M., Nam, J.-H., Chen, Q., and Fettiplace, R. (2010). Calcium balance and mechanotransduction in rat cochlear hair cells. *J Neurophysiol* 104, 18–34.
- Beutner, D., and Moser, T. (2001). The presynaptic function of mouse cochlear inner hair cells during development of hearing. *J Neurosci* 21, 4593–4599.
- Billups, B., and Forsythe, I.D. (2002). Presynaptic mitochondrial calcium sequestration influences transmission at mammalian central synapses. *J Neurosci* 22, 5840–7.
- Blackwell, D.L., Lucas, J.W., and Clarke, T.C. (2014). Summary health statistics for U.S. adults: national health interview survey, 2012. *Vital Health Stat* 10 1–161.
- Bogan, K.L., and Brenner, C. (2008). Nicotinic acid, nicotinamide, and nicotinamide riboside: a molecular evaluation of NAD⁺ precursor vitamins in human nutrition. *Annu. Rev. Nutr.* 28, 115–130.
- Bolz, H., von Brederlow, B., Ramírez, A., Bryda, E.C., Kutsche, K., Nothwang, H.G., Seeliger, M., Cabrera, M. del C.-S., Vila, M.C., Molina, O.P., et al. (2001). Mutation of

CDH23, encoding a new member of the cadherin gene family, causes Usher syndrome type 1D. *Nat Genet* 27, 108–112.

Borst, P. (1962). The aerobic oxidation of reduced diphosphopyridine nucleotide formed by glycolysis in ehrlich ascites-tumour cells. *Biochimica et Biophysica Acta* 57, 270–282.

Böttger, E.C., and Schacht, J. (2013). The mitochondrion: a perpetrator of acquired hearing loss. *Hear Res* 303, 12–19.

Boyer, C., Art, J.J., Dechesne, C.J., Lehouelleur, J., Vautrin, J., and Sans, A. (2001). Contribution of the plasmalemma to Ca^{2+} homeostasis in hair cells. *J Neurosci* 21, 2640–2650.

Brandt, A., Striessnig, J., and Moser, T. (2003). CaV1.3 channels are essential for development and presynaptic activity of cochlear inner hair cells. *J Neurosci* 23, 10832–10840.

Buck, E., Zimanyi, I., Abramson, J.J., and Pessah, I.N. (1992). Ryanodine stabilizes multiple conformational states of the skeletal muscle calcium release channel. *J. Biol. Chem.* 267, 23560–23567.

Bullen, A., West, T., Moores, C., Ashmore, J., Fleck, R.A., MacLellan-Gibson, K., and Forge, A. (2015). Association of intracellular and synaptic organization in cochlear inner hair cells revealed by 3D electron microscopy. *J Cell Sci* 128, 2529–40.

Buran, B.N., Strenzke, N., Neef, A., Gundelfinger, E.D., Moser, T., and Liberman, M.C. (2010). Onset coding is degraded in auditory nerve fibers from mutant mice lacking synaptic ribbons. *J Neurosci* 30, 7587–7597.

Burdakov, D., Petersen, O.H., and Verkhratsky, A. (2005). Intraluminal calcium as a primary regulator of endoplasmic reticulum function. *Cell Calcium* 38, 303–310.

Cai, Q., and Tammineni, P. (2016). Alterations in mitochondrial quality control in Alzheimer's disease. *Front. Cell. Neurosci.* 10, 24.

Carafoli, E. (1974). The release of calcium from heart mitochondria by sodium. *J Mol Cell Cardiol* 6, 361–371.

Carafoli, E. (2003). Historical review: mitochondria and calcium: ups and downs of an unusual relationship. *Trends Biochem. Sci.* 28, 175–181.

Carafoli, E. (2011). The plasma membrane calcium pump in the hearing process: physiology and pathology. *Sci China Life Sci* 54, 686–690.

Carafoli, E., and Lehninger, A.L. (1971). A survey of the interaction of calcium ions with mitochondria from different tissues and species. *Biochem. J.* 122, 681–690.

Cases-Langhoff, C., Voss, B., Garner, A.M., Appeltauer, U., Takei, K., Kindler, S., Veh, R.W., De Camilli, P., Gundelfinger, E.D., and Garner, C.C. (1996). Piccolo, a novel 420 kDa protein associated with the presynaptic cytomatrix. *Eur J Cell Biol* 69, 214–223.

Castellano-Muñoz, M., and Ricci, A.J. (2014). Role of intracellular calcium stores in hair-cell ribbon synapse. *Front Cell Neurosci* 8, 162.

Castellano-Muñoz, M., Schnee, M.E., and Ricci, A.J. (2016). Calcium-induced calcium release supports recruitment of synaptic vesicles in auditory hair cells. *J Neurophysiol* 115, 226–239.

Ceriani, F., Hendry, A., Jeng, J.-Y., Johnson, S.L., Stephani, F., Olt, J., Holley, M.C., Mammano, F., Engel, J., Kros, C.J., et al. (2019). Coordinated calcium signalling in cochlear sensory and non-sensory cells refines afferent innervation of outer hair cells. *EMBO J* 38, e99839.

Chang, K.T., Niescier, R.F., and Min, K.-T. (2011). Mitochondrial matrix Ca^{2+} as an intrinsic signal regulating mitochondrial motility in axons. *Proc Natl Acad Sci USA* 108, 15456–15461.

Chaudhuri, D., Sancak, Y., Mootha, V.K., and Clapham, D.E. (2013). MCU encodes the pore conducting mitochondrial calcium currents. *Elife* 2, e00704.

Chen, Y.A., and Scheller, R.H. (2001). SNARE-mediated membrane fusion. *Nat Rev Mol Cell Biol* 2, 98–106.

Chen, Z., Chou, S.-W., and McDermott, B.M. (2018). Ribeye protein is intrinsically dynamic but is stabilized in the context of the ribbon synapse. *J Physiol* 596, 409–421.

Chinnadurai, G. (2007). Transcriptional regulation by C-terminal binding proteins. *The International Journal of Biochemistry & Cell Biology* 39, 1593–1607.

Chitnis, A.B., Dalle Nogare, D., and Matsuda, M. (2012). Building the posterior lateral line system in zebrafish. *Devel Neurobio* 72, 234–255.

Chouhan, A.K., Zhang, J., Zinsmaier, K.E., and Macleod, G.T. (2010). Presynaptic mitochondria in functionally different motor neurons exhibit similar affinities for Ca^{2+} but exert little influence as Ca^{2+} buffers at nerve firing rates in situ. *J Neurosci* 30, 1869–81.

Cieri, D., Vicario, M., Giacomello, M., Vallese, F., Filadi, R., Wagner, T., Pozzan, T., Pizzo, P., Scorrano, L., Brini, M., et al. (2018). SPLICS: a split green fluorescent protein-based contact site sensor for narrow and wide heterotypic organelle juxtaposition. *Cell Death Differ.* *25*, 1131–1145.

Clerici, W.J., DiMartino, D.L., and Prasad, M.R. (1995). Direct effects of reactive oxygen species on cochlear outer hair cell shape in vitro. *Hear Res* *84*, 30–40.

Colombini, M. (2012). VDAC structure, selectivity, and dynamics. *Biochim. Biophys. Acta* *1818*, 1457–1465.

Coombs, S., and Montgomery, J.C. (1999). The Enigmatic Lateral Line System. In *Comparative Hearing: Fish and Amphibians*, R.R. Fay, and A.N. Popper, eds. (New York, NY: Springer New York), pp. 319–362.

Corey, D., and Hudspeth, A. (1983). Kinetics of the receptor current in bullfrog saccular hair cells. *J. Neurosci.* *3*, 962–976.

Court, F.A., and Coleman, M.P. (2012). Mitochondria as a central sensor for axonal degenerative stimuli. *Trends Neurosci.* *35*, 364–372.

Crompton, M. (1999). The mitochondrial permeability transition pore and its role in cell death. *Biochem. J.* *341 (Pt 2)*, 233–249.

Csordás, G., Thomas, A.P., and Hajnóczky, G. (1999). Quasi-synaptic calcium signal transmission between endoplasmic reticulum and mitochondria. *EMBO J.* *18*, 96–108.

Csordás, G., Renken, C., Várnai, P., Walter, L., Weaver, D., Buttle, K.F., Balla, T., Mannella, C.A., and Hajnóczky, G. (2006). Structural and functional features and significance of the physical linkage between ER and mitochondria. *J. Cell Biol.* *174*, 915–921.

Csordás, G., Golenár, T., Seifert, E.L., Kamer, K.J., Sancak, Y., Perocchi, F., Moffat, C., Weaver, D., de la Fuente Perez, S., Bogorad, R., et al. (2013). MICU1 controls both the threshold and cooperative activation of the mitochondrial Ca²⁺ uniporter. *Cell Metab* *17*, 976–987.

Cullen, K.E., and Minor, L.B. (2002). Semicircular canal afferents similarly encode active and passive head-on-body rotations: implications for the role of vestibular efference. *J Neurosci* *22*, RC226.

Cunningham, C.L., and Müller, U. (2019). Molecular Structure of the Hair Cell Mechanoelectrical Transduction Complex. *Cold Spring Harb Perspect Med* *9*, a033167.

Cunningham, C.D., Weber, P.C., Spicer, S.S., and Schulte, B.A. (2000). Canalicular reticulum in vestibular hair cells. *Hear Res* *143*, 69–83.

Dani, A., Huang, B., Bergan, J., Dulac, C., and Zhuang, X. (2010). Superresolution imaging of chemical synapses in the brain. *Neuron* *68*, 843–856.

De Pinto, V., Reina, S., Guarino, F., and Messina, A. (2008). Structure of the voltage dependent anion channel: state of the art. *J Bioenerg Biomembr* *40*, 139–147.

De Stefani, D., Raffaello, A., Teardo, E., Szabò, I., and Rizzuto, R. (2011). A forty-kilodalton protein of the inner membrane is the mitochondrial calcium uniporter. *Nature* *476*, 336–340.

DeBerardinis, R.J., Lum, J.J., Hatzivassiliou, G., and Thompson, C.B. (2008). The Biology of Cancer: Metabolic Reprogramming Fuels Cell Growth and Proliferation. *Cell Metabolism* 7, 11–20.

Dembla, M., Wahl, S., Katiyar, R., and Schmitz, F. (2014). ArfGAP3 is a component of the photoreceptor synaptic ribbon complex and forms an NAD(H)-regulated, redox-sensitive complex with RIBEYE that is important for endocytosis. *The Journal of Neuroscience : The Official Journal of the Society for Neuroscience* 34, 5245–60.

Denton, R.M., Randle, P.J., and Martin, B.R. (1972). Stimulation by calcium ions of pyruvate dehydrogenase phosphate phosphatase. *Biochem J* 128, 161–163.

Denton, R.M., Richards, D.A., and Chin, J.G. (1978). Calcium ions and the regulation of NAD⁺-linked isocitrate dehydrogenase from the mitochondria of rat heart and other tissues. *Biochem. J.* 176, 899–906.

Denton, R.M., McCormack, J.G., and Edgell, N.J. (1980). Role of calcium ions in the regulation of intramitochondrial metabolism. Effects of Na⁺, Mg²⁺ and ruthenium red on the Ca²⁺-stimulated oxidation of oxoglutarate and on pyruvate dehydrogenase activity in intact rat heart mitochondria. *Biochem J* 190, 107–117.

Desai, S.S., Zeh, C., and Lysakowski, A. (2005a). Comparative morphology of rodent vestibular periphery. I. Saccular and utricular maculae. *J Neurophysiol* 93, 251–266.

Desai, S.S., Ali, H., and Lysakowski, A. (2005b). Comparative morphology of rodent vestibular periphery. II. cristae ampullares. *J Neurophysiol* 93, 267–280.

Devine, M.J., and Kittler, J.T. (2018). Mitochondria at the neuronal presynapse in health and disease. *Nature Reviews Neuroscience* *19*, 63–80.

Dick, O., Hack, I., Altroock, W.D., Garner, C.C., Gundelfinger, E.D., and Brandstätter, J.H. (2001). Localization of the presynaptic cytomatrix protein Piccolo at ribbon and conventional synapses in the rat retina: comparison with Bassoon. *J Comp Neurol* *439*, 224–34.

tom Dieck, S., Sanmartí-Vila, L., Langnaese, K., Richter, K., Kindler, S., Soyke, A., Wex, H., Smalla, K.H., Kämpf, U., Fränzer, J.T., et al. (1998). Bassoon, a novel zinc-finger CAG/glutamine-repeat protein selectively localized at the active zone of presynaptic nerve terminals. *J Cell Biol* *142*, 499–509.

DiMauro, S., and Schon, E.A. (2008). Mitochondrial Disorders in the Nervous System. *Annual Review of Neuroscience* *31*, 91–123.

Dow, E., Siletti, K., and Hudspeth, A.J. (2015). Cellular projections from sensory hair cells form polarity-specific scaffolds during synaptogenesis. *Genes & Development* *29*, 1087–94.

Dow, E., Jacobo, A., Hossain, S., Siletti, K., and Hudspeth, A.J. (2018). Connectomics of the zebrafish's lateral-line neuromast reveals wiring and miswiring in a simple microcircuit. *Elife* *7*.

Eatock, R.A., and Songer, J.E. (2011). Vestibular hair cells and afferents: two channels for head motion signals. *Annu Rev Neurosci* *34*, 501–534.

Eatock, R.A., Xue, J., and Kalluri, R. (2008). Ion channels in mammalian vestibular afferents may set regularity of firing. *J Exp Biol* *211*, 1764–1774.

- Eaton, R.C., and Farley, R.D. (1973). Development of the Mauthner Neurons in Embryos and Larvae of the Zebrafish, *Brachydanio rerio*. *Copeia* 1973, 673.
- Eaton, R.C., and Farley, R.D. (1975). Mauthner neuron field potential in newly hatched larvae of the zebra fish. *J Neurophysiol* 38, 502–512.
- Eaton, R.C., Farley, R.D., Kimmel, C.B., and Schabtach, E. (1977a). Functional development in the Mauthner cell system of embryos and larvae of the zebra fish. *J Neurobiol* 8, 151–172.
- Eaton, R.C., Bombardieri, R.A., and Meyer, D.L. (1977b). The Mauthner-initiated startle response in teleost fish. *J. Exp. Biol.* 66, 65.
- Eaton, R.C., Lee, R.K.K., and Foreman, M.B. (2001). The Mauthner cell and other identified neurons of the brainstem escape network of fish. *Progress in Neurobiology* 63, 467–485.
- Eckrich, T., Blum, K., Milenkovic, I., and Engel, J. (2018). Fast Ca^{2+} transients of inner hair cells arise coupled and uncoupled to Ca^{2+} waves of inner supporting cells in the developing mouse cochlea. *Front Mol Neurosci* 11, 264.
- Emadi, G., Richter, C.-P., and Dallos, P. (2004). Stiffness of the gerbil basilar membrane: radial and longitudinal variations. *J Neurophysiol* 91, 474–488.
- Esterberg, R., Hailey, D.W., Coffin, A.B., Raible, D.W., and Rubel, E.W. (2013). Disruption of Intracellular Calcium Regulation Is Integral to Aminoglycoside-Induced Hair Cell Death. *J Neurosci* 33, 7513–7525.

Esterberg, R., Hailey, D.W., Rubel, E.W., and Raible, D.W. (2014). ER-mitochondrial calcium flow underlies vulnerability of mechanosensory hair cells to damage. *J Neurosci* *34*, 9703–19.

Esterberg, R., Linbo, T., Pickett, S.B., Wu, P., Ou, H.C., Rubel, E.W., and Raible, D.W. (2016). Mitochondrial calcium uptake underlies ROS generation during aminoglycoside-induced hair cell death. *The Journal of Clinical Investigation* *126*, 3556–66.

Fenster, S.D., Chung, W.J., Zhai, R., Cases-Langhoff, C., Voss, B., Garner, A.M., Kaempf, U., Kindler, S., Gundelfinger, E.D., and Garner, C.C. (2000). Piccolo, a Presynaptic Zinc Finger Protein Structurally Related to Bassoon. *Neuron* *25*, 203–214.

Fernández-Busnadiego, R., Zuber, B., Maurer, U.E., Cyrklaff, M., Baumeister, W., and Lučić, V. (2010). Quantitative analysis of the native presynaptic cytomatrix by cryoelectron tomography. *J Cell Biol* *188*, 145–156.

Fettiplace, R., and Nam, J.-H. (2019). Tonotopy in calcium homeostasis and vulnerability of cochlear hair cells. *Hear Res* *376*, 11–21.

Filadi, R., and Pozzan, T. (2015). Generation and functions of second messengers microdomains. *Cell Calcium* *58*, 405–414.

Fischel-Ghodsian, N., Kopke, R.D., and Ge, X. (2004). Mitochondrial dysfunction in hearing loss. *Mitochondrion* *4*, 675–694.

Fjeld, C.C., Birdsong, W.T., and Goodman, R.H. (2003). Differential binding of NAD⁺ and NADH allows the transcriptional corepressor carboxyl-terminal binding protein to serve as a metabolic sensor. *Proc Natl Acad Sci USA* *100*, 9202–9207.

- Flippo, K.H., and Strack, S. (2017). Mitochondrial dynamics in neuronal injury, development and plasticity. *J Cell Sci* *130*, 671–681.
- Flock, Å., and Cheung, H.C. (1977). Actin filaments in sensory hairs of inner ear receptor cells. *J Cell Biol* *75*, 339–343.
- Frank, T., Khimich, D., Neef, A., and Moser, T. (2009). Mechanisms contributing to synaptic Ca^{2+} signals and their heterogeneity in hair cells. *Proc Natl Acad Sci USA* *106*, 4483–4488.
- Frank, T., Rutherford, M.A., Strenzke, N., Neef, A., Pangršič, T., Khimich, D., Fejtova, A., Fejtova, A., Gundelfinger, E.D., Liberman, M.C., et al. (2010). Bassoon and the synaptic ribbon organize Ca^{2+} channels and vesicles to add release sites and promote refilling. *Neuron* *68*, 724–738.
- Fritzschnig, B., and Beisel, K.W. (2004). Keeping sensory cells and evolving neurons to connect them to the brain: molecular conservation and novelties in vertebrate ear development. *Brain Behav. Evol.* *64*, 182–197.
- Fritzschnig, B., and Wahnschaffe, U. (1983). The electroreceptive ampullary organs of urodeles. *Cell and Tissue Research* *229*, 483–503.
- Fuchs, P.A. (2005). Time and intensity coding at the hair cell's ribbon synapse. *J Physiol* *566*, 7–12.
- Fuchs, P.A., Glowatzki, E., and Moser, T. (2003). The afferent synapse of cochlear hair cells. *Current Opinion in Neurobiology* *13*, 452–458.

de la Fuente, S., Fonteriz, R.I., Montero, M., and Alvarez, J. (2013). Ca^{2+} homeostasis in the endoplasmic reticulum measured with a new low- Ca^{2+} -affinity targeted aequorin. *Cell Calcium* 54, 37–45.

Furman, A.C., Kujawa, S.G., and Liberman, M.C. (2013). Noise-induced cochlear neuropathy is selective for fibers with low spontaneous rates. *J. Neurophysiol.* 110, 577–586.

García-Berrocal, J.R., Nevado, J., Ramírez-Camacho, R., Sanz, R., González-García, J.A., Sánchez-Rodríguez, C., Cantos, B., España, P., Verdaguer, J.M., and Trinidad Cabezas, A. (2007). The anticancer drug cisplatin induces an intrinsic apoptotic pathway inside the inner ear. *Br J Pharmacol* 152, 1012–1020.

Ghysen, A., and Dambly-Chaudiere, C. (2007). The lateral line microcosmos. *Genes Dev* 21, 2118–2130.

Giacomello, M., and Pellegrini, L. (2016). The coming of age of the mitochondria-ER contact: a matter of thickness. *Cell Death and Differentiation* 23, 1417–27.

Gilmour, D., Knaut, H., Maischein, H.-M., and Nüsslein-Volhard, C. (2004). Towing of sensory axons by their migrating target cells in vivo. *Nat Neurosci* 7, 491–492.

Gincel, D., Zaid, H., and Shoshan-Barmatz, V. (2001). Calcium binding and translocation by the voltage-dependent anion channel: a possible regulatory mechanism in mitochondrial function. *Biochem. J.* 358, 147–155.

Giorgi, C., Baldassari, F., Bononi, A., Bonora, M., De Marchi, E., Marchi, S., Missiroli, S., Patergnani, S., Rimessi, A., Suski, J.M., et al. (2012). Mitochondrial Ca^{2+} and apoptosis. *Cell Calcium* 52, 36–43.

- Giorgi, C., Marchi, S., and Pinton, P. (2018). The machineries, regulation and cellular functions of mitochondrial calcium. *Nat Rev Mol Cell Biol* *19*, 713–730.
- Glancy, B., and Balaban, R.S. (2012). Role of Mitochondrial Ca²⁺ in the Regulation of Cellular Energetics. *Biochemistry* *51*, 2959–2973.
- Gleisner, L., Flock, Å., and Wersäll, J. (1973). The ultrastructure of the afferent synapse on hair cells in the frog labyrinth. *Acta Oto-Laryngologica* *76*, 199–207.
- Glowatzki, E., and Fuchs, P.A. (2002). Transmitter release at the hair cell ribbon synapse. *Nat Neurosci* *5*, 147–54.
- Goldberg, J.M., Smith, C.E., and Fernández, C. (1984). Relation between discharge regularity and responses to externally applied galvanic currents in vestibular nerve afferents of the squirrel monkey. *J. Neurophysiol.* *51*, 1236–1256.
- Goutman, J.D., and Glowatzki, E. (2007). Time course and calcium dependence of transmitter release at a single ribbon synapse. *Proceedings of the National Academy of Sciences of the United States of America* *104*, 16341–16346.
- Graydon, C.W., Manor, U., and Kindt, K.S. (2017). In Vivo Ribbon Mobility and Turnover of Ribeye at Zebrafish Hair Cell Synapses. *Sci Rep* *7*, 7467.
- Gundelfinger, E.D., and Fejtova, A. (2012). Molecular organization and plasticity of the cytomatrix at the active zone. *Curr. Opin. Neurobiol.* *22*, 423–430.
- Gundelfinger, E.D., Reissner, C., and Garner, C.C. (2016). Role of Bassoon and Piccolo in Assembly and Molecular Organization of the Active Zone. *Front. Synaptic Neurosci.* *7*, 19.

Gunter, T.E., and Sheu, S.-S. (2009). Characteristics and possible functions of mitochondrial Ca^{2+} transport mechanisms. *Biochim. Biophys. Acta* 1787, 1291–1308.

Guppy, M., Greiner, E., and Brand, K. (1993). The role of the Crabtree effect and an endogenous fuel in the energy metabolism of resting and proliferating thymocytes. *Eur J Biochem* 212, 95–99.

Haack, J.A., and Rosenberg, R.L. (1994). Calcium-dependent inactivation of L-type calcium channels in planar lipid bilayers. *Biophys J* 66, 1051–1060.

Haddon, C., and Lewis, J. (1996). Early ear development in the embryo of the zebrafish, *Danio rerio*. *J Comp Neurol* 365, 113–128.

Hagiwara, A., Fukazawa, Y., Deguchi-Tawarada, M., Ohtsuka, T., and Shigemoto, R. (2005). Differential distribution of release-related proteins in the hippocampal CA3 area as revealed by freeze-fracture replica labeling. *J Comp Neurol* 489, 195–216.

Hallermann, S., Fejtova, A., Schmidt, H., Weyhersmüller, A., Silver, R.A., Gundelfinger, E.D., and Eilers, J. (2010). Bassoon speeds vesicle reloading at a central excitatory synapse. *Neuron* 68, 710–723.

Hamasaki, K., and Rando, R.R. (1997). Specific binding of aminoglycosides to a human rRNA construct based on a DNA polymorphism which causes aminoglycoside-induced deafness. *Biochemistry* 36, 12323–12328.

Hashimoto, S., Kimura, R.S., and Takasaka, T. (1990). Computer-aided three-dimensional reconstruction of the inner hair cells and their nerve endings in the guinea pig cochlea. *Acta Otolaryngol* 109, 228–234.

van Hateren, J.H. (1992). A theory of maximizing sensory information. *Biol. Cybern.* *68*, 23–29.

Hawley, S.A., Boudeau, J., Reid, J.L., Mustard, K.J., Udd, L., Mäkelä, T.P., Alessi, D.R., and Hardie, D.G. (2003). Complexes between the LKB1 tumor suppressor, STRAD alpha/beta and MO25 alpha/beta are upstream kinases in the AMP-activated protein kinase cascade. *J. Biol.* *2*, 28.

Heinrich, U.R., Maurer, J., and Mann, W. (1999). Ultrastructural evidence for protection of the outer hair cells of the inner ear during intense noise exposure by application of the organic calcium channel blocker diltiazem. *ORL J Otorhinolaryngol Relat Spec* *61*, 321–327.

Hernández, P.P., Moreno, V., Olivari, F.A., and Allende, M.L. (2006). Sub-lethal concentrations of waterborne copper are toxic to lateral line neuromasts in zebrafish (*Danio rerio*). *Hearing Research* *213*, 1–10.

Hernández, P.P., Olivari, F.A., Sarrazin, A.F., Sandoval, P.C., and Allende, M.L. (2007). Regeneration in zebrafish lateral line neuromasts: Expression of the neural progenitor cell marker *sox2* and proliferation-dependent and-independent mechanisms of hair cell renewal. *Dev Neurobiol* *67*, 637–654.

Higashijima, S., Masino, M.A., Mandel, G., and Fetcho, J.R. (2003). Imaging Neuronal Activity During Zebrafish Behavior With a Genetically Encoded Calcium Indicator. *J Neurophysiol* *90*, 3986–3997.

Hildebrand, J.D., and Soriano, P. (2002). Overlapping and unique roles for C-terminal binding protein 1 (CtBP1) and CtBP2 during mouse development. *Mol Cell Biol* 22, 5296–5307.

Hobbie, S.N., Akshay, S., Kalapala, S.K., Bruell, C.M., Shcherbakov, D., and Böttger, E.C. (2008). Genetic analysis of interactions with eukaryotic rRNA identify the mitoribosome as target in aminoglycoside ototoxicity. *Proc Natl Acad Sci USA* 105, 20888–20893.

Holman, H.A., Poppi, L.A., Frerck, M., and Rabbitt, R.D. (2019). Spontaneous and Acetylcholine Evoked Calcium Transients in the Developing Mouse Utricle. *Front Cell Neurosci* 13, 186.

Hübler, D., Rankovic, M., Richter, K., Lazarevic, V., Altmann, W.D., Fischer, K.-D., Gundelfinger, E.D., and Fejtova, A. (2012). Differential spatial expression and subcellular localization of CtBP family members in rodent brain. *PLoS One* 7, e39710.

Huth, M.E., Han, K.-H., Sotoudeh, K., Hsieh, Y.-J., Effertz, T., Vu, A.A., Verhoeven, S., Hsieh, M.H., Greenhouse, R., Cheng, A.G., et al. (2015). Designer aminoglycosides prevent cochlear hair cell loss and hearing loss. *J Clin Invest* 125, 583–592.

Imai, S.-I. (2009). The NAD World: a new systemic regulatory network for metabolism and aging--Sirt1, systemic NAD biosynthesis, and their importance. *Cell Biochem Biophys* 53, 65–74.

Ivanova, D., Dirks, A., Montenegro-Venegas, C., Schöne, C., Altmann, W.D., Marini, C., Frischknecht, R., Schanze, D., Zenker, M., Gundelfinger, E.D., et al. (2015). Synaptic activity

controls localization and function of CtBP1 via binding to Bassoon and Piccolo. *The EMBO Journal* 34, 1056–77.

Jackson, J., Chen, C., and Buising, K. (2013). Aminoglycosides: how should we use them in the 21st century? *Curr Opin Infect Dis* 26, 516–525.

Jean, P., Lopez de la Morena, D., Michanski, S., Jaime Tobón, L.M., Chakrabarti, R., Picher, M.M., Neef, J., Jung, S., Gültas, M., Maxeiner, S., et al. (2018). The synaptic ribbon is critical for sound encoding at high rates and with temporal precision. *ELife* 7, e29275.

Jensen, J.B., Lysaght, A.C., Liberman, M.C., Qvortrup, K., and Stankovic, K.M. (2015). Immediate and delayed cochlear neuropathy after noise exposure in pubescent mice. *PLoS One* 10, e0125160.

Jensen-Smith, H.C., Hallworth, R., and Nichols, M.G. (2012). Gentamicin Rapidly Inhibits Mitochondrial Metabolism in High-Frequency Cochlear Outer Hair Cells. *PLoS ONE* 7, e38471.

Jiang, D., Zhao, L., and Clapham, D.E. (2009). Genome-wide RNAi screen identifies *Letm1* as a mitochondrial $\text{Ca}^{2+}/\text{H}^{+}$ antiporter. *Science* 326, 144–147.

Jiang, T., Kindt, K., and Wu, D.K. (2017). Transcription factor *Emx2* controls stereociliary bundle orientation of sensory hair cells. *ELife* 6, e23661.

Jing, Z., Rutherford, M.A., Takago, H., Frank, T., Fejtova, A., Khimich, D., Moser, T., and Strenzke, N. (2013). Disruption of the presynaptic cytomatrix protein bassoon degrades ribbon anchorage, multiquantal release, and sound encoding at the hair cell afferent synapse. *J Neurosci* 33, 4456–67.

- Johnson, S.L., Forge, A., Knipper, M., Munkner, S., and Marcotti, W. (2008). Tonotopic variation in the calcium dependence of neurotransmitter release and vesicle pool replenishment at mammalian auditory ribbon synapses. *J Neurosci* 28, 7670–7678.
- Johnson, S.L., Franz, C., Marcotti, W., and Marcotti, W. (2009). Functional maturation of the exocytotic machinery at gerbil hair cell ribbon synapses. *J Physiol* 587, 1715–1726.
- Johnson, S.L., Eckrich, T., Kuhn, S., Zampini, V., Franz, C., Ranatunga, K.M., Roberts, T.P., Masetto, S., Knipper, M., Kros, C.J., et al. (2011). Position-dependent patterning of spontaneous action potentials in immature cochlear inner hair cells. *Nat Neurosci* 14, 711–717.
- Johnson, S.L., Kuhn, S., Franz, C., Ingham, N., Furness, D.N., Knipper, M., Steel, K.P., Adelman, J.P., Holley, M.C., and Marcotti, W. (2013). Presynaptic maturation in auditory hair cells requires a critical period of sensory-independent spiking activity. *Proc Natl Acad Sci USA* 110, 8720–8725.
- Johnson, S.L., Safieddine, S., Mustapha, M., and Marcotti, W. (2019). Hair cell afferent synapses: function and dysfunction. *Cold Spring Harb Perspect Med* a033175.
- Jones, S.M., Erway, L.C., Bergstrom, R.A., Schimenti, J.C., and Jones, T.A. (1999). Vestibular responses to linear acceleration are absent in otoconia-deficient C57BL/6JEi-het mice. *Hear Res* 135, 56–60.
- Jones, S.M., Erway, L.C., Johnson, K.R., Yu, H., and Jones, T.A. (2004). Gravity receptor function in mice with graded otoconial deficiencies. *Hearing Research* 191, 34–40.

- Kakkar, P., and Singh, B.K. (2007). Mitochondria: a hub of redox activities and cellular distress control. *Mol. Cell. Biochem.* *305*, 235–253.
- Kalluri, R., and Monges-Hernandez, M. (2017). Spatial Gradients in the Size of Inner Hair Cell Ribbons Emerge Before the Onset of Hearing in Rats. *J. Assoc. Res. Otolaryngol.* *18*, 399–413.
- Kameoka, K., Isotani, H., Tanaka, K., Azukari, K., Fujimura, Y., Shiota, Y., Sasaki, E., Majima, M., Furukawa, K., Haginomori, S., et al. (1998). Novel mitochondrial DNA mutation in tRNA^{Lys}(8296A → G) associated with diabetes. *Biochem Biophys Res Commun* *245*, 523–527.
- Kamer, K.J., and Mootha, V.K. (2014). MICU1 and MICU2 play nonredundant roles in the regulation of the mitochondrial calcium uniporter. *EMBO Rep* *15*, 299–307.
- Kann, O., and Kovács, R. (2007). Mitochondria and neuronal activity. *Am J Physiol, Cell Physiol* *292*, C641–57.
- Karavitaki, K.D., and Mountain, D.C. (2007). Imaging electrically evoked micromechanical motion within the organ of corti of the excised gerbil cochlea. *Biophys J* *92*, 3294–3316.
- Kennedy, H.J.J. (2002). Intracellular calcium regulation in inner hair cells from neonatal mice. *Cell Calcium* *31*, 127–136.
- Kennedy, H.J., and Meech, R.W. (2002). Fast Ca²⁺ signals at mouse inner hair cell synapse: a role for Ca²⁺-induced Ca²⁺ release. *J Physiol* *539*, 15–23.

- Khan, S., and Chang, R. (2013). Anatomy of the vestibular system: a review. *NeuroRehabilitation* 32, 437–443.
- Khimich, D., Nouvian, R., Pujol, R., tom Dieck, S., Egner, A., Gundelfinger, E.D., and Moser, T. (2005). Hair cell synaptic ribbons are essential for synchronous auditory signalling. *Nature* 434, 889–894.
- Kimmel, C.B., Ballard, W.W., Kimmel, S.R., Ullmann, B., and Schilling, T.F. (1995). Stages of embryonic development of the zebrafish. *Dev Dyn* 203, 253–310.
- Kindt, K.S., Finch, G., and Nicolson, T. (2012). Kinocilia mediate mechanosensitivity in developing zebrafish hair cells. *Developmental Cell* 23, 329–41.
- Kirichok, Y., Krapivinsky, G., and Clapham, D.E. (2004). The mitochondrial calcium uniporter is a highly selective ion channel. *Nature* 427, 360–364.
- Knipper, M., Van Dijk, P., Nunes, I., Rüttiger, L., and Zimmermann, U. (2013). Advances in the neurobiology of hearing disorders: Recent developments regarding the basis of tinnitus and hyperacusis. *Progress in Neurobiology* 111, 17–33.
- Kokotas, H., Petersen, M.B., and Willems, P.J. (2007). Mitochondrial deafness. *Clin Genet* 71, 379–391.
- Kollmar, R., Fak, J., Montgomery, L.G., and Hudspeth, A.J. (1997). Hair cell-specific splicing of mRNA for the alpha1D subunit of voltage-gated Ca²⁺ channels in the chicken's cochlea. *Proc. Natl. Acad. Sci. U.S.A.* 94, 14889–14893.

- Koschak, A., Reimer, D., Huber, I., Grabner, M., Glossmann, H., Engel, J., and Striessnig, J. (2001). α 1D (Cav1.3) subunits can form l-type Ca^{2+} channels activating at negative voltages. *J. Biol. Chem.* *276*, 22100–22106.
- Krebs, H.A. (1970). Rate control of the tricarboxylic acid cycle. *Advances in Enzyme Regulation* *8*, 335–353.
- Krinner, S., Butola, T., Jung, S., Wichmann, C., and Moser, T. (2017). RIM-Binding Protein 2 promotes a large number of CaV1.3 Ca^{2+} -channels and contributes to fast synaptic vesicle replenishment at hair cell active zones. *Front Cell Neurosci* *11*, 334.
- Krols, M., van Isterdael, G., Asselbergh, B., Kremer, A., Lippens, S., Timmerman, V., and Janssens, S. (2016). Mitochondria-associated membranes as hubs for neurodegeneration. *Acta Neuropathol* *131*, 505–523.
- Kros, C.J. (2007). How to build an inner hair cell: challenges for regeneration. *Hear Res* *227*, 3–10.
- Kros, C.J., Ruppersberg, J.P., and Rüschi, A. (1998). Expression of a potassium current in inner hair cells during development of hearing in mice. *Nature* *394*, 281–284.
- Kujawa, S.G., and Liberman, M.C. (2009). Adding insult to injury: cochlear nerve degeneration after “temporary” noise-induced hearing loss. *J Neurosci* *29*, 14077–14085.
- Kwan, K.M., Fujimoto, E., Grabher, C., Mangum, B.D., Hardy, M.E., Campbell, D.S., Parant, J.M., Yost, H.J., Kanki, J.P., and Chien, C.-B. (2007). The Tol2kit: a multisite gateway-based construction kit for Tol2 transposon transgenesis constructs. *Dev Dyn* *236*, 3088–3099.

Kwon, S.-K., Sando, R., Lewis, T.L., Hirabayashi, Y., Maximov, A., and Polleux, F. (2016). LKB1 Regulates Mitochondria-Dependent Presynaptic Calcium Clearance and Neurotransmitter Release Properties at Excitatory Synapses along Cortical Axons. *PLoS Biology* *14*, e1002516.

Ladich, F. (2014). Fish bioacoustics. *Curr Opin Neurobiol* *28*, 121–127.

Lagnado, L., and Schmitz, F. (2015). Ribbon Synapses and Visual Processing in the Retina. *Annu Rev Vis Sci* *1*, 235–262.

Lai, J.C., and Cooper, A.J. (1986). Brain alpha-ketoglutarate dehydrogenase complex: kinetic properties, regional distribution, and effects of inhibitors. *J Neurochem* *47*, 1376–1386.

Lanner, J.T. (2012). Ryanodine receptor physiology and its role in disease. In *Calcium Signaling*, Md.S. Islam, ed. (Dordrecht: Springer Netherlands), pp. 217–234.

Lanner, J.T., Georgiou, D.K., Joshi, A.D., and Hamilton, S.L. (2010). Ryanodine receptors: structure, expression, molecular details, and function in calcium release. *Cold Spring Harb Perspect Biol* *2*, a003996.

Lawlis, V.B., and Roche, T.E. (1981a). Regulation of bovine kidney .alpha.-ketoglutarate dehydrogenase complex by calcium ion and adenine nucleotides. Effects on S0.5 for .alpha.-ketoglutarate. *Biochemistry* *20*, 2512–2518.

Lawlis, V.B., and Roche, T.E. (1981b). Inhibition of bovine kidney alpha-ketoglutarate dehydrogenase complex by reduced nicotinamide adenine dinucleotide in the presence or absence of calcium ion and effect of adenosine 5'-diphosphate on reduced nicotinamide adenine dinucleotide inhibition. *Biochemistry* *20*, 2519–2524.

- Lenzi, D., Runyeon, J.W., Crum, J., Ellisman, M.H., and Roberts, W.M. (1999). Synaptic vesicle populations in saccular hair cells reconstructed by electron tomography. *J Neurosci* *19*, 119–132.
- Lenzi, D., Crum, J., Ellisman, M.H., and Roberts, W.M. (2002). Depolarization redistributes synaptic membrane and creates a gradient of vesicles on the synaptic body at a ribbon synapse. *Neuron* *36*, 649–59.
- Lepeta, K., Lourenco, M.V., Schweitzer, B.C., Martino Adami, P.V., Banerjee, P., Catuara-Solarz, S., de La Fuente Revenga, M., Guillem, A.M., Haidar, M., Ijomone, O.M., et al. (2016). Synaptopathies: synaptic dysfunction in neurological disorders - A review from students to students. *J. Neurochem.* *138*, 785–805.
- Levy, M., Faas, G.C., Saggau, P., Craigen, W.J., and Sweatt, J.D. (2003). Mitochondrial regulation of synaptic plasticity in the hippocampus. *J. Biol. Chem.* *278*, 17727–17734.
- Lewis, J.A., and Tata, J.R. (1973). A rapidly sedimenting fraction of rat liver endoplasmic reticulum. *J Cell Sci* *13*, 447–459.
- Li, W., and Sauve, A.A. (2015). NAD⁺ Content and Its Role in Mitochondria. In *Mitochondrial Regulation*, C.M. Palmeira, and A.P. Rolo, eds. (New York, NY: Springer New York), pp. 39–48.
- Lieberman, M.C. (1982). Single-neuron labeling in the cat auditory nerve. *Science* *216*, 1239–1241.

Liberman, L.D., and Liberman, M.C. (2015). Dynamics of cochlear synaptopathy after acoustic overexposure. *Journal of the Association for Research in Otolaryngology* *16*, 205–219.

Liberman, L.D., and Liberman, M.C. (2016). Postnatal maturation of auditory-nerve heterogeneity, as seen in spatial gradients of synapse morphology in the inner hair cell area. *339*, 12–22.

Liberman, M.C., and Dodds, L.W. (1984). Single-neuron labeling and chronic cochlear pathology. III. Stereocilia damage and alterations of threshold tuning curves. *Hear. Res.* *16*, 55–74.

Liberman, L.D., Wang, H., and Liberman, M.C. (2011). Opposing gradients of ribbon size and AMPA receptor expression underlie sensitivity differences among cochlear-nerve/hair-cell synapses. *J Neurosci* *31*, 801–808.

Liberman, M.C., Dodds, L.W., and Pierce, S. (1990). Afferent and efferent innervation of the cat cochlea: quantitative analysis with light and electron microscopy. *The Journal of Comparative Neurology* *301*, 443–60.

Liberman, M.C., Gao, J., He, D.Z.Z., Wu, X., Jia, S., and Zuo, J. (2002). Prestin is required for electromotility of the outer hair cell and for the cochlear amplifier. *Nature* *419*, 300–304.

Lim, R., Kindig, A.E., Donne, S.W., Callister, R.J., and Brichta, A.M. (2011). Potassium accumulation between type I hair cells and calyx terminals in mouse crista. *Exp Brain Res* *210*, 607–621.

Lindquist, S.E., Neff, W.D., and Schuknecht, H.F. (1954). Stimulation deafness: a study of hearing losses resulting from exposure to noise or to blast impulses. *Journal of Comparative and Physiological Psychology* 47, 406–411.

Lioudyno, M., Hiel, H., Kong, J.-H., Katz, E., Waldman, E., Parameshwaran-Iyer, S., Glowatzki, E., and Fuchs, P.A. (2004). A “synaptoplasmic cistern” mediates rapid inhibition of cochlear hair cells. *J Neurosci* 24, 11160–11164.

Liu, Y., and Zhu, X. (2017). Endoplasmic reticulum-mitochondria tethering in neurodegenerative diseases. *Transl Neurodegener* 6, 21.

Llorente-Folch, I., Rueda, C.B., Pardo, B., Szabadkai, G., Duchen, M.R., and Satrustegui, J. (2015). The regulation of neuronal mitochondrial metabolism by calcium. *J Physiol* 593, 3447–3462.

Lukasz, D., and Kindt, K.S. (2018). In Vivo Calcium Imaging of Lateral-line Hair Cells in Larval Zebrafish. *J Vis Exp*.

Lumpkin, E.A., and Hudspeth, A.J. (1995). Detection of Ca^{2+} entry through mechanosensitive channels localizes the site of mechano-electrical transduction in hair cells. *Proc. Natl. Acad. Sci. U.S.A.* 92, 10297–10301.

Luo, D., Nakazawa, M., Yoshida, Y., Cai, J., and Imai, S. (2000). Effects of three different Ca^{2+} pump ATPase inhibitors on evoked contractions in rabbit aorta and activities of Ca^{2+} pump ATPases in porcine aorta. *Gen. Pharmacol.* 34, 211–220.

Luongo, T.S., Lambert, J.P., Gross, P., Nwokedi, M., Lombardi, A.A., Shanmughapriya, S., Carpenter, A.C., Kolmetzky, D., Gao, E., van Berlo, J.H., et al. (2017). The mitochondrial $\text{Na}^+/\text{Ca}^{2+}$ exchanger is essential for Ca^{2+} homeostasis and viability. *Nature* 545, 93–97.

Lv, C., Gould, T.J., Bewersdorf, J., and Zenisek, D. (2012). High-resolution optical imaging of zebrafish larval ribbon synapse protein RIBEYE, RIM2, and CaV 1.4 by stimulation emission depletion microscopy. *Microsc. Microanal.* 18, 745–752.

Lv, C., Stewart, W.J., Akanyeti, O., Frederick, C., Zhu, J., Santos-Sacchi, J., Sheets, L., Liao, J.C., and Zenisek, D. (2016). Synaptic Ribbons Require Ribeye for Electron Density, Proper Synaptic Localization, and Recruitment of Calcium Channels. *Cell Rep* 15, 2784–2795.

Lysakowski, A., and Goldberg, J.M. (1997). A regional ultrastructural analysis of the cellular and synaptic architecture in the chinchilla cristae ampullares. *The Journal of Comparative Neurology* 389, 419–43.

Ma, E.Y., Rubel, E.W., and Raible, D.W. (2008). Notch Signaling Regulates the Extent of Hair Cell Regeneration in the Zebrafish Lateral Line. *Journal of Neuroscience* 28, 2261–2273.

Madison, D.L., Wirz, J.A., Siess, D., and Lundblad, J.R. (2013). Nicotinamide adenine dinucleotide-induced multimerization of the co-repressor CtBP1 relies on a switching tryptophan. *J. Biol. Chem.* 288, 27836–27848.

Maeda, R., Kindt, K.S., Mo, W., Morgan, C.P., Erickson, T., Zhao, H., Clemens-Grisham, R., Barr-Gillespie, P.G., and Nicolson, T. (2014). Tip-link protein protocadherin 15 interacts

with transmembrane channel-like proteins TMC1 and TMC2. *Proceedings of the National Academy of Sciences* *111*, 12907–12912.

Magupalli, V.G., Schwarz, K., Alpadi, K., Natarajan, S., Seigel, G.M., and Schmitz, F. (2008). Multiple RIBEYE-RIBEYE interactions create a dynamic scaffold for the formation of synaptic ribbons. *J Neurosci* *28*, 7954–7967.

Makary, C.A., Shin, J., Kujawa, S.G., Liberman, M.C., and Merchant, S.N. (2011). Age-related primary cochlear neuronal degeneration in human temporal bones. *J. Assoc. Res. Otolaryngol.* *12*, 711–717.

Manchenkov, T., Pasillas, M.P., Haddad, G.G., and Imam, F.B. (2015). Novel genes critical for hypoxic preconditioning in zebrafish are regulators of Insulin and glucose metabolism. *G3: Genes, Genomes, Genetics* *5*, 1107–1116.

Mangiardi, D.A., McLaughlin-Williamson, K., May, K.E., Messana, E.P., Mountain, D.C., and Cotanche, D.A. (2004). Progression of hair cell ejection and molecular markers of apoptosis in the avian cochlea following gentamicin treatment. *J. Comp. Neurol.* *475*, 1–18.

Marcotti, W., Johnson, S.L., Rusch, A., and Kros, C.J. (2003). Sodium and calcium currents shape action potentials in immature mouse inner hair cells. *J Physiol* *552*, 743–761.

Marinelli, F., Almagor, L., Hiller, R., Giladi, M., Khananshvili, D., and Faraldo-Gómez, J.D. (2014). Sodium recognition by the Na⁺/Ca²⁺ exchanger in the outward-facing conformation. *Proc Natl Acad Sci USA* *111*, E5354–E5362.

Marshall, S.E., McCormack, J.G., and Denton, R.M. (1984). Role of Ca²⁺ ions in the regulation of intramitochondrial metabolism in rat epididymal adipose tissue. *Evidence*

against a role for Ca^{2+} in the activation of pyruvate dehydrogenase by insulin. *Biochem J* 218, 249–260.

Marti, F., Korn, H., and Faure, P. (2008). Interplay between subthreshold potentials and γ oscillations in Mauthner cells' presynaptic inhibitory interneurons. *Neuroscience* 151, 983–994.

Maruyama, T., Kanaji, T., Nakade, S., Kanno, T., and Mikoshiba, K. (1997). 2APB, 2-Aminoethoxydiphenyl Borate, a Membrane-Penetrable Modulator of $\text{Ins}(1,4,5)\text{P}_3$ -Induced Ca^{2+} Release. *J Biochem* 122, 498–505.

Matlib, M.A., Zhou, Z., Knight, S., Ahmed, S., Choi, K.M., Krause-Bauer, J., Phillips, R., Altschuld, R., Katsube, Y., Sperelakis, N., et al. (1998). Oxygen-bridged dinuclear ruthenium amine complex specifically inhibits Ca^{2+} uptake into mitochondria in vitro and in situ in single cardiac myocytes. *Journal of Biological Chemistry* 273, 10223–10231.

Matsushima, S., Sakai, Y., and Aida, I. (1983). Effects of melatonin on synaptic ribbons in pinealocytes of the Chinese hamster, *Cricetulus griseus*. *Cell and Tissue Research* 233, 59–67.

Matthews, G., and Fuchs, P. (2010). The diverse roles of ribbon synapses in sensory neurotransmission. *Nat Rev Neurosci* 11, 812–822.

Maxeiner, S., Luo, F., Tan, A., Schmitz, F., and Südhof, T.C. (2016). How to make a synaptic ribbon: RIBEYE deletion abolishes ribbons in retinal synapses and disrupts neurotransmitter release. *EMBO J* 35, 1098–1114.

- McCormack, J.G., and Denton, R.M. (1979). The effects of calcium ions and adenine nucleotides on the activity of pig heart 2-oxoglutarate dehydrogenase complex. *Biochem. J.* *180*, 533–544.
- McHenry, M.J., Feitl, K.E., Strother, J.A., and Van Trump, W.J. (2009). Larval zebrafish rapidly sense the water flow of a predator's strike. *Biology Letters* *5*, 477–9.
- Mellado Lagarde, M.M., Drexler, M., Lukashkin, A.N., Zuo, J., and Russell, I.J. (2008). Prestin's role in cochlear frequency tuning and transmission of mechanical responses to neural excitation. *Curr Biol* *18*, 200–202.
- Mendoza Schulz, A., Jing, Z., María Sánchez Caro, J., Wetzel, F., Dresbach, T., Strenzke, N., Wichmann, C., and Moser, T. (2014). Bassoon-disruption slows vesicle replenishment and induces homeostatic plasticity at a CNS synapse. *EMBO J* *33*, 512–527.
- Merchan-Perez, A., and Liberman, M.C. (1996). Ultrastructural differences among afferent synapses on cochlear hair cells: correlations with spontaneous discharge rate. *J Comp Neurol* *371*, 208–21.
- Metcalf, W.K. (1985). Sensory neuron growth cones comigrate with posterior lateral line primordial cells in zebrafish. *J Comp Neurol* *238*, 218–224.
- Metcalf, W.K., Kimmel, C.B., and Schabtach, E. (1985). Anatomy of the posterior lateral line system in young larvae of the zebrafish. *J Comp Neurol* *233*, 377–389.
- Metcalf, W.K., Mendelson, B., and Kimmel, C.B. (1986). Segmental homologies among reticulospinal neurons in the hindbrain of the zebrafish larva. *J. Comp. Neurol.* *251*, 147–159.

- Meyer, A.C., Frank, T., Khimich, D., Hoch, G., Riedel, D., Chapochnikov, N.M., Yarin, Y.M., Harke, B., Hell, S.W., Egner, A., et al. (2009). Tuning of synapse number, structure and function in the cochlea. *Nat Neurosci* *12*, 444–453.
- Michalski, N., and Petit, C. (2015). Genetics of auditory mechano-electrical transduction. *Pflugers Arch* *467*, 49–72.
- Michanski, S., Smaluch, K., Steyer, A.M., Chakrabarti, R., Setz, C., Oestreicher, D., Fischer, C., Möbius, W., Moser, T., Vogl, C., et al. (2019). Mapping developmental maturation of inner hair cell ribbon synapses in the apical mouse cochlea. *Proc Natl Acad Sci USA* *116*, 6415–6424.
- Mikaelian, D., and Ruben, R.J. (1965). Development of hearing in the normal Cba-J mouse: correlation of physiological observations with behavioral responses and with cochlear anatomy. *Acta Otolaryngol* *59*, 451–461.
- Mikoshiya, K. (2015). Role of IP3 receptor signaling in cell functions and diseases. *Adv Biol Regul* *57*, 217–227.
- Mirjany, M., and Faber, D.S. (2011). Characteristics of the anterior lateral line nerve input to the Mauthner cell. *J Exp Biol* *214*, 3368.
- Mogami, H., Tepikin, A.V., and Petersen, O.H. (1998). Termination of cytosolic Ca²⁺ signals: Ca²⁺ reuptake into intracellular stores is regulated by the free Ca²⁺ concentration in the store lumen. *EMBO J* *17*, 435–442.

- Moglie, M.J., Fuchs, P.A., Elgoyhen, A.B., and Goutman, J.D. (2018). Compartmentalization of antagonistic Ca²⁺ signals in developing cochlear hair cells. *Proc Natl Acad Sci USA* *115*, E2095–E2104.
- Montgomery, J.C., McDonald, F., Baker, C.F., Carton, A.G., and Ling, N. (2003). Sensory integration in the hydrodynamic world of rainbow trout. *Proc. R. Soc. Lond. B* *270*.
- Monzack, E.L., and Cunningham, L.L. (2013). Lead roles for supporting actors: Critical functions of inner ear supporting cells. *Hearing Research* *303*, 20–29.
- Moorman, S.J., Burrell, C., Cordova, R., and Slater, J. (1999). Stimulus dependence of the development of the zebrafish (*Danio rerio*) vestibular system. *J Neurobiol* *38*, 247–258.
- Moser, T., and Beutner, D. (2000). Kinetics of exocytosis and endocytosis at the cochlear inner hair cell afferent synapse of the mouse. *Proc Natl Acad Sci USA* *97*, 883–888.
- Moser, T., and Starr, A. (2016). Auditory neuropathy--neural and synaptic mechanisms. *Nat Rev Neurol* *12*, 135–149.
- Moser, T., Brandt, A., and Lysakowski, A. (2006). Hair cell ribbon synapses. *Cell Tissue Res* *326*, 347–359.
- Mukherjee, K., Yang, X., Gerber, S.H., Kwon, H.-B., Ho, A., Castillo, P.E., Liu, X., and Sudhof, T.C. (2010). Piccolo and bassoon maintain synaptic vesicle clustering without directly participating in vesicle exocytosis. *Proceedings of the National Academy of Sciences* *107*, 6504–6509.

Mulkey, R.M., and Malenka, R.C. (1992). Mechanisms underlying induction of homosynaptic long-term depression in area CA1 of the hippocampus. *Neuron* *9*, 967–975.

Müller, T.M., Gierke, K., Joachimsthaler, A., Sticht, H., Izsvák, Z., Hamra, F.K., Fejtová, A., Ackermann, F., Garner, C.C., Kremers, J., et al. (2019). A multiple Piccolino-RIBEYE interaction supports plate-shaped synaptic ribbons in retinal neurons. *J Neurosci* *39*, 2606–2619.

Murakami, S.L., Cunningham, L.L., Werner, L.A., Bauer, E., Pujol, R., Raible, D.W., and Rubel, E.W. (2003). Developmental differences in susceptibility to neomycin-induced hair cell death in the lateral line neuromasts of zebrafish (*Danio rerio*). *Hearing Research* *186*, 47–56.

Murphy, A.N., Kelleher, J.K., and Fiskum, G. (1990). Submicromolar Ca^{2+} regulates phosphorylating respiration by normal rat liver and AS-30D hepatoma mitochondria by different mechanisms. *J Biol Chem* *265*, 10527–10534.

Nagiel, A., Andor-Ardo, D., and Hudspeth, A.J. (2008). Specificity of afferent synapses onto plane-polarized hair cells in the posterior lateral line of the zebrafish. *J Neurosci* *28*, 8442–8453.

Nagiel, A., Patel, S.H., Andor-Ardo, D., and Hudspeth, A.J. (2009). Activity-independent specification of synaptic targets in the posterior lateral line of the larval zebrafish. *PNAS* *106*, 21948–21953.

Naidu, R.C., and Mountain, D.C. (1998). Measurements of the stiffness map challenge a basic tenet of cochlear theories. *Hear Res* *124*, 124–131.

- Nakamura, K., Bossy-Wetzler, E., Burns, K., Fadel, M.P., Lozyk, M., Goping, I.S., Opas, M., Bleackley, R.C., Green, D.R., and Michalak, M. (2000). Changes in Endoplasmic Reticulum Luminal Environment Affect Cell Sensitivity to Apoptosis. *J Cell Biol* *150*, 731–740.
- Namkung, Y., Skrypnik, N., Jeong, M.-J., Lee, T., Lee, M.-S., Kim, H.-L., Chin, H., Suh, P.-G., Kim, S.-S., and Shin, H.-S. (2001). Requirement for the L-type Ca^{2+} channel $\alpha 1\text{D}$ subunit in postnatal pancreatic β cell generation. *J. Clin. Invest.* *108*, 1015–1022.
- Neef, J., Gehrt, A., Bulankina, A.V., Meyer, A.C., Riedel, D., Gregg, R.G., Strenzke, N., and Moser, T. (2009). The Ca^{2+} channel subunit beta2 regulates Ca^{2+} channel abundance and function in inner hair cells and is required for hearing. *J Neurosci* *29*, 10730–10740.
- Neef, J., Urban, N.T., Ohn, T.-L., Frank, T., Jean, P., Hell, S.W., Willig, K.I., and Moser, T. (2018). Quantitative optical nanophysiology of Ca^{2+} signaling at inner hair cell active zones. *Nat Commun* *9*, 290.
- Nemzou N, R.M., Bulankina, A.V., Khimich, D., Giese, A., and Moser, T. (2006). Synaptic organization in cochlear inner hair cells deficient for the $\text{CaV}1.3$ ($\alpha 1\text{D}$) subunit of L-type Ca^{2+} channels. *Neuroscience* *141*, 1849–60.
- Nicholls, D.G. (2005). Mitochondria and calcium signaling. *Cell Calcium* *38*, 311–317.
- Nicolson, T. (2005). The genetics of hearing and balance in zebrafish. *Annu Rev Genet* *39*, 9–22.
- Nicolson, T. (2017). The genetics of hair-cell function in zebrafish. *J. Neurogenet.* *31*, 102–112.

Nissanov, J., Eaton, R.C., and DiDomenico, R. (1990). The motor output of the Mauthner cell, a reticulospinal command neuron. *Brain Res* 517, 88–98.

Nordemar, H. (1983). Embryogenesis of the Inner Ear: II. The Late Differentiation of the Mammalian Crista Ampullaris in Vivo and in Vitro. *Acta Oto-Laryngologica* 96, 1–8.

Nouvian, R., Beutner, D., Parsons, T.D., and Moser, T. (2006). Structure and Function of the Hair Cell Ribbon Synapse. *J Membrane Biol* 209, 153–165.

Nouvian, R., Neef, J., Bulankina, A.V., Reisinger, E., Pangršič, T., Frank, T., Sikorra, S., Brose, N., Binz, T., and Moser, T. (2011). Exocytosis at the hair cell ribbon synapse apparently operates without neuronal SNARE proteins. *Nature Neuroscience* 14, 411–3.

Obholzer, N., Wolfson, S., Trapani, J.G., Mo, W., Nechiporuk, A., Busch-Nentwich, E., Seiler, C., Sidi, S., Söllner, C., Duncan, R.N., et al. (2008). Vesicular glutamate transporter 3 is required for synaptic transmission in zebrafish hair cells. *J Neurosci* 28, 2110–2118.

Ohinata, Y., Miller, J.M., Altschuler, R.A., and Schacht, J. (2000). Intense noise induces formation of vasoactive lipid peroxidation products in the cochlea. *Brain Res.* 878, 163–173.

Ohn, T.-L., Rutherford, M.A., Jing, Z., Jung, S., Duque-Afonso, C.J., Hoch, G., Picher, M.M., Scharinger, A., Strenzke, N., and Moser, T. (2016). Hair cells use active zones with different voltage dependence of Ca²⁺ influx to decompose sounds into complementary neural codes. *Proc. Natl. Acad. Sci. U.S.A.* 113, E4716-4725.

Ohtsuka, T., Takao-Rikitsu, E., Inoue, E., Inoue, M., Takeuchi, M., Matsubara, K., Deguchi-Tawarada, M., Satoh, K., Morimoto, K., Nakanishi, H., et al. (2002). Cast: a novel protein of

the cytomatrix at the active zone of synapses that forms a ternary complex with RIM1 and munc13-1. *J Cell Biol* 158, 577–590.

Oishi, N., and Schacht, J. (2011). Emerging treatments for noise-induced hearing loss. *Expert Opin Emerg Drugs* 16, 235–245.

Okerlund, N.D., Schneider, K., Leal-Ortiz, S., Montenegro-Venegas, C., Kim, S.A., Garner, L.C., Waites, C.L., Gundelfinger, E.D., Reimer, R.J., and Garner, C.C. (2017). Bassoon Controls Presynaptic Autophagy through Atg5. *Neuron* 93, 897-913.e7.

Olivari, F.A., Hernández, P.P., and Allende, M.L. (2008). Acute copper exposure induces oxidative stress and cell death in lateral line hair cells of zebrafish larvae. *Brain Research* 1244, 1–12.

Ollion, J., Cochenec, J., Loll, F., Escudé, C., and Boudier, T. (2013). TANGO: a generic tool for high-throughput 3D image analysis for studying nuclear organization. *Bioinformatics* 29, 1840–1841.

Orrenius, S., Zhivotovsky, B., and Nicotera, P. (2003). Regulation of cell death: the calcium-apoptosis link. *Nat Rev Mol Cell Biol* 4, 552–565.

van den Ouweland, J.M.W., Lemkes, H.H.P.J., Ruitenbeek, W., Sandkuijl, L.A., de Vijlder, M.F., Struyvenberg, P.A.A., van de Kamp, J.J.P., and Maassen, J.A. (1992). Mutation in mitochondrial tRNA^{Leu}(UUR) gene in a large pedigree with maternally transmitted type II diabetes mellitus and deafness. *Nat Genet* 1, 368–371.

Owens, K.N., Cunningham, D.E., Macdonald, G., Rubel, E.W., Raible, D.W., and Pujol, R. (2007). Ultrastructural analysis of aminoglycoside-induced hair cell death in the zebrafish lateral line reveals an early mitochondrial response. *J. Comp. Neurol.* *502*, 522–543.

Palma, F.D., Holme, R.H., Bryda, E.C., Belyantseva, I.A., Pellegrino, R., Kachar, B., Steel, K.P., and Noben-Trauth, K. (2001). Mutations in *Cdh23*, encoding a new type of cadherin, cause stereocilia disorganization in *waltzer*, the mouse model for Usher syndrome type 1D. *Nat Genet* *27*, 103–107.

Palty, R., Silverman, W.F., Hershinkel, M., Caporale, T., Sensi, S.L., Parnis, J., Nolte, C., Fishman, D., Shoshan-Barmatz, V., Herrmann, S., et al. (2010). NCLX is an essential component of mitochondrial $\text{Na}^+/\text{Ca}^{2+}$ exchange. *Proc. Natl. Acad. Sci. U.S.A.* *107*, 436–441.

Pang, Z.P., and Südhof, T.C. (2010). Cell biology of Ca^{2+} -triggered exocytosis. *Current Opinion in Cell Biology* *22*, 496–505.

Pangršič, T., Lasarow, L., Reuter, K., Takago, H., Schwander, M., Riedel, D., Frank, T., Tarantino, L.M., Bailey, J.S., Strenzke, N., et al. (2010). Hearing requires otoferlin-dependent efficient replenishment of synaptic vesicles in hair cells. *Nat Neurosci* *13*, 869–876.

Pangršič, T., Reisinger, E., and Moser, T. (2012). Otoferlin: a multi-C2 domain protein essential for hearing. *Trends Neurosci* *35*, 671–680.

Pangršič, T., Singer, J.H., and Koschak, A. (2018). Voltage-gated calcium channels: key players in sensory coding in the retina and the inner ear. *Physiol Rev* *98*, 2063–2096.

- Parsons, T.D., Lenzi, D., Almers, W., and Roberts, W.M. (1994). Calcium-triggered exocytosis and endocytosis in an isolated presynaptic cell: capacitance measurements in saccular hair cells. *Neuron* 13, 875–883.
- Parthier, D., Kuner, T., and Körber, C. (2018). The presynaptic scaffolding protein Piccolo organizes the readily releasable pool at the calyx of Held: Bassoon and Piccolo in synaptic transmission. *J Physiol* 596, 1485–1499.
- Patron, M., Raffaello, A., Granatiero, V., Tosatto, A., Merli, G., De Stefani, D., Wright, L., Pallafacchina, G., Terrin, A., Mammucari, C., et al. (2013). The Mitochondrial calcium uniporter (MCU): Molecular identity and physiological roles. *J Biol Chem* 288, 10750–10758.
- Peng, T.-I., and Jou, M.-J. (2010). Oxidative stress caused by mitochondrial calcium overload. *Ann N Y Acad Sci* 1201, 183–188.
- Pfeiffer, T., Schuster, S., and Bonhoeffer, S. (2001). Cooperation and Competition in the Evolution of ATP-Producing Pathways. *Science* 292, 504–507.
- Pickett, C.B., Montisano, D., Eisner, D., and Cascarano, J. (1980). The physical association between rat liver mitochondria and rough endoplasmic reticulum. I. Isolation, electron microscopic examination and sedimentation equilibrium centrifugation analyses of rough endoplasmic reticulum-mitochondrial complexes. *Exp. Cell Res.* 128, 343–352.
- Pickett, S.B., Thomas, E.D., Sebe, J.Y., Linbo, T., Esterberg, R., Hailey, D.W., and Raible, D.W. (2018). Cumulative mitochondrial activity correlates with ototoxin susceptibility in zebrafish mechanosensory hair cells. *Elife* 7, e38062.

- Pinton, P., Brini, M., Bastianutto, C., Tuft, R.A., Pozzan, T., and Rizzuto, R. (1998). New light on mitochondrial calcium. *Biofactors* 8, 243–253.
- Pinton, P., Ferrari, D., Rapizzi, E., Di Virgilio, F., Pozzan, T., and Rizzuto, R. (2001). The Ca^{2+} concentration of the endoplasmic reticulum is a key determinant of ceramide-induced apoptosis: significance for the molecular mechanism of Bcl-2 action. *EMBO J.* 20, 2690–2701.
- Pinton, P., Giorgi, C., Siviero, R., Zecchini, E., and Rizzuto, R. (2008). Calcium and apoptosis: ER-mitochondria Ca^{2+} transfer in the control of apoptosis. *Oncogene* 27, 6407–6418.
- Platt, C. (1993). Zebrafish inner ear sensory surfaces are similar to those in goldfish. *Hear. Res.* 65, 133–140.
- Platzer, J., Engel, J., Schrott-Fischer, A., Stephan, K., Bova, S., Chen, H., Zheng, H., and Striessnig, J. (2000). Congenital deafness and sinoatrial node dysfunction in mice lacking class D L-type Ca^{2+} channels. *Cell* 102, 89–97.
- Popper, A.N., and Fay, R.R. (1993). Sound detection and processing by fish: critical review and major research questions. *Brain Behav Evol* 41, 14–25.
- Popper, A.N., and Fay, R.R. (2011). Rethinking sound detection by fishes. *Hear Res* 273, 25–36.
- Popper, A.N., Ramcharitar, J., and Campana, S.E. (2005). Why otoliths? Insights from inner ear physiology and fisheries biology. *Mar. Freshwater Res.* 56, 497.

- Poulikakos, P., and Falagas, M.E. (2013). Aminoglycoside therapy in infectious diseases. *Expert Opin Pharmacother* *14*, 1585–1597.
- Pozzan, T., Bragadin, M., and Azzone, G.F. (1977). Disequilibrium between steady-state Ca^{2+} accumulation ratio and membrane potential in mitochondria. Pathway and role of Ca^{2+} efflux. *Biochemistry* *16*, 5618–5625.
- Puel, J.L., Pujol, R., Tribillac, F., Ladrech, S., and Eybalin, M. (1994). Excitatory amino acid antagonists protect cochlear auditory neurons from excitotoxicity. *J. Comp. Neurol.* *341*, 241–256.
- Pujol, R., Lenoir, M., Robertson, D., Eybalin, M., and Johnstone, B.M. (1985). Kainic acid selectively alters auditory dendrites connected with cochlear inner hair cells. *Hear. Res.* *18*, 145–151.
- Qi, H., Li, L., and Shuai, J. (2015). Optimal microdomain crosstalk between endoplasmic reticulum and mitochondria for Ca^{2+} oscillations. *Sci Rep* *5*, 7984.
- Qiu, J., Tan, Y.-W., Hagenston, A.M., Martel, M.-A., Kneisel, N., Skehel, P.A., Wyllie, D.J.A., Bading, H., and Hardingham, G.E. (2013). Mitochondrial calcium uniporter Mcu controls excitotoxicity and is transcriptionally repressed by neuroprotective nuclear calcium signals. *Nat Commun* *4*, 2034.
- Raible, D.W., and Kruse, G.J. (2000). Organization of the lateral line system in embryonic zebrafish. *J Comp Neurol* *421*, 189–198.
- Rapizzi, E., Pinton, P., Szabadkai, G., Wieckowski, M.R., Vandecasteele, G., Baird, G., Tuft, R.A., Fogarty, K.E., and Rizzuto, R. (2002). Recombinant expression of the voltage-

dependent anion channel enhances the transfer of Ca^{2+} microdomains to mitochondria. *J Cell Biol.* 159, 613–624.

Reardon, W., Pembrey, M.E., Trembath, R.C., Ross, R.J.M., Sweeney, M.G., Harding, A.E., and Luxon, L.M. (1992). Diabetes mellitus associated with a pathogenic point mutation in mitochondrial DNA. *The Lancet* 340, 1376–1379.

Regus-Leidig, H., Ott, C., Löhner, M., Atorf, J., Fuchs, M., Sedmak, T., Kremers, J., Fejtová, A., Gundelfinger, E.D., and Brandstätter, J.H. (2013). Identification and immunocytochemical characterization of Piccolino, a novel Piccolo splice variant selectively expressed at sensory ribbon synapses of the eye and ear. *PLoS ONE* 8, e70373.

Reichenbach, T., and Hudspeth, A.J. (2014). The physics of hearing: fluid mechanics and the active process of the inner ear. *Rep. Prog. Phys.* 77, 076601.

Ricci, A.J., and Fettiplace, R. (1998). Calcium permeation of the turtle hair cell mechanotransducer channel and its relation to the composition of endolymph. *J. Physiol. (Lond.)* 506 (Pt 1), 159–173.

Riley, B.B., and Moorman, S.J. (2000). Development of utricular otoliths, but not saccular otoliths, is necessary for vestibular function and survival in zebrafish. *J Neurobiol* 43, 329–337.

Risner, J.R., and Holt, J.R. (2006). Heterogeneous potassium conductances contribute to the diverse firing properties of postnatal mouse vestibular ganglion neurons. *J. Neurophysiol.* 96, 2364–2376.

Rizzuto, R., Nakase, H., Darras, B., Francke, U., Fabrizi, G.M., Mengel, T., Walsh, F., Kadenbach, B., DiMauro, S., and Schon, E.A. (1989). A gene specifying subunit VIII of human cytochrome c oxidase is localized to chromosome 11 and is expressed in both muscle and non-muscle tissues. *J. Biol. Chem.* *264*, 10595–10600.

Rizzuto, R., Brini, M., Murgia, M., and Pozzan, T. (1993). Microdomains with high Ca^{2+} close to IP₃-sensitive channels that are sensed by neighboring mitochondria. *Science* *262*, 744–747.

Rizzuto, R., Pinton, P., Carrington, W., Fay, F.S., Fogarty, K.E., Lifshitz, L.M., Tuft, R.A., and Pozzan, T. (1998). Close contacts with the endoplasmic reticulum as determinants of mitochondrial Ca^{2+} responses. *Science* *280*, 1763–1766.

Rizzuto, R., De Stefani, D., Raffaello, A., and Mammucari, C. (2012). Mitochondria as sensors and regulators of calcium signalling. *Nat Rev Mol Cell Biol* *13*, 566–578.

Roberts, L.E., Eggermont, J.J., Caspary, D.M., Shore, S.E., Melcher, J.R., and Kaltenbach, J.A. (2010). Ringing Ears: The Neuroscience of Tinnitus. *J Neurosci* *30*, 14972–14979.

Robertson, D. (1983). Functional significance of dendritic swelling after loud sounds in the guinea pig cochlea. *Hear Res* *9*, 263–278.

Rossi, A., Pizzo, P., and Filadi, R. (2019). Calcium, mitochondria and cell metabolism: A functional triangle in bioenergetics. *Biochim Biophys Acta Mol Cell Res* *1866*, 1068–1078.

Roux, I., Safieddine, S., Nouvian, R., Grati, M., Simmler, M.-C., Bahloul, A., Perfettini, I., Le Gall, M., Rostaing, P., Hamard, G., et al. (2006). Otoferlin, defective in a human deafness form, is essential for exocytosis at the auditory ribbon synapse. *Cell* *127*, 277–289.

Roux, I., Hosie, S., Johnson, S.L., Bahloul, A., Cayet, N., Nouaille, S., Kros, C.J., Petit, C., and Safieddine, S. (2009). Myosin VI is required for the proper maturation and function of inner hair cell ribbon synapses. *Hum Mol Genet* 18, 4615–4628.

Ruel, J., Emery, S., Nouvian, R., Bersot, T., Amilhon, B., Van Rybroek, J.M., Rebillard, G., Lenoir, M., Eybalin, M., Delprat, B., et al. (2008). Impairment of SLC17A8 encoding vesicular glutamate transporter-3, VGLUT3, underlies nonsyndromic deafness DFNA25 and inner hair cell dysfunction in null mice. *The American Journal of Human Genetics* 83, 278–292.

Russell, I.J., and Richardson, G.P. (1987). The morphology and physiology of hair cells in organotypic cultures of the mouse cochlea. *Hear Res* 31, 9–24.

de Ruyter van Steveninck, R.R., and Laughlin, S.B. (1996). The rate of information transfer at graded-potential synapses. *Nature* 379, 642–645.

Safieddine, S., and Wenthold, R.J. (1999). SNARE complex at the ribbon synapses of cochlear hair cells: analysis of synaptic vesicle- and synaptic membrane-associated proteins: SNARE complex of the ribbon-synapses of hair cells. *Eur J Neurosci* 11, 803–812.

Safieddine, S., El-Amraoui, A., and Petit, C. (2012). The auditory hair cell ribbon synapse: from assembly to function. *Annu Rev Neurosci* 35, 509–528.

Salvinelli, F., Firrisi, L., Casale, M., Trivelli, M., D’Ascanio, L., Lamanna, F., Greco, F., and Costantino, S. (2004). Benign paroxysmal positional vertigo: diagnosis and treatment. *Clin Ter* 155, 395–400.

Santos, F., MacDonald, G., Rubel, E.W., and Raible, D.W. (2006). Lateral line hair cell maturation is a determinant of aminoglycoside susceptibility in zebrafish (*Danio rerio*). *Hearing Research* 213, 25–33.

Satrústegui, J., and Bak, L.K. (2015). Fluctuations in Cytosolic Calcium Regulate the Neuronal Malate-Aspartate NADH Shuttle: Implications for Neuronal Energy Metabolism. *Neurochem. Res.* 40, 2425–2430.

Scaglia, F., Hsu, C.-H., Kwon, H., Bai, R.-K., Perng, C.-L., Chang, H.-M., Dai, P., Smith, E.O., Whiteman, D.A.H., Feigenbaum, A., et al. (2006). Molecular bases of hearing loss in multi-systemic mitochondrial cytopathy. *Genet Med* 8, 641–652.

Schein, S.J., Colombini, M., and Finkelstein, A. (1976). Reconstitution in planar lipid bilayers of a voltage-dependent anion-selective channel obtained from paramecium mitochondria. *J. Membr. Biol.* 30, 99–120.

Schindelin, J., Arganda-Carreras, I., Frise, E., Kaynig, V., Longair, M., Pietzsch, T., Preibisch, S., Rueden, C., Saalfeld, S., Schmid, B., et al. (2012). Fiji: an open-source platform for biological-image analysis. *Nat. Methods* 9, 676–682.

Schmitz, F. (2009). The Making of Synaptic Ribbons: How They Are Built and What They Do. *The Neuroscientist* 15, 611–624.

Schmitz, F., Königstorfer, A., and Südhof, T.C. (2000). RIBEYE, a component of synaptic ribbons: a protein's journey through evolution provides insight into synaptic ribbon function. *Neuron* 28, 857–72.

- Schnee, M.E., and Ricci, A.J. (2003). Biophysical and pharmacological characterization of voltage-gated calcium currents in turtle auditory hair cells. *J Physiol* *549*, 697–717.
- Schnee, M.E., Lawton, D.M., Furness, D.N., Benke, T.A., and Ricci, A.J. (2005). Auditory hair cell-afferent fiber synapses are specialized to operate at their best frequencies. *Neuron* *47*, 243–254.
- Seal, R.P., Akil, O., Yi, E., Weber, C.M., Grant, L., Yoo, J., Clause, A., Kandler, K., Noebels, J.L., Glowatzki, E., et al. (2008). Sensorineural deafness and seizures in mice lacking vesicular glutamate transporter 3. *Neuron* *57*, 263–275.
- Sebe, J.Y., Cho, S., Sheets, L., Rutherford, M.A., von Gersdorff, H., and Raible, D.W. (2017). Ca²⁺-Permeable AMPARs mediate glutamatergic transmission and excitotoxic damage at the hair cell ribbon synapse. *J Neurosci* *37*, 6162–6175.
- Seiler, C., Finger-Baier, K.C., Rinner, O., Makhankov, Y.V., Schwarz, H., Neuhaus, S.C.F., and Nicolson, T. (2005). Duplicated genes with split functions: independent roles of protocadherin15 orthologues in zebrafish hearing and vision. *Development* *132*, 615–623.
- Sekler, I. (2015). Standing of giants shoulders the story of the mitochondrial Na⁺Ca²⁺ exchanger. *Biochemical and Biophysical Research Communications* *460*, 50–52.
- Sendin, G., Bourien, J., Rassendren, F., Puel, J.-L., and Nouvian, R. (2014). Spatiotemporal pattern of action potential firing in developing inner hair cells of the mouse cochlea. *Proc Natl Acad Sci USA* *111*, 1999–2004.
- Sha, S.-H., Taylor, R., Forge, A., and Schacht, J. (2001). Differential vulnerability of basal and apical hair cells is based on intrinsic susceptibility to free radicals. *Hear Res* *155*, 1–8.

Shaw, R.J., Kosmatka, M., Bardeesy, N., Hurley, R.L., Witters, L.A., DePinho, R.A., and Cantley, L.C. (2004). The tumor suppressor LKB1 kinase directly activates AMP-activated kinase and regulates apoptosis in response to energy stress. *Proceedings of the National Academy of Sciences* *101*, 3329–3335.

Sheets, L. (2017). Excessive activation of ionotropic glutamate receptors induces apoptotic hair-cell death independent of afferent and efferent innervation. *Sci Rep* *7*, 41102.

Sheets, L., Trapani, J.G., Mo, W., Obholzer, N., and Nicolson, T. (2011). Ribeye is required for presynaptic Ca(V)1.3a channel localization and afferent innervation of sensory hair cells. *Development* *138*, 1309–19.

Sheets, L., Kindt, K.S., and Nicolson, T. (2012). Presynaptic CaV1.3 channels regulate synaptic ribbon size and are required for synaptic maintenance in sensory hair cells. *J Neurosci* *32*, 17273–17286.

Sheets, L., Hagen, M.W., and Nicolson, T. (2014). Characterization of Ribeye subunits in zebrafish hair cells reveals that exogenous Ribeye B-domain and CtBP1 localize to the basal ends of synaptic ribbons. *PLoS ONE* *9*, e107256.

Sheets, L., He, X.J., Olt, J., Schreck, M., Petralia, R.S., Wang, Y.-X., Zhang, Q., Beirl, A., Nicolson, T., Marcotti, W., et al. (2017). Enlargement of Ribbons in Zebrafish Hair Cells Increases Calcium Currents But Disrupts Afferent Spontaneous Activity and Timing of Stimulus Onset. *J Neurosci* *37*, 6299–6313.

Shen, H.-M., and Liu, Z. (2006). JNK signaling pathway is a key modulator in cell death mediated by reactive oxygen and nitrogen species. *Free Radical Biology and Medicine* 40, 928–939.

Shen, H., Zhang, B., Shin, J.-H., Lei, D., Du, Y., Gao, X., Wang, Q., Ohlemiller, K.K., Piccirillo, J., and Bao, J. (2007). Prophylactic and therapeutic functions of T-type calcium blockers against noise-induced hearing loss. *Hear Res* 226, 52–60.

Sheng, Z.-H., and Cai, Q. (2012). Mitochondrial transport in neurons: impact on synaptic homeostasis and neurodegeneration. *Nat Rev Neurosci* 13, 77–93.

Shin, J.-B., Streijger, F., Beynon, A., Peters, T., Gadzala, L., McMillen, D., Bystrom, C., Van der Zee, C.E.E.M., Wallimann, T., and Gillespie, P.G. (2007). Hair bundles are specialized for ATP delivery via creatine kinase. *Neuron* 53, 371–386.

Shore, G.C., and Tata, J.R. (1977). Two fractions of rough endoplasmic reticulum from rat liver. I. Recovery of rapidly sedimenting endoplasmic reticulum in association with mitochondria. *J. Cell Biol.* 72, 714–725.

Shoshan-Barmatz, V., and Gincel, D. (2003). The voltage-dependent anion channel: characterization, modulation, and role in mitochondrial function in cell life and death. *Cell Biochem. Biophys.* 39, 279–292.

Shoshan-Barmatz, V., De Pinto, V., Zweckstetter, M., Raviv, Z., Keinan, N., and Arbel, N. (2010). VDAC, a multi-functional mitochondrial protein regulating cell life and death. *Molecular Aspects of Medicine* 31, 227–285.

- Sidi, S. (2004). *gemini* Encodes a Zebrafish L-Type Calcium Channel That Localizes at Sensory Hair Cell Ribbon Synapses. *J Neurosci* *24*, 4213–4223.
- Simmler, M.-C., Cohen-Salmon, M., El-Amraoui, A., Guillaud, L., Benichou, J.-C., Petit, C., and Panthier, J.-J. (2000). Targeted disruption of *Otog* results in deafness and severe imbalance. *Nat Genet* *24*, 139–143.
- Sjöstrand, F.S. (1958). Ultrastructure of retinal rod synapses of the guinea pig eye as revealed by three-dimensional reconstructions from serial sections. *Journal of Ultrastructure Research* *2*, 122–170.
- Smith, C.A., and Sjostrand, F.S. (1961). Structure of the nerve endings on the external hair cells of the guinea pig cochlea as studied by serial sections. *J. Ultrastruct. Res.* *5*, 523–556.
- Sobkowicz, H.M., Bereman, B., and Rose, J.E. (1975). Organotypic development of the organ of Corti in culture. *J Neurocytol* *4*, 543–572.
- Sobkowicz, H.M., Rose, J.E., Scott, G.E., and Slapnick, S.M. (1982). Ribbon synapses in the developing intact and cultured organ of Corti in the mouse. *J Neurosci* *2*, 942–957.
- Sobkowicz, H.M., Rose, J.E., Scott, G.L., and Levenick, C.V. (1986). Distribution of synaptic ribbons in the developing organ of Corti. *J Neurocytol* *15*, 693–714.
- Sobkowicz, H.M., Loftus, J.M., and Slapnick, S.M. (1993). Tissue Culture of the Organ of Corti: Part I. *Acta Oto-Laryngologica* *113*, 1–19.

Söllner, C., Rauch, G.-J., Siemens, J., Geisler, R., Schuster, S.C., Müller, U., Nicolson, T., and Tübingen 2000 Screen Consortium (2004). Mutations in cadherin 23 affect tip links in zebrafish sensory hair cells. *Nature* 428, 955–959.

Sollner, C., Schwarz, H., Geisler, R., and Nicolson, T. (2004). Mutated otopectrin 1 affects the genesis of otoliths and the localization of Starmaker in zebrafish. *Dev Genes Evol* 214, 582–590.

Söllner, T., Whiteheart, S.W., Brunner, M., Erdjument-Bromage, H., Geromanos, S., Tempst, P., and Rothman, J.E. (1993). SNAP receptors implicated in vesicle targeting and fusion. *Nature* 362, 318–324.

Solovyova, N., Veselovsky, N., Toescu, E.C., and Verkhratsky, A. (2002). Ca^{2+} dynamics in the lumen of the endoplasmic reticulum in sensory neurons: direct visualization of Ca^{2+} -induced Ca^{2+} release triggered by physiological Ca^{2+} entry. *EMBO J* 21, 622–630.

Song, H., Nie, L., Rodriguez-Contreras, A., Sheng, Z.-H., and Yamoah, E.N. (2003). Functional interaction of auxiliary subunits and synaptic proteins with $Ca(v)1.3$ may impart hair cell Ca^{2+} current properties. *J. Neurophysiol.* 89, 1143–1149.

Song, Q., Shen, P., Li, X., Shi, L., Liu, L., Wang, J., Yu, Z., Stephen, K., Aiken, S., Yin, S., et al. (2016). Coding deficits in hidden hearing loss induced by noise: the nature and impacts. *Sci Rep* 6, 25200.

Sonntag, M., Blosa, M., Schmidt, S., Reimann, K., Blum, K., Eckrich, T., Seeger, G., Hecker, D., Schick, B., Arendt, T., et al. (2018). Synaptic coupling of inner ear sensory cells is

controlled by brevican-based extracellular matrix baskets resembling perineuronal nets. *BMC Biol* 16, 99.

Sood, A., Jeyaraju, D.V., Prudent, J., Caron, A., Lemieux, P., McBride, H.M., Laplante, M., Tóth, K., and Pellegrini, L. (2014). A Mitofusin-2-dependent inactivating cleavage of Opa1 links changes in mitochondria cristae and ER contacts in the postprandial liver. *Proc Natl Acad Sci USA* 111, 16017–16022.

Spassova, M.A., Avissar, M., Furman, A.C., Crumling, M.A., Saunders, J.C., and Parsons, T.D. (2004). Evidence that rapid vesicle replenishment of the synaptic ribbon mediates recovery from short-term adaptation at the hair cell afferent synapse. *J. Assoc. Res. Otolaryngol.* 5, 376–390.

Spicer, S.S., Thomopoulos, G.N., and Schulte, B.A. (1999). Novel membranous structures in apical and basal compartments of inner hair cells. *J Comp Neurol* 409, 424–437.

Spinelli, K.J., Klimek, J.E., Wilmarth, P.A., Shin, J.-B., Choi, D., David, L.L., and Gillespie, P.G. (2012). Distinct energy metabolism of auditory and vestibular sensory epithelia revealed by quantitative mass spectrometry using MS2 intensity. *PNAS* 109, E268–E277.

Spoendlin, H. (1971). Primary Structural Changes in the Organ of Corti After Acoustic Overstimulation. *Acta Otolaryngol* 71, 166–176.

Srivastava, S. (2016). Emerging therapeutic roles for NAD⁺ metabolism in mitochondrial and age-related disorders. *Clin Trans Med* 5, 25.

Stamatakis, S., Francis, H.W., Lehar, M., May, B.J., and Ryugo, D.K. (2006). Synaptic alterations at inner hair cells precede spiral ganglion cell loss in aging C57BL/6J mice. *Hear Res* 221, 104–118.

Stankiewicz, T.R., Gray, J.J., Winter, A.N., and Linseman, D.A. (2014). C-terminal binding proteins: central players in development and disease. *Biomolecular Concepts* 5, 489–511.

Stefanelli, C., Stanic, I., Bonavita, F., Flamigni, F., Pignatti, C., Guarnieri, C., and Calderera, C.M. (1998). Inhibition of glucocorticoid-induced apoptosis with 5-aminoimidazole-4-carboxamide ribonucleoside, a cell-permeable activator of AMP-activated protein kinase. *Biochem. Biophys. Res. Commun.* 243, 821–826.

Stowe, D.F., and Camara, A.K.S. (2009). Mitochondrial reactive oxygen species production in excitable cells: modulators of mitochondrial and cell function. *Antioxid Redox Signal* 11, 1373–1414.

Strenzke, N., Chanda, S., Kopp-Scheinflug, C., Khimich, D., Reim, K., Bulankina, A.V., Neef, A., Wolf, F., Brose, N., Xu-Friedman, M.A., et al. (2009). Complexin-I is required for high-fidelity transmission at the endbulb of Held auditory synapse. *J. Neurosci.* 29, 7991–8004.

Suli, A., Pujol, R., Cunningham, D.E., Hailey, D.W., Prendergast, A., Rubel, E.W., and Raible, D.W. (2016). Innervation regulates synaptic ribbons in lateral line mechanosensory hair cells. *J Cell Sci* 129, 2250–2260.

Suzuki, J., Kanemaru, K., Ishii, K., Ohkura, M., Okubo, Y., and Iino, M. (2014). Imaging intraorganellar Ca^{2+} at subcellular resolution using CEPIA. *Nat Commun* 5, 4153.

- Szabo, T.M., Weiss, S.A., Faber, D.S., and Preuss, T. (2006). Representation of auditory signals in the M-Cell: Role of electrical synapses. *J Neurophysiol* *95*, 2617–2629.
- Szabo, T.M., McCormick, C.A., and Faber, D.S. (2007). Otolith endorgan input to the Mauthner neuron in the goldfish. *J. Comp. Neurol.* *505*, 511–525.
- Szabo, I., and Zoratti, M. (2014). Mitochondrial channels: ion fluxes and more. *Physiol. Rev.* *94*, 519–608.
- Tait, S.W.G., and Green, D.R. (2013). Mitochondrial regulation of cell death. *Cold Spring Harb Perspect Biol* *5*, a008706.
- Tajeddine, N. (2016). How do reactive oxygen species and calcium trigger mitochondrial membrane permeabilisation? *Biochim. Biophys. Acta* *1860*, 1079–1088.
- Takao-Rikitsu, E., Mochida, S., Inoue, E., Deguchi-Tawarada, M., Inoue, M., Ohtsuka, T., and Takai, Y. (2004). Physical and functional interaction of the active zone proteins, CAST, RIM1, and Bassoon, in neurotransmitter release. *J Cell Biol* *164*, 301–311.
- Teudt, I.U., and Richter, C.P. (2014). Basilar membrane and tectorial membrane stiffness in the CBA/CaJ mouse. *J Assoc Res Otolaryngol* *15*, 675–694.
- Thastrup, O., Cullen, P.J., Drøbak, B.K., Hanley, M.R., and Dawson, A.P. (1990). Thapsigargin, a tumor promoter, discharges intracellular Ca^{2+} stores by specific inhibition of the endoplasmic reticulum Ca^{2+} -ATPase. *Proc. Natl. Acad. Sci. U.S.A.* *87*, 2466–2470.
- Thevenaz, P., Ruttimann, U.E., and Unser, M. (1998). A pyramid approach to subpixel registration based on intensity. *IEEE Transactions on Image Processing* *7*, 27–41.

Thio, S.S.C., Bonventre, J.V., and Hsu, S.I.-H. (2004). The CtBP2 co-repressor is regulated by NADH-dependent dimerization and possesses a novel N-terminal repression domain. *Nucleic Acids Res* *32*, 1836–1847.

Todorova, V., and Blokland, A. (2017). Mitochondria and synaptic plasticity in the mature and aging nervous system. *Curr Neuropharmacol* *15*, 166–173.

tom Dieck, S., Altmann, W.D., Kessels, M.M., Qualmann, B., Regus, H., Brauner, D., Fejtová, A., Bracko, O., Gundelfinger, E.D., and Brandstätter, J.H. (2005). Molecular dissection of the photoreceptor ribbon synapse. *The Journal of Cell Biology* *168*, 825–836.

Torre, V., Ashmore, J.F., Lamb, T.D., and Menini, A. (1995). Transduction and adaptation in sensory receptor cells. *J Neurosci* *15*, 7757–7768.

Torres, V.I., and Inestrosa, N.C. (2018). Vertebrate Presynaptic Active Zone Assembly: a Role Accomplished by Diverse Molecular and Cellular Mechanisms. *Mol Neurobiol* *55*, 4513–4528.

Tritsch, N.X., and Bergles, D.E. (2010). Developmental Regulation of Spontaneous Activity in the Mammalian Cochlea. *J Neurosci* *30*, 1539–1550.

Tritsch, N.X., Yi, E., Gale, J.E., Glowatzki, E., and Bergles, D.E. (2007). The origin of spontaneous activity in the developing auditory system. *Nature* *450*, 50–55.

Tritsch, N.X., Rodríguez-Contreras, A., Crins, T.T.H., Wang, H.C., Borst, J.G.G., and Bergles, D.E. (2010). Calcium action potentials in hair cells pattern auditory neuron activity before hearing onset. *Nat Neurosci* *13*, 1050–1052.

Trune, D.R., and Lim, D.J. (1983). The Behavior and Vestibular Nuclear Morphology of Otoconia-Deficient Pallid Mutant Mice. *J Neurogenet* 1, 53–69.

Tucker, T., and Fettiplace, R. (1995). Confocal imaging of calcium microdomains and calcium extrusion in turtle hair cells. *Neuron* 15, 1323–35.

Uthaiyah, R.C., and Hudspeth, A.J. (2010). Molecular anatomy of the hair cell's ribbon synapse. *J Neurosci* 30, 12387–12399.

Vakifahmetoglu-Norberg, H., Ouchida, A.T., and Norberg, E. (2017). The role of mitochondria in metabolism and cell death. *Biochemical and Biophysical Research Communications* 482, 426–431.

Valero, M.D., Burton, J.A., Hauser, S.N., Hackett, T.A., Ramachandran, R., and Liberman, M.C. (2017). Noise-induced cochlear synaptopathy in rhesus monkeys (*Macaca mulatta*). *Hear. Res.* 353, 213–223.

Vance, J.E. (2014). MAM (mitochondria-associated membranes) in mammalian cells: lipids and beyond. *Biochim. Biophys. Acta* 1841, 595–609.

Vandecaetsbeek, I., Vangheluwe, P., Raeymaekers, L., Wuytack, F., and Vanoevelen, J. (2011). The Ca^{2+} pumps of the endoplasmic reticulum and Golgi apparatus. *Cold Spring Harb Perspect Biol* 3, a004184–a004184.

Vaughan, H., and Newsholme, E.A. (1969). The effects of Ca^{2+} and ADP on the activity of NAD-linked isocitrate dehydrogenase of muscle. *FEBS Lett* 5, 124–126.

Venkatesan, J.K., Natarajan, S., Schwarz, K., Mayer, S.I., Alpadi, K., Magupalli, V.G., Sung, C.-H., and Schmitz, F. (2010). Nicotinamide adenine dinucleotide-dependent binding of the neuronal Ca^{2+} sensor protein GCAP2 to photoreceptor synaptic ribbons. *The Journal of Neuroscience : The Official Journal of the Society for Neuroscience* 30, 6559–76.

Verhoeven, K., Ensink, R.J., Tiranti, V., Huygen, P.L., Johnson, D.F., Schatteman, I., Van Laer, L., Verstreken, M., Van de Heyning, P., Fischel-Ghodsian, N., et al. (1999). Hearing impairment and neurological dysfunction associated with a mutation in the mitochondrial tRNASer(UCN) gene. *Eur J Hum Genet* 7, 45–51.

Verkhatsky, A. (2005). Physiology and pathophysiology of the calcium store in the endoplasmic reticulum of neurons. *Physiol Rev* 85, 201–279.

Verkhatsky, A., and Petersen, O.H. (2002). The endoplasmic reticulum as an integrating signalling organelle: from neuronal signalling to neuronal death. *Eur J Pharmacol* 447, 141–154.

Vialettes, B.H., Paquis-Flucklinger, V., Pelissier, J.F., Bendahan, D., Narbonne, H., Silvestre-Aillaud, P., Montfort, M.F., Righini-Chossegros, M., Pouget, J., Cozzone, P.J., et al. (1997). Phenotypic expression of diabetes secondary to a T14709C mutation of mitochondrial DNA: Comparison with MIDD syndrome (A3243G mutation): a case report. *Diabetes Care* 20, 1731–1737.

Vincent, P.F.Y., Bouleau, Y., Safieddine, S., Petit, C., and Dulon, D. (2014). Exocytotic machineries of vestibular type I and cochlear ribbon synapses display similar intrinsic Otoferlin-dependent Ca^{2+} sensitivity but a different coupling to Ca^{2+} channels. *J Neurosci* 34, 10853–10869.

Vollrath, L., Schultz, R.L., and McMillan, P.J. (1983). “Synaptic” ribbons and spherules of the guinea pig pineal gland: Inverse day/night differences in number. *Am. J. Anat.* 168, 67–74.

Von Békésy, G., and Wever, E.G. (1989). *Experiments in hearing* (New York: Acoustical Society of America through the American Institute of Physics by arrangement with McGraw-Hill Book Co).

Vos, M., Lauwers, E., and Verstreken, P. (2010). Synaptic mitochondria in synaptic transmission and organization of vesicle pools in health and disease. *Front Synaptic Neurosci* 2, 139.

Wahl, S., Magupalli, V.G., Dembla, M., Katiyar, R., Schwarz, K., Köblitz, L., Alpađi, K., Krause, E., Rettig, J., Sung, C.-H., et al. (2016). The disease protein Tulp1 is essential for periaxonal zone endocytosis in photoreceptor ribbon synapses. *J Neurosci* 36, 2473–2493.

Waites, C.L., Leal-Ortiz, S.A., Okerlund, N., Dalke, H., Fejtova, A., Altroek, W.D., Gundelfinger, E.D., and Garner, C.C. (2013). Bassoon and Piccolo maintain synapse integrity by regulating protein ubiquitination and degradation. *EMBO J* 32, 954–969.

Wallace, D.C. (2012). Mitochondria and cancer. *Nature Reviews Cancer* 12, 685–698.

Wan, G., and Corfas, G. (2015). No longer falling on deaf ears: Mechanisms of degeneration and regeneration of cochlear ribbon synapses. 329.

Wan, L., Almers, W., and Chen, W. (2005). Two ribeye genes in teleosts: the role of Ribeye in ribbon formation and bipolar cell development. *The Journal of Neuroscience: The Official Journal of the Society for Neuroscience* 25, 941–949.

- Wan, Q.-F., Nixon, E., and Heidelberger, R. (2012). Regulation of presynaptic calcium in a mammalian synaptic terminal. *J Neurophysiol* *108*, 3059–67.
- Wang, X., Kibschull, M., Laue, M.M., Lichte, B., Petrasch-Parwez, E., and Kilimann, M.W. (1999). Aczonin, a 550-Kd Putative Scaffolding Protein of Presynaptic Active Zones, Shares Homology Regions with Rim and Bassoon and Binds Profilin. *J Cell Biol* *147*, 151–162.
- Wang, X., Zhu, Y., Long, H., Pan, S., Xiong, H., Fang, Q., Hill, K., Lai, R., Yuan, H., and Sha, S.-H. (2019). Mitochondrial calcium transporters mediate sensitivity to noise-induced losses of hair cells and cochlear synapses. *Front Mol Neurosci* *11*, 469.
- Wanson, J.C., Drochmans, P., May, C., Penasse, W., and Popowski, A. (1975). Isolation of centrolobular and perilobular hepatocytes after phenobarbital treatment. *J. Cell Biol.* *66*, 23–41.
- Warburg, O. (1956). On the Origin of Cancer Cells. *Science* *123*, 309–314.
- Weaver, S.P., and Schweitzer, L. (1994). Development of gerbil outer hair cells after the onset of cochlear function: an ultrastructural study. *Hear. Res.* *72*, 44–52.
- Whitfield, T.T., Riley, B.B., Chiang, M.-Y., and Phillips, B. (2002). Development of the zebrafish inner ear. *Dev. Dyn.* *223*, 427–458.
- Wiederhold, M.L. (1976). Mechanosensory Transduction in “Sensory” and “Motile” Cilia. *Annu. Rev. Biophys. Bioeng.* *5*, 39–62.

- Wiemer, E.A., Michels, P.A., and Opperdoes, F.R. (1995). The inhibition of pyruvate transport across the plasma membrane of the bloodstream form of *Trypanosoma brucei* and its metabolic implications. *Biochem. J.* *312 (Pt 2)*, 479–484.
- Williams, J.A., and Holder, N. (2000). Cell turnover in neuromasts of zebrafish larvae. *Hearing Research* *143*, 171–181.
- Williams, G.S.B., Boyman, L., Chikando, A.C., Khairallah, R.J., and Lederer, W.J. (2013). Mitochondrial calcium uptake. *Proc Natl Acad Sci USA* *110*, 10479–10486.
- Williamson, D.H., Lund, P., and Krebs, H.A. (1967). The redox state of free nicotinamide-adenine dinucleotide in the cytoplasm and mitochondria of rat liver. *Biochem J* *103*, 514–527.
- Wong, A.B., Rutherford, M.A., Gabrielaitis, M., Pangrsic, T., Göttfert, F., Frank, T., Michanski, S., Hell, S., Wolf, F., Wichmann, C., et al. (2014). Developmental refinement of hair cell synapses tightens the coupling of Ca²⁺ influx to exocytosis. *EMBO J.* *33*, 247–264.
- Woods, A., Johnstone, S.R., Dickerson, K., Leiper, F.C., Fryer, L.G.D., Neumann, D., Schlattner, U., Wallimann, T., Carlson, M., and Carling, D. (2003). LKB1 is the upstream kinase in the AMP-activated protein kinase cascade. *Curr. Biol.* *13*, 2004–2008.
- Wu, H., Carvalho, P., and Voeltz, G.K. (2018). Here, there, and everywhere: The importance of ER membrane contact sites. *Science* *361*.
- Xing, G., Chen, Z., and Cao, X. (2007). Mitochondrial rRNA and tRNA and hearing function. *Cell Res.* *17*, 227–239.

Xu, W., and Lipscombe, D. (2001). Neuronal Ca(V)1.3alpha(1) L-type channels activate at relatively hyperpolarized membrane potentials and are incompletely inhibited by dihydropyridines. *J. Neurosci.* 21, 5944–5951.

Yamane, H., Nakai, Y., Takayama, M., Iguchi, H., Nakagawa, T., and Kojima, A. (1995). Appearance of free radicals in the guinea pig inner ear after noise-induced acoustic trauma. *Eur Arch Otorhinolaryngol* 252, 504–508.

Yamoah, E.N., Lumpkin, E.A., Dumont, R.A., Smith, P.J., Hudspeth, A.J., and Gillespie, P.G. (1998). Plasma membrane Ca²⁺-ATPase extrudes Ca²⁺ from hair cell stereocilia. *J Neurosci* 18, 610–624.

Yasunaga S, Grati M, Cohen-Salmon M, El-Amraoui A, Mustapha M, Salem N, El-Zir E, Loiselet J, Petit C. (1999) A mutation in OTOF, encoding otoferlin, a FER-1-like protein, causes DFNB9, a nonsyndromic form of deafness. *Nat Genet* 21(4):363–369.

Yin, Y., Liberman, L.D., Maison, S.F., and Liberman, M.C. (2014). Olivocochlear innervation maintains the normal modiolar-pillar and habenular-cuticular gradients in cochlear synaptic morphology. *Journal of the Association for Research in Otolaryngology : JARO* 15, 571–83.

Zammit, V.A., and Newsholme, E.A. (1976). Effects of calcium ions and adenosine diphosphate on the activities of NAD⁺-linked isocitrate dehydrogenase from the radular muscles of the whelk and flight muscles of insects. *Biochemical Journal* 154, 677–687.

Zenisek, D., and Matthews, G. (2000). The role of mitochondria in presynaptic calcium handling at a ribbon synapse. *Neuron* 25, 229–37.

Zenisek, D., Davila, V., Wan, L., and Almers, W. (2003). Imaging calcium entry sites and ribbon structures in two presynaptic cells. *J. Neurosci.* *23*, 2538–2548.

Zhang, Q., Li, S., Wong, H.-T.C., He, X.J., Beirl, A., Petralia, R.S., Wang, Y.-X., and Kindt, K.S. (2018). Synaptically silent sensory hair cells in zebrafish are recruited after damage. *Nature Communications* *9*, 1388.

Zhang, Q.X., He, X.J., Wong, H.C., and Kindt, K.S. (2016). Functional calcium imaging in zebrafish lateral-line hair cells. In *Methods in Cell Biology*, (Elsevier), pp. 229–252.

Zhang, Y.-Z., Ouyang, Y.-C., Hou, Y., Schatten, H., Chen, D.-Y., and Sun, Q.-Y. (2008). Mitochondrial behavior during oogenesis in zebrafish: A confocal microscopy analysis: Mitochondrial behavior during oogenesis. *Development, Growth & Differentiation* *50*, 189–201.

Zhao, H., Li, R., Wang, Q., Yan, Q., Deng, J.-H., Han, D., Bai, Y., Young, W.-Y., and Guan, M.-X. (2004). Maternally inherited aminoglycoside-induced and nonsyndromic deafness is associated with the novel C1494T mutation in the mitochondrial 12S rRNA gene in a large Chinese family. *Am J Hum Genet* *74*, 139–152.

Zhao, H., Young, W.-Y., Yan, Q., Li, R., Cao, J., Wang, Q., Li, X., Peters, J.L., Han, D., and Guan, M.-X. (2005). Functional characterization of the mitochondrial 12S rRNA C1494T mutation associated with aminoglycoside-induced and non-syndromic hearing loss. *Nucleic Acids Res* *33*, 1132–1139.

Zheng, J., Du, G.-G., Anderson, C.T., Keller, J.P., Orem, A., Dallos, P., and Cheatham, M. (2006). Analysis of the oligomeric structure of the motor protein Prestin. *J. Biol. Chem.* *281*, 19916–19924.

Curriculum Vitae

Hiu-Tung Candy Wong

hue.tone@gmail.com

LinkedIn /wonghc

734-560-8550

35 Convent Drive 1D-931

Bethesda, MD 20892

Education

Johns Hopkins University (Biology)

Ph.D. 2013-present

Baltimore, MD

University of Michigan (Biomedical Engineering)

M.S.E. May 2013

Ann Arbor, MI

University of Michigan (Cellular and Molecular Biology)

B.S. May 2012

Ann Arbor, MI

Research Experiences

Ph.D. Candidate

2014-present

Location: Bethesda, MD | Advisor: Dr. Katie Kindt

Studied zebrafish lateral line hair cell synapse formation using microscopy, immunohistochemistry, pharmacology, and genetically-encoded fluorescent indicators.

Independent Research

2012-2013

Location: Ann Arbor, MI | Faculty sponsor: Dr. Karl Grosh

Reviewed the use of electrical impedance spectroscopy in assessing fibrotic tissue response to cochlea implants.

Research Assistant

2008-2013

Location: Ann Arbor, MI | Faculty sponsor: Dr. Yehoash Raphael

Trained in otopathology related surgery in guinea pig inner ear; dissection, immunohistology and analysis of the organ of Corti and spiral ganglion. **Honors thesis: Comparing neurotrophin effects on auditory neurofiber regrowth in deafened guinea pig ear.**

Senior team member and championship participant

2010-2012

Location: Ann Arbor, MI | Faculty Sponsor: Dr. Marcus Ammerlaan

Design and development of genetically modified *Escherichia coli* to adhere to specific dsDNA on microarray.

Research Assistant as part of Undergraduate Research Opportunity Program

2008-2010

Location: Ann Arbor, MI | Faculty sponsor: Dr. John Schiefelbein

Investigated the role of germin-like protein on *Arabidopsis thaliana* in regulating root epidermis development.

Awards

Best presentation in Mid-Atlantic Regional Zebrafish meeting, Nov 2019

NIDCD Director's Recognition Group Awards for
NIDCD Fellows Committee Leadership
NIDCD Green Team
EARssential Lab Series Instructors
Educate Children in the Community, Nov 2018

Best trainee presentation in NIDCD Retreat, Feb 2018

Best poster in NIDCD Retreat, Feb 2017

International Genetically Engineered Machine competition award
Gold in Americas East Region, 2012
Bronze in Americas East Region, 2011

Teaching Experiences

“Microscopy” (single lecture) 2017

Using the framework of a “photon budget”, introduce students of university-level general science background to concepts of epifluorescence and confocal microscopy, as well as broad overview of advances in super-resolution microscopy,

“Microscopy” and “High-throughput screening” (2 lectures) 2015

Introduce students with university-level general science background to history and concepts of light and epifluorescence microscopy.

Explain the concept of screening, limitation of manual protocols that can be overcome by automation.

Publications

H.C. Wong, Q.X. Zhang, A.J. Beirl, R.S. Petralia, Y.X. Wang, K.S. Kindt. *Synaptic mitochondria regulate hair-cell synapse size and junction.* *eLife* 2019;8:e48914

Q.X. Zhang, S. Li, **H.C. Wong**, J.X. He, A. Beirl, R.S. Petralia, Y.X. Wang, K.S. Kindt. *Synaptically silent sensory hair cells in zebrafish are recruited after damage.* *Nat Commun.* 2018 Apr 11;9(1):1388.

G.P. Wang, I. Basu, L.A. Beyer, **H.T. Wong**, D.L. Swiderski, S.S. Gong, Y. Raphael. *Severe streptomycin ototoxicity in the mouse utricle leads to a flat epithelium but the peripheral neural degeneration is delayed.* *Hear Res.* 2017 Nov;355:33-41.

Q.X. Zhang, X.J. He, **H.C. Wong**, K.S. Kindt. *Functional imaging in zebrafish lateral-line hair cells.* *Methods Cell Biol.* 2016;133:229-52.

C.L. Budenz, **H.T. Wong**, D.L. Swiderski, S.B. Shibata, B.E. Pflug BE, Y. Raphael. *Differential effects of AAV.BDNF and AAV.Ntf3 in the deafened adult guinea pig ear.* *Sci Rep.* 2015; 5:8619.

Y.H. Park, K.F. Wilson, Y. Ueda, **H.T. Wong**, L.A. Beyer, D.L. Swiderski, D.F. Dolan, Y. Raphael. *Conditioning the cochlea to facilitate survival and integration of exogenous cells into the auditory epithelium.* *Mol Ther.* 2014; 22(4):873-80.

H. Fukui, **H.T. Wong**, L.A. Beyer, B.G. Case, D.L. Swiderski, A. Di Polo, A.F. Ryan, Y. Raphael. *BDNF gene therapy induces*

auditory nerve survival and fiber sprouting in deaf Pou4f3 mutant mice. Sci Rep. 2012; 2:838.

G.C. Lin, G.J. Basura, **H.T. Wong**, K.D. Heidenreich. *Canal switch after canalith repositioning procedure for benign paroxysmal positional vertigo.* Laryngoscope. 2012 Sep;122(9):2076-8.

G.P. Wang, I. Chatterjee, S.A. Batts, **H.T. Wong**, T.W. Gong, S.S. Gong, Y. Raphael. *Notch signaling and Atob1 expression during hair cell regeneration in the mouse utricle.* Hear Res. 2010 Aug;267(1-2):61-70.

Presentations

“The Role of Mitochondrial Calcium at Hair Cell Synapses”

Mid-Atlantic Regional Zebrafish meeting, Nov 2019 (oral presentation)

“Mitochondrial Ca²⁺ and NAD(H) Regulates Hair-cell Synapse Formation”

Mid-Atlantic Regional Zebrafish meeting, Dec 2018 (poster)

“Linking Mitochondrial Calcium uptake, metabolism, and sensory synapse formation”

Neurobiology Seminar Series, Oct 2018 (oral presentation)

“Mitochondrial Ca²⁺ and NAD(H) Regulate Hair-cell Synapse Formation”

Graduate Student Symposium, Apr 2018 (poster)

Association for Research in Otolaryngology MidWinter Meeting, Feb 2018 (oral presentation)

“Hair-cell Ribbon Synapse Formation is Controlled by Calcium Levels in Synaptic Mitochondria and NAD(H) Redox Homeostasis”

Mid-Atlantic Regional Zebrafish meeting, Sep 2017 (poster)

“Regulation of Hair-cell Ribbon Synapse Size by Mitochondrial Ca²⁺ Uptake”

Eastern Auditory Retreat, Jun 2017 (poster)

Mid-Atlantic Regional Zebrafish meeting, Mar 2017 (poster)

“Regulation of Hair-cell Ribbon Synapse Size by Ribeye NAD-binding”

Graduate Student Symposium, Apr 2017 (poster)

Association for Research in Otolaryngology MidWinter Meeting, Feb 2017 (poster)

Mid-Atlantic Regional Zebrafish meeting, Dec 2016 (oral presentation)

“Regulation of Synaptic Ribbon Formation by Intracellular Calcium Stores”

Association for Research in Otolaryngology MidWinter Meeting, Feb 2016 (poster)

Association for Research in Otolaryngology MidWinter Meeting, Feb 2015 (poster)

“Utilizing FimE and HbiF Recombinases to Tightly Control a Bi-directional and Inheritable Switch”

International Genetically Engineered Machine competition 2012 (oral presentation)

“Comparing neurotrophin effects on auditory neurofiber regrowth in deafened guinea pig ear”

Association for Research in Otolaryngology MidWinter Meeting, Feb 2012. (poster)

“DNA directed cell immobilization using outer membrane protein containing zinc finger domain” International Genetically Engineered Machine competition 2011 (oral presentation)

“Role of germin-like protein on *Arabidopsis thaliana* in regulating root epidermis development.” Undergraduate Poster Symposium, 2009 and 2010. (posters)

Other writing experience

Independently researched and wrote grant proposal as fulfillment of graduate school curriculum requirement: “Uncoupling Nodal and actin-dependent cardiac left-right patterning”

Professional activities

Steering committee member of Neurobiology Interest Group 2018-present

Member of the NIDCD Green Team 2016-present

Poster judge for the NIH Postbac Poster Day 2017, 2019

Member of the NIH Fellows Committee 2016-2018

Community engagement

Letters to a Pre-scientist program participant 2018-present

NIH Take Your Child to Work Day volunteer 2017- 2019